AEDC-TR-81-14

High Power MHD System — Facility Status and Magnet Test Results

G. L. Whitehead
ARO, Inc.

February 1982

Final Report for Period July 1, 1977 – September 30, 1980

Approved for public release, distribution unlimited.

ARNOLD ENGINEERING DEVELOPMENT CENTER
ARNOLD AIR FORCE STATION, TENNESSEE
AIR FORCE SYSTEMS COMMAND
UNITED STATES AIR FORCE

NOTICES

When U. S. Government drawings, specifications, or other data are used for any purpose other than a definitely related Government procurement operation, the Government thereby incurs no responsibility nor any obligation whatsoever, and the fact that the government may have formulated, furnished, or in any way supplied the said drawings, specifications, or other data, is not to be regarded by implication or otherwise, or in any manner licensing the holder or any other person or corporation, or conveying any rights or permission to manufacture, use, or sell any patented invention that may in any way be related thereto.

Qualified users may obtain copies of this report from the Defense Technical Information Center.

References to named commercial products in this report are not to be considered in any sense as an endorsement of the product by the United States Air Force or the Government.

This report has been reviewed by the Office of Public Affairs (PA) and is releasable to the National Technical Information Service (NTIS). At NTIS, it will be available to the general public, including foreign nations.

APPROVAL STATEMENT

This report has been reviewed and approved.

ROSS G. ROEPKE
Directorate of Technology
Deputy for Operations

Approved for publication:

FOR THE COMMANDER

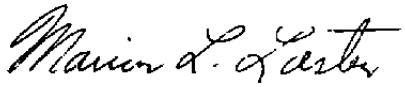

MARION L. LASTER
Director of Technology
Deputy for Operations

REPORT DOCUMENTATION PAGE		READ INSTRUCTIONS BEFORE COMPLETING FORM
1 REPORT NUMBER AEDC-TR-81-14	2 GOVT ACCESSION NO.	3 RECIPIENT'S CATALOG NUMBER
4 TITLE (and Subtitle) HIGH POWER MHD SYSTEM - FACILITY STATUS AND MAGNET TEST RESULTS		5 TYPE OF REPORT & PERIOD COVERED Final Report-July 1, 1977 - Sept. 30, 1980 6 PERFORMING ORG REPORT NUMBER
7 AUTHOR(s) G. L. Whitehead, ARO, Inc., a Sverdrup Corporation Company		8 CONTRACT OR GRANT NUMBER(s)
9 PERFORMING ORGANIZATION NAME AND ADDRESS Arnold Engineering Development Center/DOT Air Force Systems Command Arnold Air Force Station, TN 37389		10 PROGRAM ELEMENT, PROJECT, TASK AREA & WORK UNIT NUMBERS Program Element 62203F
11 CONTROLLING OFFICE NAME AND ADDRESS Arnold Engineering Development Center/DOS Air Force Systems Command Arnold Air Force Station, TN 37389		12 REPORT DATE February 1982 13 NUMBER OF PAGES 103
14 MONITORING AGENCY NAME & ADDRESS(if different from Controlling Office)		15 SECURITY CLASS. (of this report) UNCLASSIFIED 15a DECLASSIFICATION/DOWNGRADING SCHEDULE N/A

16 DISTRIBUTION STATEMENT (of this Report)

Approved for public release; distribution unlimited.

17 DISTRIBUTION STATEMENT (of the abstract entered in Block 20, if different from Report)

18 SUPPLEMENTARY NOTES

Available in Defense Technical Information Center (DTIC).

19 KEY WORDS (Continue on reverse side if necessary and identify by block number)

magnetohydrodynamic generators
magnet coils
hot gases
combustors
water cooling
oxidizers
test and evaluation

20 ABSTRACT (Continue on reverse side if necessary and identify by block number)

AEDC has been requested by the Aero Propulsion Laboratory to design, fabricate, and install facility hardware necessary to conduct tests to demonstrate the performance of high power MHD generator systems developed by AFWAL contractors. This report summarizes the AEDC effort since program inception, describes the facility under development, gives the status of each major facility component, and summarizes the results of the data acquired during

DD FORM 1 JAN 73 1473 EDITION OF 1 NOV 65 IS OBSOLETE

20. ABSTRACT (Continued)

magnet checkout tests. The report also describes the future effort required to make the facility a useful tool for MHD generator system and component development.

AFSC
Arnold AFS Tenn

PREFACE

The work reported herein was conducted by the Arnold Engineering Development Center (AEDC), Air Force Systems Command (AFSC), Arnold Air Force Station, Tennessee, under Program Element 62203F. The results were obtained by ARO, Inc., AEDC Group (a Sverdrup Corporation Company), during the period from July 1, 1977 to September 30, 1980. The manuscript was submitted for publication on July 6, 1981.

AEDC has been requested by the Aero Propulsion Laboratory (AFWAL), Wright-Patterson Air Force Base, Dayton, OH, to design, fabricate, and install facility hardware necessary to conduct tests to demonstrate the performance of high power MHD generator systems developed by AFWAL contractors. Funding limitations have temporarily halted the project and the only major facility component completed to the point of operational testing was the high field strength magnet. This report summarizes the AEDC effort since the program inception, describes the facility under development, gives the status of each major facility component, and summarizes the results of the data acquired during magnet checkout tests. The report also describes the future effort required to make the facility a useful tool for MHD generator system and component development.

CONTENTS

ILLUSTRATIONS

Figure | Page

Figure Page

TABLE

1.0 INTRODUCTION

For more than a decade the Aero Propulsion Laboratory (AFWAL) has maintained an interest in lightweight, compact, high power electrical systems for possible airborne applications. The magnetohydrodynamic (MHD) generator has been advocated as a prime candidate to fulfill that requirement, and significant effort has been expended to attain that goal. Reference 1 describes an initial effort to produce a nominal 1-MW device (Project BRILLIANT), and Ref. 2 describes the successful development of a submegawatt generator installed and operated at AFWAL. Those efforts were conducted in the late sixties and early seventies. Since that time, the original scope of the research has been expanded to include even higher power density generators at much higher power levels. Numerous studies have investigated the feasibility of these larger systems, resulting in the development of a set of operating parameters covering the range of interest and defining a typical development program (Ref. 3).

As a result, Arnold Engineering Development Center (AEDC) has been under contract since 1977 to design, fabricate, and install the facility hardware necessary to conduct tests to demonstrate the performance of high power MHD generator systems developed by AFWAL contractors. The facility includes a high field strength magnet and its power supply, an exhaust and scrubber system, a fuel and oxidizer system, facility utilities, and a data acquisition and control system. This report describes the work accomplished toward facility development since project inception and gives the present status of all major components. The only facility component completed to the point of operational checkout is the High Power Magnetohydrodynamic System (HPMS) magnet. The major emphasis of this report will be on the fabrication, assembly, installation, and testing of the HPMS magnet system. Although not part of the AEDC effort, the test articles will also be briefly discussed for the sake of completeness.

2.0 PROGRAM DESCRIPTION

2.1 PROJECT GOALS

The AFWAL HPMS project has as its objective the testing of an advanced MHD generator system operating into a single resistive load. The test articles consist of a liquid fueled high performance combustor/nozzle combination and a diagonal wall MHD generator channel/diffuser combination. The performance objectives of this system, when installed in the HPMS test facility, are shown in Table 1.

The first three listed parameters are the more critical because they demonstrate the design objectives. The remaining parameters, while important, are more operational in nature.

Although thermal efficiency is not a design requirement, a 10-percent enthalpy extraction is expected to be achieved.

2.2 AREAS OF RESPONSIBILITY

Four government agencies or contractor organizations have been involved in the attempt to meet the objectives given in Table 1 and to fulfill the overall program goals. The procuring and funding organization is AFWAL. Maxwell Labs, Inc. (MLI) served as prime contractor for the hot gas flow train with the Rocketdyne Division of Rockwell International as subcontractor. AEDC is under direct contract to AFWAL as the testing organization. The system under development is shown in Fig. 1.

2.2.1 Channel Development

As prime contractor for the design of the hot gas flow train, MLI was also chartered to develop the design of the channel/diffuser combination. The design of the generator channel is complete, but procurement of the channel hardware has not begun.

The existing design calls for a slant-wall channel in which the electrode frames are oriented approximately 40 deg to the flow direction in the active portion of the channel and undergo transition 90 deg to the flow direction at the channel ends, as shown in Fig. 2. The electrodes are supported in a molded fiberglass composite outer structure which acts as a pressure vessel to contain the static pressure during operation. Figure 3 presents an external view which also shows the water cooling manifolds.

The channel electrodes are constructed of oxygen-free high conductivity (OFHC) copper strips brazed into a trapezoidal window frame shape, with copper tubing brazed to the outside surfaces for water cooling. Inconel® inserts immersed in castable ceramic are used as current collectors. The channel is designed to operate supersonically in a tailored magnetic field with a peak field strength of 4 Tesla (T). The channel output will be dissipated into a single resistive load as indicated in Fig. 2. The pertinent channel parameters are in Table 2.

2.2.2 Combustor Development

The Rocketdyne Division of Rockwell International, under contract to MLI, developed the combustor. Design, fabrication, and shakedown testing have been completed at the Rocketdyne Santa Susana facility. Preliminary results of those tests have been published (Ref. 4) and indicate that combustor design requirements will be achieved.

The combustor provides a uniform flow of hot gas to the generator channel while minimizing energy losses caused by cooling and aerodynamics. The combustor is a high performance, liquid fuel, rocket-type combustor which uses JP-4 as the fuel and liquid oxygen (LOX) as the oxidizer. The design incorporates a rectangular combustion chamber to minimize flow nonuniformity to the rectangular MHD channel. The assembly consists of a water cooled combustion chamber, an injector, and a dual augmented spark ignition system. Methane and gaseous oxygen are used as reactants in the ignition system.

To make the resulting products of combustion an electrical conductor, cesium seed is added to the flow as CS_2CO_3 dissolved in water. The seed solution, approximately 72 percent cesium by weight, is stored in a separate tank and is injected into the fuel line before injection into the burner. Span-80, a hydrocarbon surfactant, is added to the JP-4 in a ratio of 7 percent by weight to improve dispersion of the seed solution as it is injected into the fuel mixture. Operating parameters of the combustion system are listed in Table 3.

The combustor, control system, and reactant feed systems are to be supplied for installation into the HPMS test facility. Figure 4 shows the combustor system and the control panels. The seed system is also to be supplied to AEDC and is shown in Fig. 5.

2.3 INTERFACE INFORMATION

The division of responsibilities among project participants has been controlled by various interface documents. An Interface Control Working Group (ICWG), consisting of one member from each organization and chaired by the Rocketdyne member, was organized to establish interfaces between subsystem elements subject to interface control, and to prepare a list of all interface items to use as a control document. The resulting document is the Interface Control Document, (ICD) Document No. MHD 2.2 IC (Ref. 5). This document establishes the specific requirements, rules, and operating methods for coordinating, documenting, and controlling physical and functional interface within the HPMS. The ICD also defines the system for generation, control, and change of documents that identify the physical, environmental, and functional interface requirements.

The test plan (Ref. 6) contains additional information on division of responsibilities and establishes operational sequences and procedures to be followed during testing of the HPMS system.

AEDC is responsible for defining physical interface limits within the test facility. The critical area is the test clear volume in or near the magnet; test clear volume has been

designated as shown in Figs. 6, 7, and 8. The zero point is located at the nominal magnet entrance centerline. Contractor-supplied components must comply with the dimensions shown in the figures previously mentioned.

3.0 AEDC PROJECT DESCRIPTION

3.1 FACILITY DEVELOPMENT

The original scope of the AEDC HPMS project included the development of a test facility to test complete systems or given system components developed by AFWAL contractors. This included modification of existing test hardware, and design, fabrication, and installation of new hardware to accomplish that objective. The initial concept for the facility was oriented toward the HPMS flow train under development in 1977. As previously noted, this flow train consisted of a combustor/nozzle combination and a channel/ diffuser combination to be supplied as test articles. The test facility itself consisted of a fuel and oxidizer system, an exhaust and scrubber system, a high field strength electromagnet, and the ancillary equipment necessary to support these systems. Delay in the HPMS project resulted in a postponement of facility completion. A detailed description of the facility and development status is presented in Section 4.0.

3.2 HPMS MAGNET SYSTEM

The delay in the HPMS effort resulted in a reduction in the scope of the AEDC effort. In FY78, the effort was reduced to procurement, installation, and checkout of the magnet system, which has been completed. The magnet system is described briefly in Section 4.0, and the detailed design, fabrication, and installation information, along with the magnet test results, is presented in later sections. The magnet test was the final scheduled effort on the AFWAL project. No effort is scheduled for FY81, and the project is scheduled to resume in FY82.

4.0 DESCRIPTION OF TEST FACILITY

4.1 TEST FACILITY LAYOUT

The HPMS Test Facility is located in the High Temperature Laboratory (HTL) of the Propulsion Wind Tunnel Facility (PWT). The layout of the facility is shown in Fig. 9. Note that the LOX system is located near the test unit, eliminating the piping of high pressure LOX through any congested area. The fuel system is located along the west side of the fenced area, as far as it can conveniently be located from the oxidizer system.

4.2 FACILITY COMPONENTS

4.2.1 Liquid Oxygen System

The LOX supply system includes tanks, piping, valves, and controls required to deliver it to the HPMS combustor. The entire LOX and fuel system was moved, essentially intact, from an adjacent wind tunnel and installed at the HTL.

Two high-pressure stainless steel uninsulated run tanks are used for pressurizing the LOX for injection into the combustor. Each tank has a volume of 2.43 cum (86 cu ft), of which 0.28 cum (10 cu ft) is for ullage. The tanks are 304 stainless steel and are ASME code rated for 122.5 atm (1,800 psi) for a temperature range from 311°K (100°F) to 88°K (-300°F). The inlet gas nozzle for tank pressurization is equipped with a diffuser to prevent impingement of the nitrogen gas on the liquid oxygen surface.

The tanks are equipped with relief valves, rupture discs, and automatic electrically operated vent valves to limit the tank pressure to a selected value below the tank rating. The tanks are also instrumented to supply local and remote indications of tank pressure and LOX level. The tank vents and relief devices are manifolded into a 15-m (50-ft) high vent stack to eliminate the release of oxygen at ground level.

The LOX tanks are pressurized by a nitrogen pressure control system supplied from High Performance Demonstration Experiment (HPDE) nitrogen/oxygen storage tanks which can be pressurized to 150 atm (2,200 psi). The nitrogen supply gas is filtered by parallel 40 μ rated filters. The nitrogen pressure is controlled by four large capacity dome-type regulators manifolded in parallel and equipped with remotely-operated pressure loaders to set the regulator dome pressure. The LOX tank nitrogen pressurization manifold is equipped with shutoff valves, relief valves, vent valves, and remote pressure indicating devices. The nitrogen pressure control system will also automatically shut off the supply of nitrogen gas into the LOX tanks if the maximum safe tank pressure is exceeded. The nitrogen pressure control system is designed for a nitrogen flow rate of 1,275 scmm (45,000 scfm) at 122 atm (1,800 psi) to the run tanks if the storage tank pressure is above 136 atm (2,000 psi). This nitrogen flow rate should provide for LOX flow rates up to 36.4 kg/sec (80 lb/sec). Present maximum design requirements are for a flow rate of 26 kg/sec (57.2 lb/sec).

The liquid oxygen is supplied from the run tanks by a manifold consisting of 7.62-cm (3-in.) pipe and shutoff valves. A similar pipeline with vents and pressure relief devices completes the connections to the combustor located approximately 25 m from the LOX run tanks.

Design of the oxidizer system is complete and system installation is approximately 75-percent complete. The piping and tanks have been installed and cleaned except for the line between the run tank manifold and the combustor. The vent line has been fabricated but not installed. Installation of control wiring and pneumatic and instrument tubing for the instrumentation and control valves has not been completed. The LOX system will be completed upon resumption of the HPMS project, now scheduled for FY82. The LOX system is shown in Fig. 10a, and the partially installed system is pictured in Fig. 10b.

4.2.2 JP-4 Fuel System

The fuel system provides filtered, metered, conditioned fuel at a nominal flow rate of 6.8 kg/sec (15 lb/sec) at a pressure of 122.5 atm (1,800 psi). The liquid fuel supply system includes a run tank, piping, valves, and controls to supply JP-4 fuel at the required pressure and flow rate.

One high pressure stainless steel run tank is used to supply the fuel for the combustor. The tank is identical to the liquid oxygen tanks except the code rated temperature is 311°K (100°F). The tank is also equipped with the same type pressure protection devices.

The fuel tank is pressurized with gaseous nitrogen to obtain the pressure and flow rates required by the combustor. The nitrogen pressurization is similar to the LOX system except that the nitrogen flow rate is much lower since the nitrogen will remain essentially at ambient temperature. The single small dome-type pressure regulator will supply approximately 78 scmm (2,750 scfm) at 109 atm (1,600 psi) from the Propulsion Wind Tunnel (16S) nitrogen storage unit, which can deliver nitrogen gas up to 150 atm (2,200 psi). This nitrogen flow rate should provide for fuel flow rate up to a maximum of 10 kg/sec (22 lb/sec) to the combustor. The system is shown in Fig. 11a and as installed in Fig. 11b.

The fuel is supplied to the combustor located approximately 40 m from the fuel tank by a 7.62-cm (3-in.) pipeline with a shutoff valve at the end of the line near the combustor.

The fuel system design is complete, and all piping except the tank vent has been installed. The wiring and tubing for the instrumentation and control valves have not been installed. The fuel system can be completed with minimal effort upon project resumption.

4.2.3 Load Bank

The existing load bank which will be used to dissipate the HPMS generator output consists of a series of stainless steel tubes mounted between supply and discharge water

manifolds. Each tube has an effective length of 18 ft, and is constructed of thin-wall 304 stainless steel isolated at either end by reinforced flexible hose, with the flexible hose connected to an 8-in. water supply and discharge line. Table 4 lists the various tube sizes and capacities which comprise the load bank. The current ratings in the table assume a ΔT of 55°K (100°F) at a pressure differential of 24 atm (350 psid). The system was originally designed for 12,000 VDC, but it has been upgraded and tested to 15,000 VDC with cooling water supplied from the 15,000 gpm raw water pump. When operated at design condition, the ballast tubes are capable of continuous operation. In reality, the system is limited to 15 min because of the pump.

The maximum resistance of a given tube is determined from its size and length. However, sliding connectors provided on each tube lower the resistance at the sacrifice of the amount of power which can be dissipated in that tube. The tubes can be connected in series, parallel, or some combination of both to achieve essentially any desired resistance up to 160 ohm. A ballast terminal board is used to patch between the various sets of tubes, and once a given resistance range is determined and the proper connections are made at the tubes, most wiring can be accomplished at the terminal board.

A second load bank consisting of 730 individually insulated liquid rheostats is also located at the HTL Building. Each rheostat is designed to dissipate 90 kw at a resistance up to 40 ohm, with less than a 10-percent change in resistance for 15 sec of run time at the design condition. The total capability is 66 MW for 15 sec, with progressively longer times at lower power levels. The individual rheostats can be connected in parallel or series and were designed as the resistive load for an MHD generator operating in the segmented Faraday mode. The load bank is designed to use a standard configuration consisting of a rectangular plastic container, two copper plates with variable separation capability, inlet and discharge water piping, and appropriate plate supports and electrical connections. The mechanical mounting is designed so the resistance can be varied by changing the plate spacing, thus providing a linear relationship between resistance and plate position.

4.2.4 Data Acquisition

The data system uses a DEC PDP 11/50 computer for data acquisition and an IBM 370 for bulk data reductions and processing, as shown in Fig. 12. Instrumentation readings from the 200 planned channels of pressure, flow rate, temperature, voltage, current, and magnetic flux data will be transferred to magnetic tape by the acquisition computer at a scan rate of fifty samples of each instrumentation item per second. From this tape, the reduction program will convert the data into engineering units for each scan and create an engineering unit data file. Average data points consisting of a specified number of scans are normally

calculated to provide some smoothing and then printed for engineering analysis and permanent record. From the data file, the data can be used with a sophisticated interactive graphics routine to generate data plots of any measured parameter versus any other parameter of User-selected scale. This option is used extensively to study performance transients on the HPDE tests and to analyze the distribution of measured parameters. The data can also be corrected and reprinted in the interactive mode.

4.2.5 HPMS Magnet

The HPMS magnet is a high field strength, iron frame electromagnet designed to produce a peak magnetic field of 4 T when it operates with an input power of 17.5 MW. The design is such that 4.5 T can be achieved, if required, by increasing the power level to 23 MW. A detailed description of the magnet and its capabilities is presented in Section 5.0.

4.2.6 Peripheral Facility Hardware

In addition to the major system components, general items of support equipment which will be required for HPMS operation are located in the HTL Building. A 27-MW power supply will provide 17,000 amp to the magnet coils. Cooling to the stainless steel load bank tubes, the magnet coils, and other system components is supplied by a 2,000-hp pump which can deliver 6,000 gpm of raw water at high pressure on a continuous basis, or 15,000 gpm for 5 min duration. A demineralized water system supplies 1,300 gpm of filtered demineralized water at 55 atm (800 psi). Other utilities, such as low-pressure raw water and various a-c and d-c power supplies, are installed and are available to support the HPMS facility.

The exhaust system will diffuse the high velocity plasma exiting from the generator channel, turn it 90 deg, and vent it to the atmosphere. In the process, cooling water spray banks will cool the flow and scrub out the cesium seed to reduce the expelled pollutants to an acceptable level.

5.0 HPMS MAGNET SYSTEM

5.1 MAGNET DESCRIPTION

The HPMS magnet is a high field strength, iron frame, water cooled electromagnet designed to produce the centerline axial magnetic field strength distribution shown in Fig. 13. The magnet was designed and the coils were fabricated by the Magnetic Corporation of

America (MCA) in Waltham, Massachusetts. The magnet iron and force containment structures were designed by MCA and fabricated at AEDC. Final assembly of the magnet was also performed at AEDC.

The magnet coils are square, hollow, copper conductor, of epoxy impregnated construction. Four coils were fabricated as two nested pairs. The coils were numbered 1 through 4, with coils 1 and 2 being inner coils and coils 3 and 4 being outer coils.

Coils 1 and 3 and coils 2 and 4 each make a nested pair. Each coil is made up of three two-layer pancakes, epoxy impregnated into a single construction. Single-turn water cooling is employed throughout. A summary of operating characteristics is given in Table 5 and the magnet mechanical and hydraulic design parameters are given in Tables 6 and 7.

5.2 COIL FABRICATION

As previously noted, the magnet coils were designed and fabricated by MCA with design criteria supplied by AEDC. The primary criterion was to produce the field strength profile shown in Fig. 13 with a set of coils capable of continuous operation. The high input power required to achieve the high field levels precluded the use of single path water cooling, which means that each coil turn had to be individually cooled. This required coil fabrication which would permit installation of water cooling tubes in each coil turn. As a result, each coil was made up of three two-layer pancakes. Water blocks and cooling tubes were then installed on each side of the pancakes before assembly as a single coil.

Each pancake was wound with a continuous copper conductor with the stipulation that no conductor joint be located in a high stress region or in a location which would require the joint to be bent during winding (in the saddle region, for example). Scarf joints were used throughout except for the pancake crossover turn which is discussed later. A typical scarf joint is shown in Fig. 14. Each joint was fabricated by torch brazing using a fluxless brazing alloy (Phoson 15, 15-percent Ag). Sample joints were made and tested prior to initiating winding of the coil.

A fairly complex coil geometry was required to meet all design considerations. The configuration designed to achieve the rapid rise to the high peak field, followed by a step decreasing gradient along the bore, is shown in Fig. 15. Although not a standard saddle configuration, the coils were wound on a fixture very similar to that normally used for saddle coils. One of the coils is shown in Fig. 16 as it appeared after removal from the winding fixture. Also shown is a portion of another coil with water blocks and cooling tubes partially installed.

Electrical and mechanical checks were made on a continuing basis during coil winding and assembly. Electrical tests were made on each brazed joint to ensure that the electrical resistance of a short specimen containing the joint was essentially equal to an equal specimen of the parent conductor. Flow blockage was also checked by passing a ball through the conductor to ensure that no blockage was created at the joint. In addition, all cooling passages were flow tested individually after fabrication. The criterion specified was that the flow for any individual cooling passage with a water pressure differential of 0.045 atm/m not differ from the average of all passages in the coil by more than 10 percent.

All coils were also hydrostatically tested to 55 atm, which is 1.5 times the maximum anticipated operating pressure in the coil.

After winding and installation of the water cooling tubes, each coil was sandblasted, cleaned, and the insulation was handwrapped. Figure 17 shows one pancake separated for installation of turn-to-turn insulation.

Note that the two-layer pancake has been separated into single layers for applying the insulation. A first attempt was made to apply the turn-to-turn insulation without separating the pancakes, but that proved to be too tedious and time-consuming. Separation of the individual pancakes required cutting the crossover coil (see Fig. 16). That had to be respliced and it was that joint which was the exception to the scarf joint requirement. Because that particular location is a low stress region and it is also extremely difficult to produce a reliable scarf joint there, a standard butt joint was used instead. The butt joint was produced exactly like the scarf joint in Fig. 14 except the cut is perpendicular to the conductor, and a ferrule of only 2.54 cm was required. The butt joints were subjected to the same tests as the scarf joints.

After applying the turn-to-turn insulation, resplicing into a single pancake, and insulating the spliced area, the pancakes were stacked to form a single coil. The electrical connections between pancakes were designed to be made external to the coil, so no interpancake connections were required before coil impregnation. Figure 18 shows two pancakes after installation of turn-to-turn insulation.

As the insulated pancakes were stacked into a final unit, phenolic spacers were installed to fill the voids near the water blocks and to prevent the water blocks from being heavily loaded under the magnetic loads which exist during operation. A final ground wrap was also applied at this point. Figure 19 shows the coils as the final ground wrap is being applied.

A fiberglass reinforced laminate was installed in each saddle region to distribute the load on the coils as they act upon the force containment structure (FCS) during operation. One of those installations is shown in Fig. 19. Note that the laminate is designed to be contained inside the final ground wrap. The voids within the end blocks were filled with shredded fiberglass as shown in Fig. 20.

After the final ground wrap was installed, each coil was "cocooned" or vacuum bagged in preparation for impregnation. One coil in that stage is shown in Fig. 21. The coils were then placed as a nested pair into a sizing fixture for final sizing before impregnation. The final impregnation was performed by vacuum pumping from one end of the coil while pouring the liquid epoxy into the other end. Both connections can be seen in Fig. 21. The epoxy seal used with the HPMS coils, as well as a full materials list, is given in Table 8.

Although both coils of a nested pair were installed in the sizing fixture for accurate nesting, the coils were impregnated one at a time. The time required for the epoxy to saturate a given coil completely was such that the hardening process would begin before two coils could be completely saturated.

After each coil was completely saturated, the entire sizing fixture was placed in an oven for final curing. The nested coils in the sizing fixture ready for impregnation are shown in Fig. 22, and Fig. 23 shows a single coil after impregnation and removal from the sizing fixture. After the coil was removed from the sizing fixture, the excess epoxy was removed, the coils were painted with varnish, the power connections were made, and the water fittings were installed on the cooling tubes. The completed coils were then shipped to AEDC for final magnet assembly. The completed coils, as received, are shown in Figs. 24 and 25.

Significant difficulties were experienced during fabrication of the HPMS coils. Electrical checks performed as fabrication progressed revealed numerous turn-to-turn electrical shorts which required correction before proceeding. In general, these shorts were located in the end turn regions and usually developed after the coils were placed in the sizing fixture. The coils were subjected to high loads as they were being clamped to conform to their final configuration, resulting in the insulation being crushed in some locations. Shorts were also caused by the plate in the sizing fixture which maintains the proper divergent angle. In each case, the coils had to be removed from the sizing fixture for repair.

The continued difficulty with these shorts finally led to installation of additional tape in the end turn regions and other areas which were subject to high stress. Perforated Mylar® tape was also used between turns in the high stress areas. The outer coils experienced the most shorting and one of those (Coil No. 3) had to be completely disassembled for reinsulation.

The electrical shorts were detected by sensitive resistive measurements and coil ringing tests (or Q tests). The Q tests involved applying a capacitive discharge to the coil and observing the voltage decay with an oscilloscope. Figure 26 is a photograph of the results of such a test. The top figure shows the standard decay with a nonshorted coil, with a superimposed decay trace using one intentionally shorted turn, and finally with two intentionally shorted turns. The bottom figure is a trace of the voltage decay with two intentionally shorted turns. A shorted turn has marked effect on the voltage decay. In the case shown, the turns were intentionally shorted, which would simulate a dead short between turns. In the case of a high resistance short, there is less effect on the voltage decay and the test results require some engineering evaluation. In other words, the capacitive discharge test is adequate to detect a dead or low resistance short, but this test method becomes questionable for a high resistance short.

Another difficulty was experienced with a shorted turn after impregnation. Electrical tests were performed after Coil No. 4 was installed in the sizing fixture just before impregnation. The checks did not indicate any discrepancy. After the coil was impregnated and removed from the sizing fixture, however, additional checks indicated a shorted turn. The difficulty was apparently the result of the premature hardening of the epoxy resin as the coil was being impregnated. That resulted in a failure to achieve complete saturation, and the coil moved when the sizing fixture clamps were released. Attempts to repair the coil without removal of the epoxy were unsuccessful. Furthermore, no solvent could be located to effectively strip the coils of the epoxy. Coil separation was finally achieved by wrapping the coil in foil to prevent flaming of the epoxy, placing it in the oven, and gradually raising the oven temperature to 750°K (≈ 900°F) for 36 hrs. The epoxy was completely charred, allowing coil separation for cleaning. The coils were cleaned, sandblasted, reinsulated, reassembled, and finally impregnated for the second time.

The high temperature required to bake off the epoxy raised some doubts about having compromised the integrity of the brazed joints in Coil No. 4. As a result, eight sample joints were fabricated, heated to a temperature higher than that used for burning away the insulation, and subjected to tensile pull tests to determine the degradation in joint strength. The results of those tests are shown in Fig. 27. The data indicate that the integrity of the joints was not compromised. In fact, very little degradation occurred until the sample joints were exposed to a temperature within 50°K of the published melting temperature of the brazing alloy. MCA was therefore given permission to reuse the existing coil.

Acceptance tests were made on all coils after delivery to AEDC. No discrepancies were revealed during the electrical checks.

5.3 MAGNET IRON FABRICATION

The magnet iron was designed by MCA, with inputs from AEDC. The force containment structures were similarly designed. The cooling water manifolds were designed at AEDC in accordance with required coil cooling connections. Fabrication of those components, as well as fabrication of the coil divergence spacers, was performed at AEDC.

The magnet iron was fabricated by modifying the iron frame from an existing magnet (originally designed for a 20-MW accelerator). Although extensive modifications were required, the modification was essentially straightforward torch cutting, machining, and rewelding. Each half of the magnet iron is supported by four casters so the magnet can be separated along the centerplane and rolled back for ease of channel installation or other operations. The original magnet steel is shown in Fig. 28 and the modified return frame is shown in Fig. 29.

The force containment structures are massive welded steel beams designed to contain the magnetic loads generated by the coils during operation. The primary FCS beams contain the axial forces which tend to straighten the saddle coils; the smaller composite beams are designed to contain the transverse forces which attempt to force the saddle end turns into a circle. The axial force containment structures are shown in Fig. 30 before final cleaning and painting. The end turn FCS beams are shown in Fig. 31 with all fabrication complete except cleaning and painting. Also shown are the aluminum attractive load spacers which are installed in the divergent areas of the coils to maintain the proper divergence angle and to support the attractive loads on the coils during operation. The only other items fabricated at AEDC were the water cooling manifolds which are shown in Fig. 32.

5.4 MAGNET ASSEMBLY

Final assembly of the HPMS magnet was performed at AEDC. As previously noted, the magnet was designed to separate along the centerplane, permitting independent assembly of each magnet half. Assembly was accomplished by placing the magnet steel on its side so the coils could be lowered horizontally onto the magnet steel. Delrin® sheets were placed between the coils and the steel to prevent direct contact of the coils with the metal and to provide a slip plane for coil movements. The inner coils were placed on the steel and properly positioned, and then the outer coils were lowered onto the inner coil. Proper positioning of the coils was critical to the assembly, and precaution was taken to achieve accurate placement. The aluminum attractive load spacers were then installed and the gap between the coils and spacer was measured. The spacers were then removed and the gap was filled with fiberglass-reinforced silicone rubber of 70 durometer hardness. This prevents the

coil from making direct contact with the metal surfaces, avoiding possible abrasive rubbing as the coil attempts to move during operation. The rubber also provides some cushion to allow some slight coil movement, and its hardness does not allow excessive movement. This is discussed in more detail later.

With the attractive load spacers in place, the axial force containment trial fit was initiated. During the acceptance inspection of the coils, it was determined that the specified dimensional tolerances for the coils had not been met. This was further confirmed by measurements taken during placement of the coils. The trial fit of the force containment structure was necessary to ascertain the corrective action required to overcome the dimensional discrepancies. The overall length of the coils was longer than designed and the coil saddle face was irregular. This complicated the assembly process significantly and required corrective action as discussed below.

The magnet coils were designed so the coil saddle face would be parallel to the face of the magnet iron. With that design the axial FCS could be installed parallel to the magnet iron and uniformly support the coil forces. The FCS beams are mounted to the magnet iron by six 5.08-cm-diam threaded rods. The beams are properly spaced from the iron by six "thick-wall" pipe segments which also support the preload on the threaded rods. Assembly procedures called for installing a sheet of fiberglass-reinforced silicone rubber on the FCS, measuring the amount of extension of the coil beyond the magnet iron face, and machining the spacers so the rubber sheet would be uniformly compressed by 0.080 cm when the specified preload was applied to the threaded rods. The dimensional nonuniformity of the saddle face prevented assembly in that fashion. Furthermore, the preload cylinders had been precut to approximate length and the excessive extension of the coils resulted in some of the cylinders being too short. Additional doughnut spacers were fabricated to achieve proper length. The dimensional nonuniformity can be seen in Figs. 33 and 34. As can be seen, the gap between the coils and the FCS varies significantly.

The coil nonuniformity caused a similar problem between the inner coil and outer coil saddle region. The coils were designed for placement of phenolic spacer boards in the void between the coils in the saddle region to prevent the inner coil from bending under the magnetic load during operation. The irregularity in the coil dimensions made it impossible to install a phenolic spacer board to support the inner coils uniformly. The irregularities can be seen in Figs. 35 and 36.

To circumvent the difficulty with the dimensional irregularity and to assure that the coils would be uniformly supported, a castable epoxy was poured in the void between coils and in

the void between the outer coil and the FCS. Ren® 1710 epoxy was selected because of its high strength and rapid cure characteristics.

Final installation of the axial FCS was accomplished by mounting the FCS at a uniform distance from the iron face (resulting in nonuniform voids between coil and FCS) and tightening the bolts to the specified preload value before filling the voids. After the FCS was properly mounted, the two-part epoxy was mixed, shredded fiberglass was added to the mixture to increase its final cured strength, and the voids were filled with the mixture. This method ensures that the coils will be uniformly supported and that very little initial movement will result when the coils are energized. Compression of the rubber sheet will allow the slight increase in coil length as the coils grow thermally. Figure 37 shows the saddle region after pouring of the epoxy.

After installation of the axial force containment structure, the tranverse FCS beams were installed. These beams span from the side of the magnet iron to the flange on the axial FCS beams, across the coil end turns. The coil nonuniformity in that region also required the use of the Ren epoxy mixture. Figure 38 shows one of those beams installed and also shows the spacers or preload cylinders as installed. The epoxy filler can also be seen between the coils and between the coils and FCS. The black rubber shown was used as a dam for pouring the epoxy and was later removed. The two magnet halves, after assembly, are shown in Fig. 39.

5.5 MAGNET INSTALLATION

The magnet halves were moved separately to the HTL Building, the V-groove casters were installed, and the magnet was set in place on the previously installed track. Final connections were then made to the cooling water supply lines and to the power bus. Figure 40 shows a portion of these connections. Final hookup between the water manifolds and the individual coil coolant tubes was then made as shown in Fig. 41, completing the magnet installation. A closeup of the cooling connections, the power connections, and the interpancake electrical connections is shown in Fig. 42.

Very little difficulty was experienced in the magnet installation phase until final hydrostatic testing of the cooling system was attempted. That test revealed numerous leaks where the water fittings were attached to the coil coolant tubes. Repair of those leaks was very tedious and time-consuming. The fittings were a swage-type fitting; a flared fitting or sweat joint should be considered for future magnets of this type.

6.0 MAGNET CHECKOUT

6.1 PRETEST PREPARATION

Extensive tests were made to determine the integrity of the installed magnet before operation. The integrity of the electrical isolation was of paramount concern since the power dissipated at a field strength of 4 T is about 17 MW, and at 4.5 T is above 24 MW. High voltage tests were from coil to coil and from coil to ground, with and without cooling water flowing. With cooling water flowing, the resistance to ground was calculated from current leakage rates to be 15,000 ohm. That value was found to be consistent with the resistance calculation based on the measured conductivity of the raw water. There are 348 parallel paths to ground through the water flowing in the flexible hoses, which means that each path has a resistance of approximately 5 MΩ. Assuming the maximum open circuit voltage of 2,800 v from the magnet power supply, the current leakage through all paths would be less than 200 ma.

The HPMS coils are connected in series, which means that the total current flows through each magnet turn. This also means that the voltage drop per turn is quite low. There are 348 turns, so the voltage differential between turns is only 8 v, assuming a maximum open circuit voltage of 2,800 v. Since the magnet power supply is ungrounded, the positive bus can float between 0 and- 2,800 v and the negative bus can float between 0 and -2,800 v. The coil-to-ground voltage could then be as much as 2,800 v at some point in the coil. To limit this value, the center tap of the magnet coils was grounded through a high resistance ground. This ensures that the center tap of the coil will remain at ground potential, thereby limiting the positive bus to no more than 1,400 v and the negative bus to a minimum of -1,400 v. The maximum differential voltage to ground is thus limited to no more than 1,400 v. The centertap circuit also serves as a ground fault detection circuit. If a fault to ground occurs, the grounded center tap would provide the path to complete the circuit back to the floating power supply. A current sensor is installed in that circuit with a 0.5-amp trip limit. If a current in excess of 0.5 amp flows in that circuit, a relay furnishes a signal to the computer to automatically trip the power supply circuit breaker.

A second computer interlock limits the maximum current flow from the power supply. A predetermined maximum current value is input to the computer before each run. If the total current from the power supply exceeds the set point for four consecutive data scans ($\approx$ 80 msec), the computer automatically trips the circuit breaker. The limit is normally set at 500 amp above the anticipated current on each run.

An accurate resistance check of each coil pancake was made to determine if internal coil shorts were present. Each pancake was measured individually, then a measurement was

made across the entire coil to verify that the sum of the individual resistances was equal to the total resistance. This was performed for all four coils and no discrepancies were noted. Total magnet resistance at room temperature was found to be 0.00998 ohms.

A phasing test was conducted to ensure that each pancake had been would properly and to ensure that all interpancake connections had been made properly. A constant current power supply was connected between the positive bus and the first magnet pancake. With a constant 5-amp current flowing in that one pancake, the magnetic field strength was measured with a sensitive low range gaussmeter. With the gaussmeter in a fixed position, the electrical connection was changed to include two pancakes, thereby doubling the number of ampere-turns generating the magnetic field. The strength was again measured to ensure that the field strength increased. The procedure was continued until all pancakes had been added to the circuit one at a time. A decrease in field strength after including an additional pancake would indicate a reversed electrical connection with current flowing in a direction opposite to that desired. A failure to increase in field strength after adding an additional pancake would indicate an internal short. The phasing test indicated no discrepancy, with the field strength rising almost uniformly with addition of each succeeding pancake.

Finally, high pressure water flow was established and allowed to flow for some time to ensure that no water leaks had developed at the water fitting connections. Although no quantitative measurement could be made, care was exercised to ensure that cooling water was flowing in each magnet turn by grasping each flexible hose to feel the water flow.

The original magnet design called for mounting 48 Klixon® thermostats to selected cooling tubes. These thermostats were to be interlocked to trip the magnet power supply if any of the selected cooling tubes exceeded the 350°K allowable temperature limit. However, the thermostats had a published voltage insulation rating of 1,200 v and, as a precaution, some were tested to failure. Electrical breakdown occurred at under 2,000 v on some of the sample thermostats. This led to concern that installation of these thermostats could compromise the electrical integrity of the system and it was decided to delete the thermostats and rely on the water temperature measurements in the supply and discharge manifolds.

6.2 INSTRUMENTATION

Instrumentation for the magnet checkout consisted of cooling water supply and discharge pressure and temperature, magnet current and voltage, Hall probes, and Hall probe current supply. Pressure transducers were installed in each water manifold to measure the pressure drop across the coils. Thermocouples were similarly installed to determine the temperature rise of the water flowing through the coils. The magnetic field probes were the

primary instrumentation for the test. Six probes were installed along the axial centerline, and an additional eight probes were installed to map the field strength distribution at a given axial location. Figure 43 shows the location of the installed probes. Location C is the point of maximum field strength down the bore, and the bulk of the distribution data was acquired at that location. Probe support fixtures were fabricated to obtain distribution measurements at Locations B and E in addition to Location C. Figure 44 shows the installation of the magnetic field strength probes with the uniformity grid installed at Location C.

F. W. Bell Model BHT-900 probes were used to obtain the data during this test. The probe calibrations are linear to within one-half of one percent up to 3 T. Calibration data were not available above 3 T, but the manufacturer estimated no more than one percent deviation up to 4.5 T (the capability of the HPMS magnet). A 100-ma constant current must be supplied to the probes, and these currents were monitored throughout the test to ensure that no current drift occurred.

Data were acquired with the DEC PDP 11/50 computer. Real time display of the cooling water pressures, water temperatures, magnet current and voltage, and the centerline magnet field strength at Location C were used to monitor test conditions.

6.3 MAGNET OPERATION

Magnet checkout was performed in late FY80. The first application of power was essentially a check for electrical integrity at minimum voltage and currents; successive runs increased voltage and current in discrete increments. The operating characteristics of the magnet power supply are such that not all desired operating points are achievable. The minimum open circuit voltage is 1,400 v and the maximum is 2,800 v. Open circuit voltage is controlled by a tap changer whose tap changing under load capability allows the voltage to be varied without interruption in 33 discrete increments from 1,400 v to 2,800 v. Maximum current (short circuit) varies from 25,000 amp to 41,000 amp, depending on the tap setting. The actual operating point depends on the tap setting and the load impedance. Figure 45 shows the operating characteristics if operating into a purely resistive load. The operating line for the HPMS magnet ($\approx$ 0.10 ohm) is also shown in the figure.

To expand the operating envelope of the power supply, external reactance can be installed to reduce the current flow at a given power supply tap setting. The present system allows prerun insertion of seventeen different reactance values by proper configuration of the reactor bank. Each configuration is also denoted as a reactor tap setting. Unlike the open circuit voltage, the reactance values cannot be changed remotely during a run. The

power supply operating characteristics, including reactance, are shown in Fig. 46. For clarity, only three reactance values are shown but those shown cover the entire operating envelope. The HPMS load line is also shown in the figure.

Minimum voltage and minimum current were desired for initial operation of the magnet. That condition is incompatible with the operating characteristics of the power supply. As shown in Fig. 47, the magnet resistance is such that the load line falls below the power supply crossover point when reactance is installed in the circuit. The minimum voltage setting in that case gives the maximum current value. Figure 47 shows that a steady-state current of 6,400 amp would flow with a Tap No. 1 power supply setting. The lowest voltage was desired, so the first run was made with maximum reactance on Tap 1, and the computer interlock was set at 2,000 amp maximum current.

After all prerun operational checks were completed, the first run was performed as described above. The run duration was approximately 1 sec, at which time the magnet current had reached 2,000 amp and the computer terminated the run as anticipated. During the run, personnel outside the evacuation limits observed the magnet. The operation was also monitored by television inside the control room, and video recordings were made of each run.

After close inspection of the magnet revealed no indication of faults, a second run was made at the identical setting, except the current limit was raised to 4,000 amp, which is the minimum steady current for the HPMS system at any combination of settings (as shown in Fig. 47). The second run was also properly terminated at 4,000 amp by the computer. The third run was identical to Runs 1 and 2 except that the open circuit voltage was increased to 2,100 v (Tap 17) which would have resulted in a steady-state current of 5,300 amp. The computer properly terminated the run at 4,000 amp. Run 4 was identical to Run 3 except the open circuit voltage was increased to 2,800 v (Tap 33). Again the computer properly terminated the run. No electrical or mechanical difficulties were noted.

After the sequence, the current limit was increased to 4,200 amp to prevent the computer from tripping the power supply, and Run 5 was conducted with the same setup as Run 4. The magnet was allowed to reach steady-state current of just over 4,000 amp, and it was operated for approximately 1 min, thereby allowing the system to reach total equilibrium. The magnet current reaches equilibrium in some 4 to 5 sec, but thermal equilibrium requires 15 to 20 sec.

Run 6 was identical to Run 5 at its inception. The magnet was powered and allowed to equilibrate at 4,000 amp. After coming to equilibrium, the tap changer was reduced to Tap

17, allowed to equilibrate, and then started toward Tap 1. The run was terminated at 88 sec when a metal shield in the building began to be pulled toward the magnet. Run 7 picked up where Run 6 was stopped. The magnet was brought on at Tap 17 and allowed to equilibrate; the tap setting was decreased to Tap 1 and allowed to reach steady state. The run was manually terminated at 76 sec after reaching a steady-state value of 6,400 amp.

Before Run 8 the reactor bank was reconfigured to Configuration 10 (3.62-ohm reactance). The run was initiated with a tap setting of 33, came to a steady-state value of 6,400 amp, and was then incrementally increased to 8,400 amp, maximum current for that configuration. The run was manually terminated at 105 sec.

The reactor bank was reconfigured to Configuration 8 before Run 9. The magnet was brought up to 8,300 amp (Tap 33) and allowed to equilibrate. The tap setting was then lowered in increments until the computer terminated the run at 84 sec at the preset current limit of 10,000 amp.

Finally, all reactance was removed, leaving the power supply with operating characteristics as shown in Fig. 45. With this configuration, the load line falls above the crossover point and the minimum voltage also gives the minimum current. When Run 10 was initiated at a Tap 1 setting, the current came to steady state at 11,500 amp. Just as steady state was being achieved, the magnetic field again began to move a metal shield in the building and the run was terminated at 9 sec.

Run 11 was identical in configuration to Run 10 except the grid measurement system was stationed at Location B. The run was initiated using a Tap 1 setting, came to steady state at 11,500 amp, and the current was incrementally increased to 12,100 amp. Just as the run was being manually terminated at 49 sec, two water cooling tubes arced together, creating a turn-to-turn short in the lower east coil quadrant. Some shrinkable tubing was burned away, but no permanent damage of any type was sustained. The fault was the result of vibration of the flexible cooling lines at the relatively high water flow velocity ($\approx$ 5 m/sec). The movement was transmitted to the closely-packed copper cooling tubes on the coils. The cooling tubes and the bulky water fittings were insulated with shrinkable tubing, but the weight of the water in the cooling lines had apparently caused one tube to sag against another, and the vibration between the two water fittings had rubbed through the shrinkable tube, causing metal-to-metal contact. Inspection revealed that the contact was slight, giving a relatively high resistance short (much greater than the 0.00028 ohm of a single turn), which means that most of the current continued to flow through the coil. Much greater damage would have been sustained with a dead short. The fact that the run was being terminated manually at the time of failure also limited the damage.

One other run had been planned for the test sequence, with the intention of increasing the current until a peak field strength of 4 T was achieved (≈ 13,000 amp). Repair of the damaged area would have been minimal, but since a potential problem had been identified, there was considerable concern that a similar problem would develop at other locations. In view of the amount of data already acquired, it was deemed unwise to risk potentially extensive damage for the minimal amount of additional information to be gained. The test sequence was therefore concluded, and no additional runs will be made until a complete re-insulation can be completed.

Operational checkout of the HPMS magnet was considered to be quite successful. Eleven of twelve planned runs were completed with excellent data acquired. The total test sequence is given in Table 9.

7.0 ANALYSIS OF MAGNET DATA

The performance of the magnet can be most simply summarized by its magnetization curve giving the magnetic field strength at a particular location in the bore as a function of the magnetomotive force, or equivalently for a given number of turns, the coil current. A comparison of the magnetization curve based on the original design with the data acquired at the peak field strength location is given in Fig. 48. The data given in Fig. 48 were all taken at steady-state conditions and therefore can be compared directly with theoretical predictions. No steady-state data were acquired below 4,000 amp, so no details were considered for the low field strength where the magnet steel becomes saturated.

Figure 48 indicates that the steel did saturate as predicted, indicated by the fact that above the knee of the curve, the data are consistent with the slope of the design magnetization curve. Although the data have the proper slope, the data are consistently 0.1 T lower than the design curve up to 3.5 T. There appears to be a slight inflection in the curve above 3.5 T, but no definite conclusion can be drawn from that single data point. With the inflection at the maximum field point, extrapolation must be done with caution, but it appears that 4 T is readily achievable at a current flow of just over 13,000 amp.

The transient data for Runs 3 through 11 are shown in Figs. 49 through 57. Runs 1 and 2 were of such short duration (≈ 0.5 sec) that no data are presented for those runs. The efficiency of the magnet trip limit is shown clearly in Fig. 49 where a current limit of 4,000 amp was established. The circuit breaker was automatically tripped less than 0.1 sec after reaching that limit.

The data for Run 4 (Fig. 50) indicate that steady state had been achieved just before run termination at 3.5 sec. In general, the data on all runs with external reactance indicate that 4 to 6 sec were required to reach steady state (except for the minor change in current caused by the change in coil resistance as the coil temperature increases to thermal equilibrium). On Runs 10 and 11 (Figs. 56 and 57), with all external reactance removed, steady state was achieved in 8 to 10 sec.

Magnet Runs 4, 5, and 6 were all identical at their outset, and Figs. 50, 51, and 52 indicate repeatable performance characteristics. Run 5 was simply a longer duration run than Run 4 where complete equilibrium was achieved. The tap changing under load capability can be seen in Run 6, Fig. 52. The first 20 sec were a repeat of the first 20 sec of Run 5 and then the voltage was changed during the run to increase magnet current. Each flat portion on the amperage curve represents an operating point where the magnet was allowed to come to equilibrium before proceeding. The first 35 sec of Run 7 (Fig. 53) reproduce the time span from 50 to 70 sec on Run 6 (Fig. 52), then continue to higher current levels. Run 8 (Fig. 54) was the first run without maximum external reactance and that run traversed the full power supply operating envelope for the Tap 10 reactor setting. Run 9 (Fig. 55) was similar to Run 8, the increased current level again provided by decreased external reactance. Run 10 (Fig. 56) was the first run with no external reactance and Fig. 56 indicates that a slightly longer rise time resulted. Run 10 was approaching equilibrium when it became necessary to terminate the run. The initial portion of Run 11 (Fig. 57) repeated Run 10 and comparison of Figs. 56 and 57 indicates equivalent performance. In general, Figs. 49 through 57 indicate both repeatable and stable performance.

The design axial magnetic field strength profile was previously presented in Fig. 13. That figure is reproduced in Fig. 58 with the actual profiles included for comparison. The shape of the actual profile compares very favorably with the prediction over the full range. The good agreement can be seen more easily in the normalized data shown in Fig. 59. The data fall very near the design prediction in the increasing field region and compare favorably through the steep decreasing gradient. The actual data are above the design prediction, which means that the field strength does not drop as rapidly as desired. However, such a variation is preferable to a gradient which is steeper than design prediction since a lower field strength would reduce the amount of energy that could be extracted from the generator channel. In general, the overall comparison is quite good.

As previously noted, the power required to generate the high magnetic field in the HPMS magnet is not small. Figure 60 shows the power required as a function of the centerline peak field strength. Two points which are worth noting are illustrated in the data. First, the steep slope of the data below 2 T and the sharp knee of the curve around 2 T indicate that the iron

saturated as predicted. Second, the power required to achieve 4 T will be approximately 18 MW. This is consistent with the data shown in Fig. 48. Since the achieved field strength falls slightly below the predicted field strength, the current required to achieve a given field is higher than predicted. Since the power is proportional to the current squared, the power level increases quite rapidly. The original design predicted a power requirement of 17.5 MW for a 4 T peak field and 24.7 MW for a 4.5 T peak field. While adequate power is available to achieve the 4 T point, it is doubtful that 4.5 T can be achieved. When operating into a 0.1 ohm load, the power supply is capable of 26 MW which may not be sufficient to provide adequate power to achieve 4.5 T, assuming that the trend noted in Fig. 60 is valid up to that level.

The power dissipated in the magnet coil was determined by direct measurement of the current and voltage. The voltage measurement was subject to some fluctuation, however, and the voltage plots in Figs. 49 through 57 are time averaged to generate smooth data. The measured coil resistance, along with the current, provides a direct secondary measurement of power dissipation which is equivalent to the calculation using the measured voltage, and the data presented in Fig. 60 use the coil resistance instead of the averaged voltage measurements.

The coil resistance varies during a given run but the variation is slight. During the initial portion of the run, the current heats the magnet coils and the power dissipated is a combination of thermal energy stored in the coil and the energy transmitted to the cooling water. At thermal equilibrium the total energy is transmitted to the cooling water and the temperature rise along with the water flow rate gives a third power calculation ($\dot{m}C_p\Delta T$). At maximum power input, the ΔT between the coils and cooling water is estimated to be approximately 8°K. The coil temperature is therefore 8°K higher than the final cooling water exit temperature. Figure 61 gives the coil resistance as a function of temperature over the range of interest. The change in resistance is shown to be around 8 percent for maximum ΔT achieved in Run 11. The cooling water temperature as a function of run time is shown for several runs in Fig. 62. Comparison of Fig. 62 with the transient data in Figs. 49 through 57 shows that thermal equilibrium lags the electrical equilibrium by several seconds. Power calculations were made at several points of thermal equilibrium on Runs 6, 8, and 11. The results of these calculations are shown as closed symbols in Fig. 60. The heat balance calculations compare favorably with the I^2R calculation.

8.0 CONCLUDING REMARKS

Procurement and installation of HPMS facility components, excluding the magnet system, was approximately 75 percent complete when the scope of the project was reduced

to completion of the magnet system only. The fuel and liquid oxygen systems have been secured at that stage of completion, valves and piping not yet installed have been stored for later use, and all facility installation efforts have been suspended until resumption of the HPMS project.

Magnet installation and checkout are complete. Dimensional nonuniformities and difficulty with the water fittings created significant mechanical problems and delays, but the performance characteristics were very close to the design requirements. The magnetic field strength generated was within 0.1 T of the design value over the full current range. The axial centerline profile was slightly higher than the design profile in the steep decreasing field region, but overall the profile was judged to be quite satisfactory. No internal electrical discrepancies were revealed during testing, but external cooling tube insulation was found to be inadequate. Improvement of that insulation will be required before further operation.

REFERENCES

1. Pape, Thomas A. "One Megawatt Diagonal Conducting Wall MHD Generator." Chrysler Corporation, AFAPL-TR-69-3, 1969.

2. Sonju, O. K., et al. "Experimental Research on a 400 KW High Power Density MHD Generator." AVCO-Everett Research Laboratory, AFAPL-TR-71-5, December 1970.

3. Sonju, O. K., and Teno, J. "Study of High Power, High Performance Portable MHD Generator Power Supply Systems." Maxwell Laboratories, Inc., AFAPL-TR-76-87, August 1976.

4. Sonju, O. K., Burry, R. V., Cooper, R. F., et al. "Development of a Compact, Lightweight High Performance 30 MW MHD Generator System." Presented at the Seventeenth Symposium on the Engineering Aspects of Magnetohydrodynamics, Stanford, California, March 1978.

5. Huebner, Alan W., Thompson, E., and Swallom, D. W. "Hot Gas Flow Train Interface Control Document for Gas Generator and the High Power Channel MHD Tests." Rocketdyne Division, Rockwell International, RI/RD 78-142, February 1978.

6. Huebner, Alan W., et al. "Hot Gas Flow Train Performance Test Plan for Gas Generator and the High Power Channel MHD Tests." Rocketdyne Division, Rockwell International, RI/RD 78-125, January 1978.

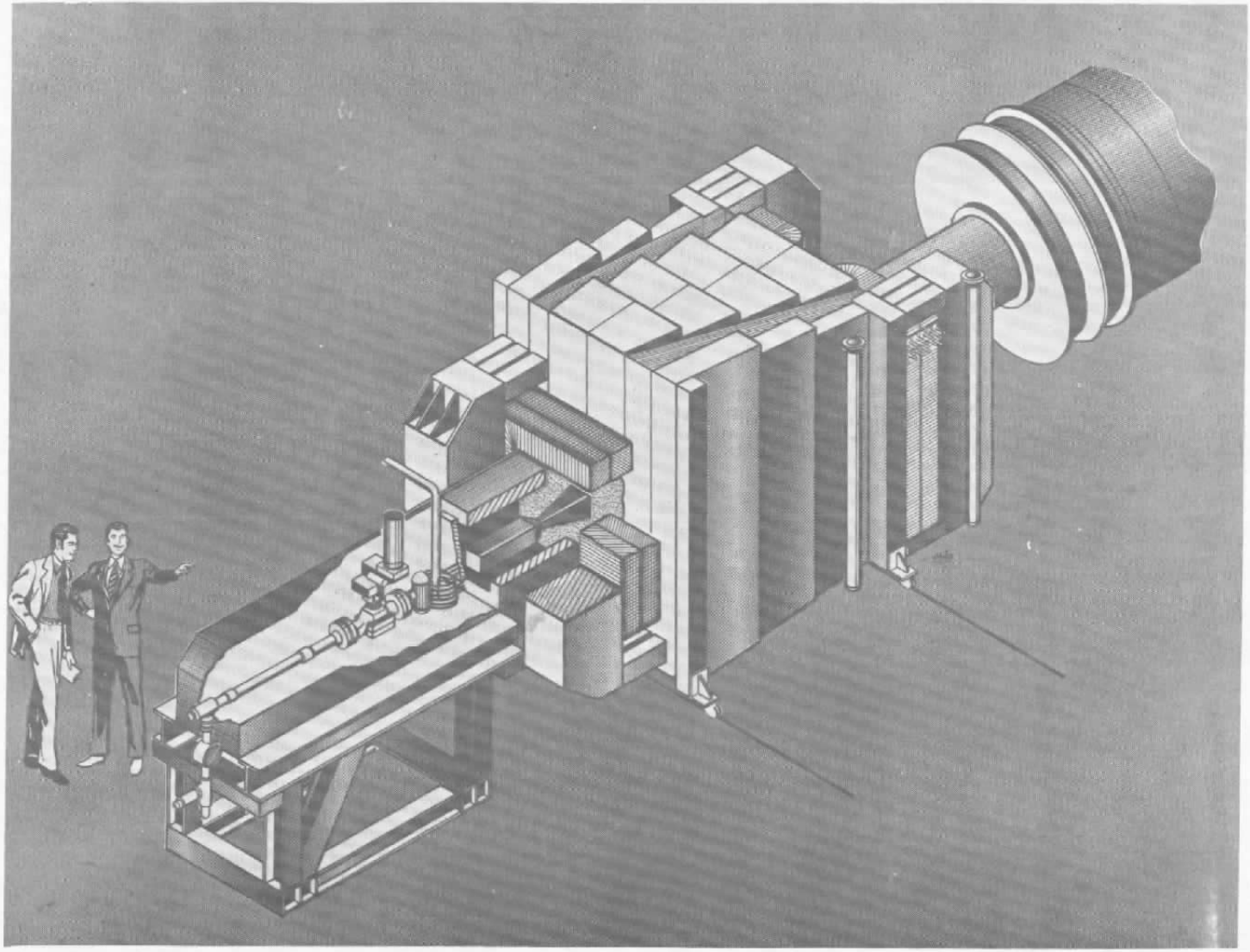

Figure 1. Schematic - High Power MHD System (HPMS).

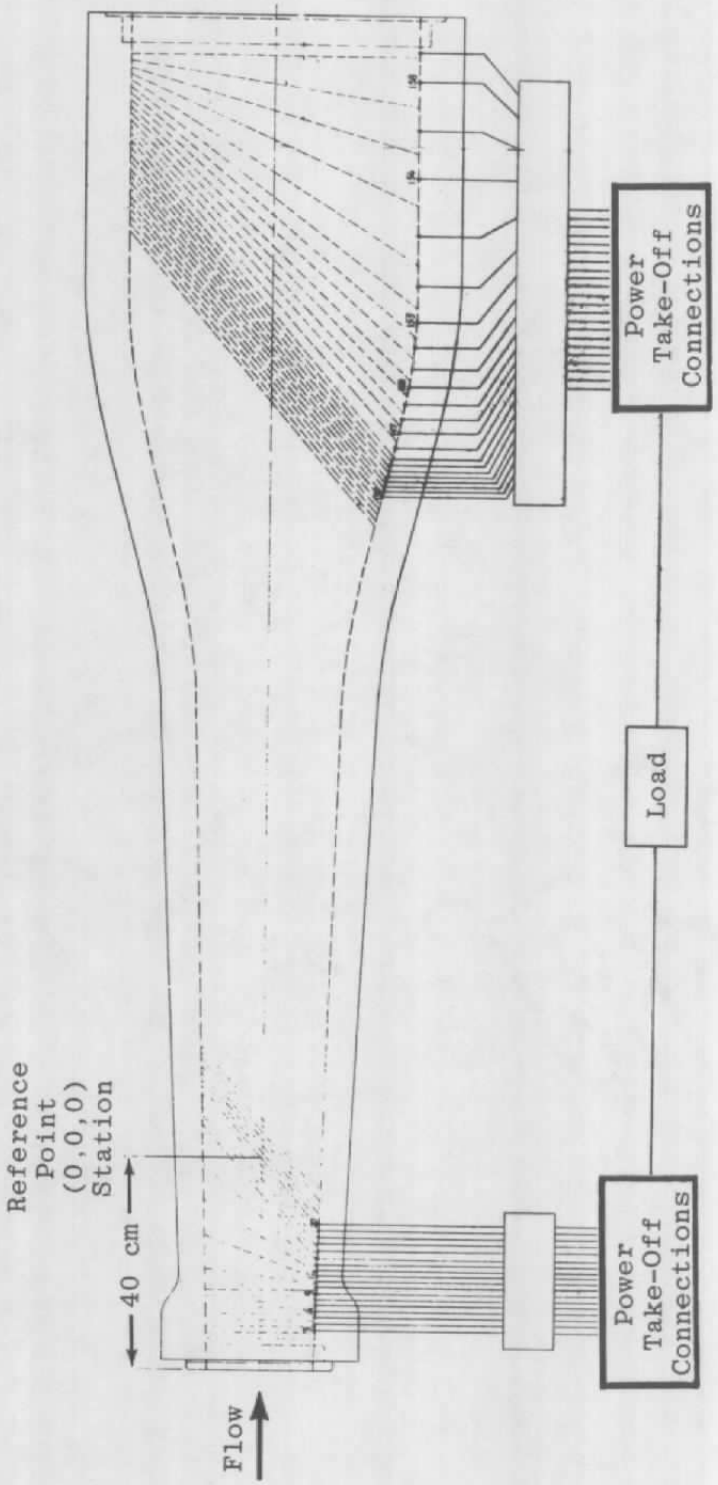

Figure 2. HPMS channel frame orientation.

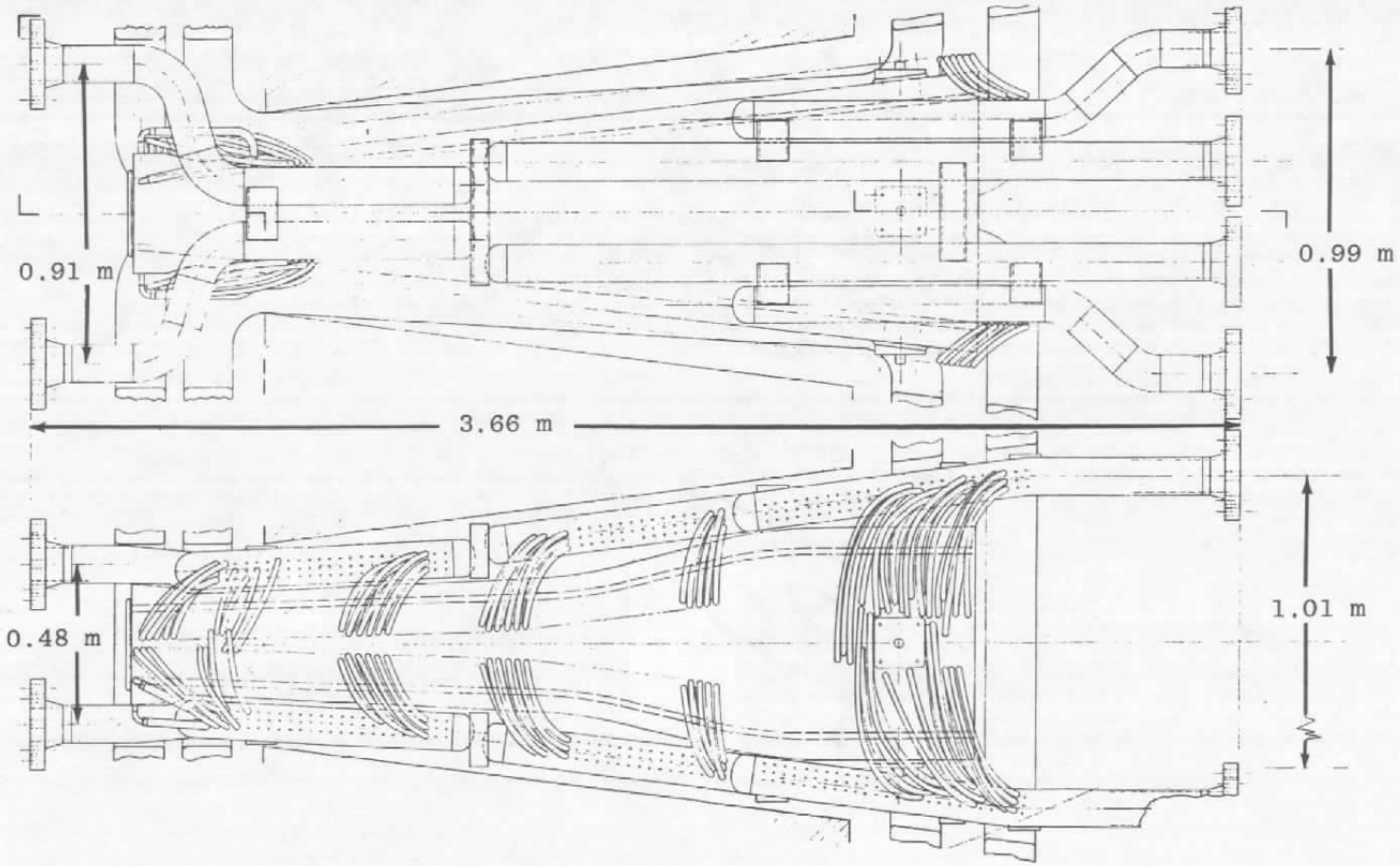

Figure 3. View of HPMS channel.

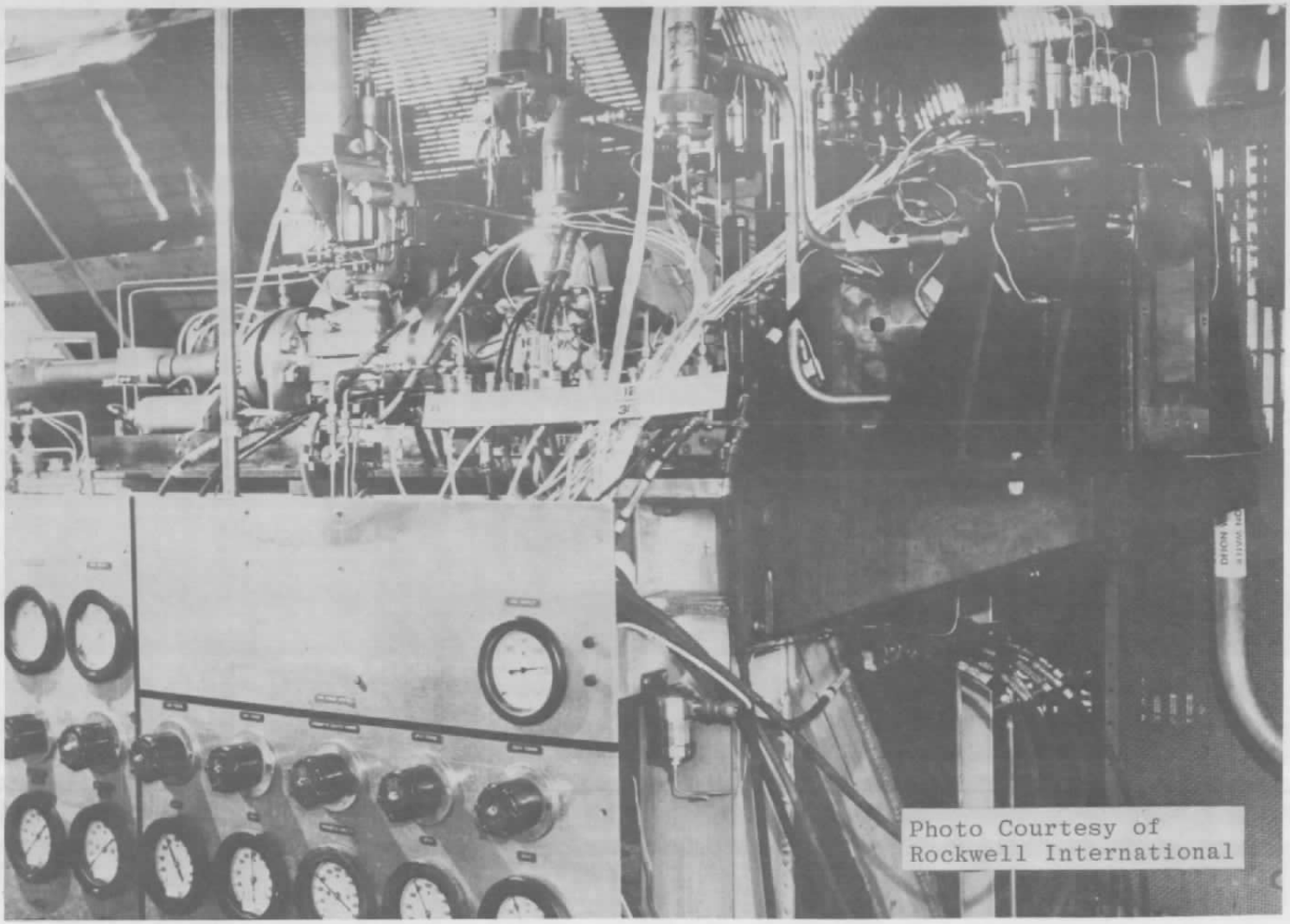

Figure 4. HPMS combustor system and control panels.

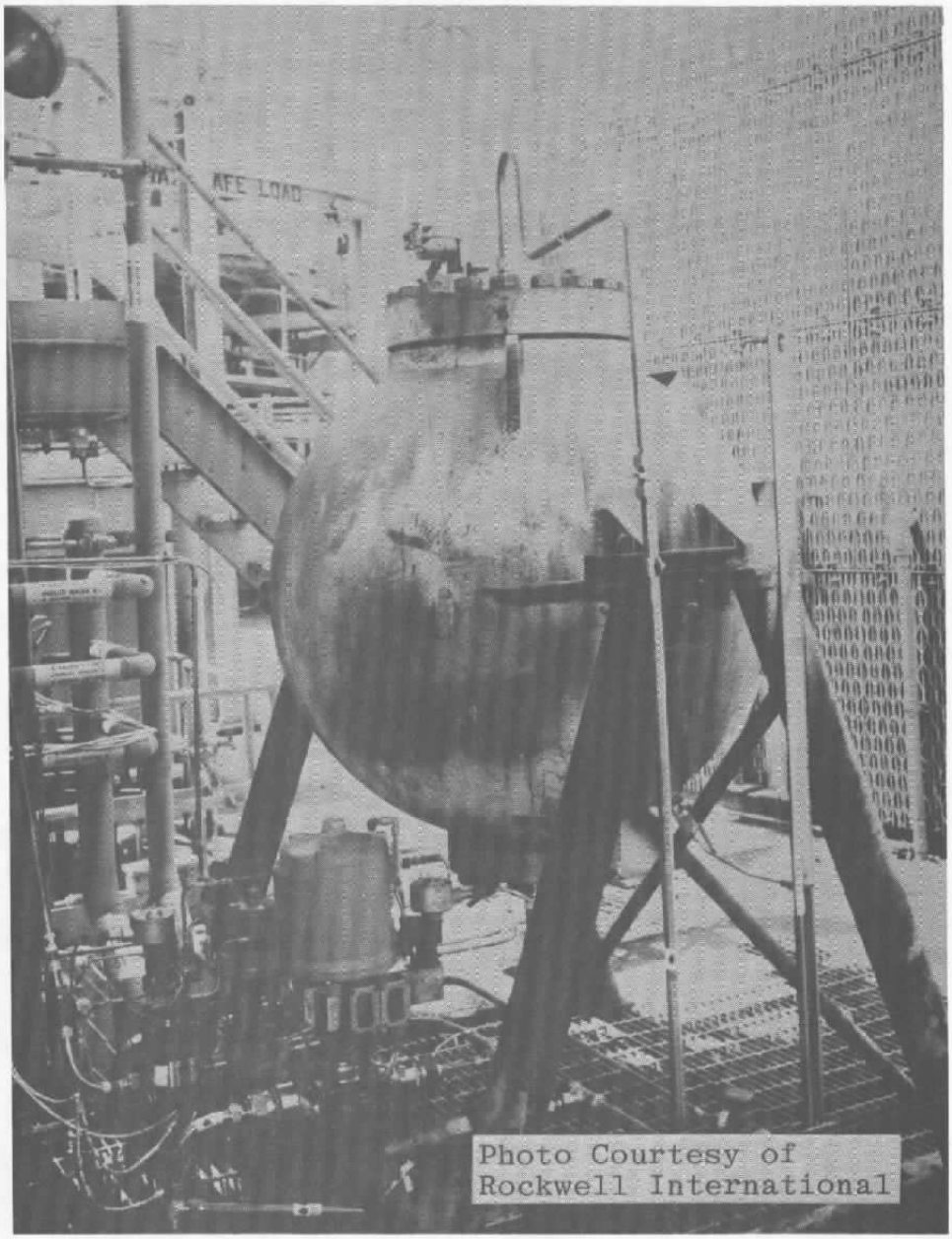

Figure 5. HPMS seed supply system.

Note: All Dimensions in Meters

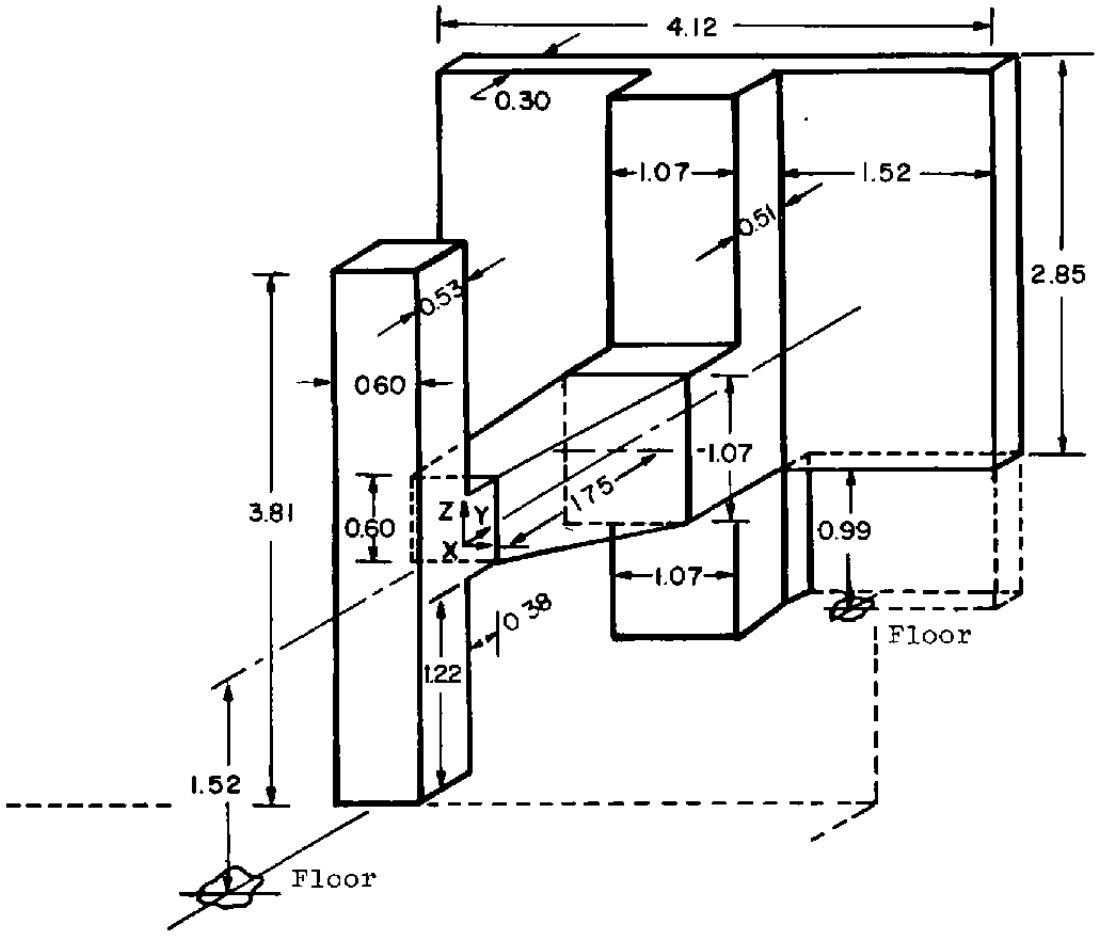

Figure 6. AEDC test clear area, MCA magnet envelope.

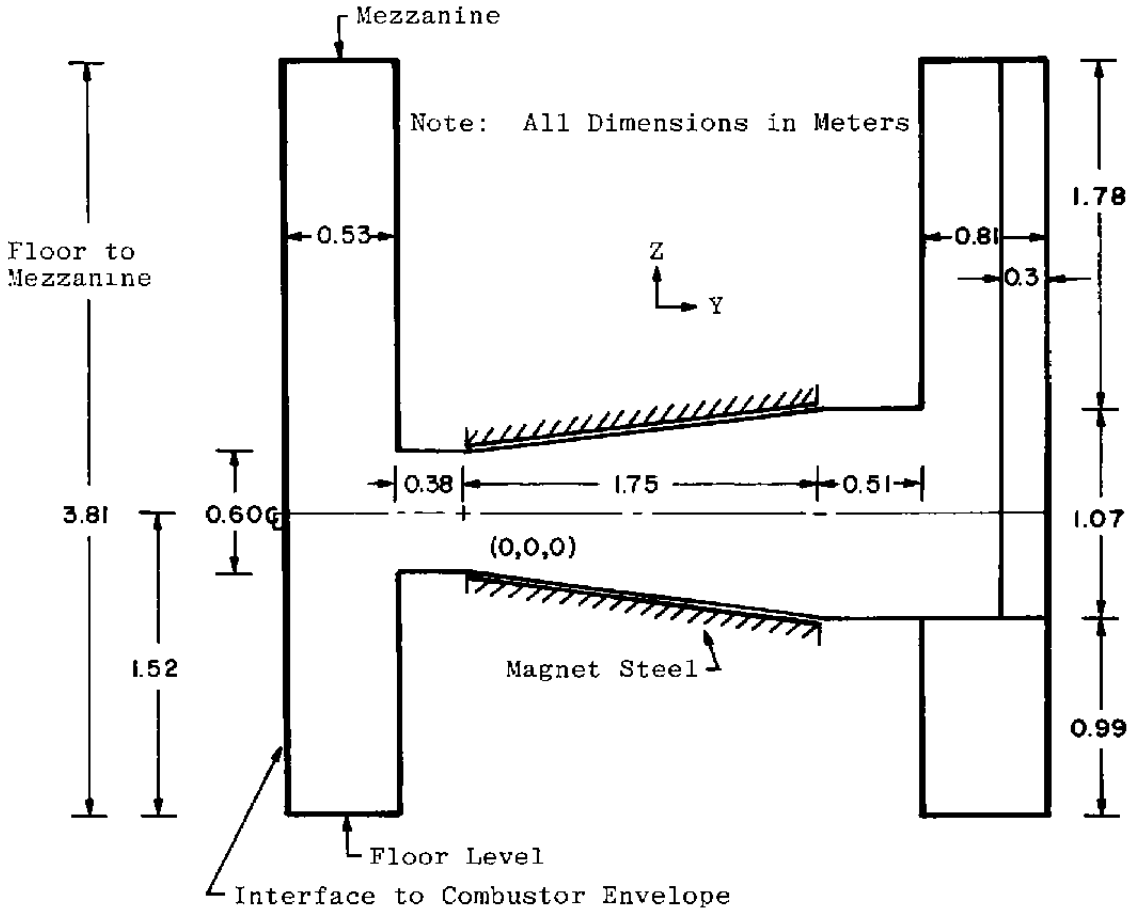

Figure 7. AEDC test clear area, MCA magnet - side view.

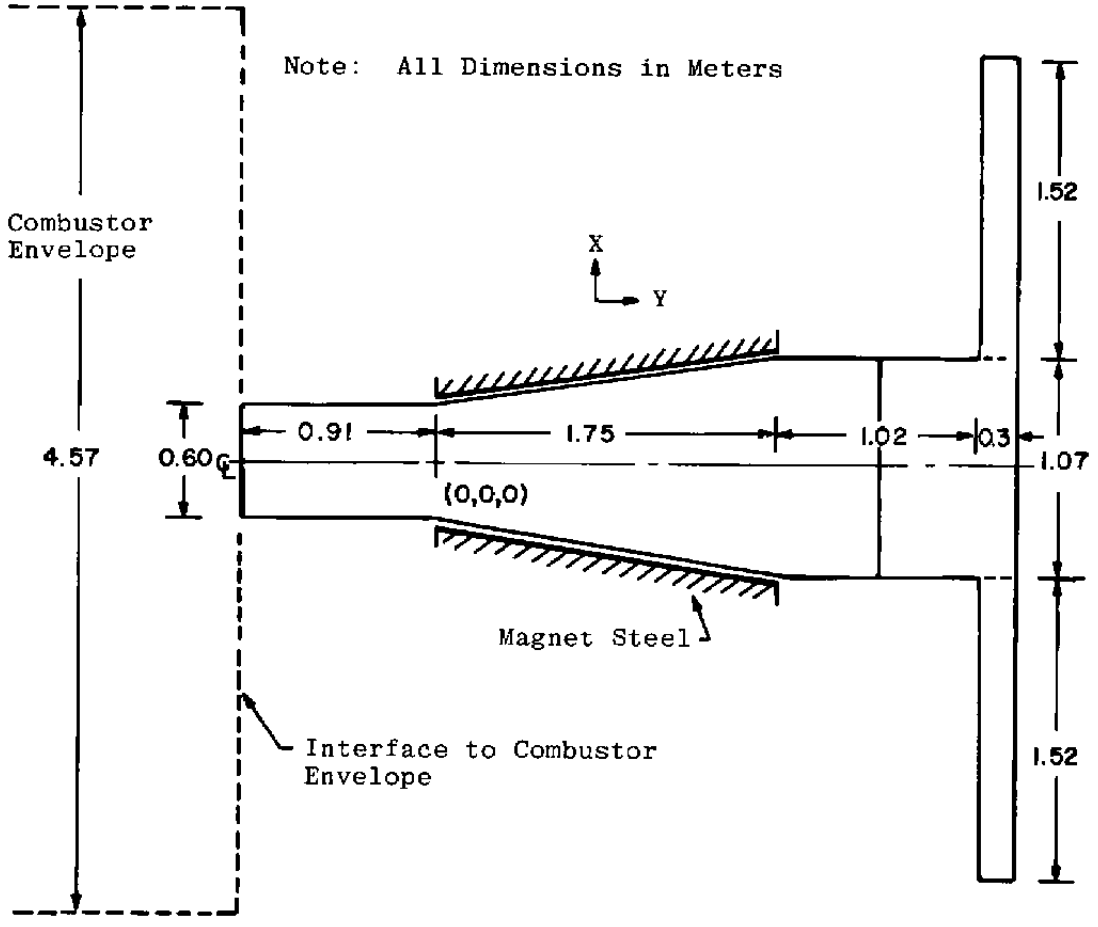

Figure 8. AEDC test clear area, MCA magnet - top view.

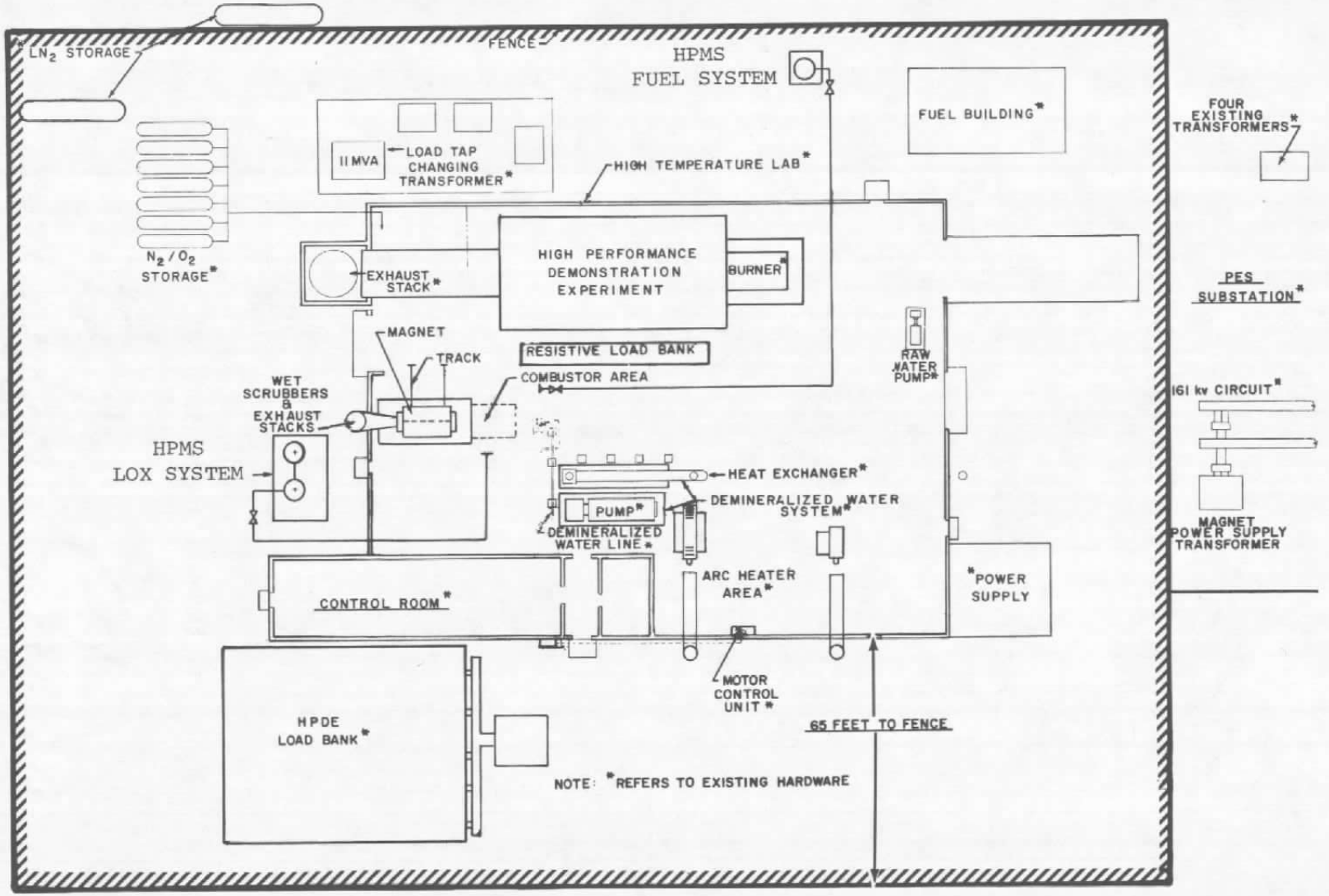

Figure 9. Layout of high temperature laboratory (HTL) building.

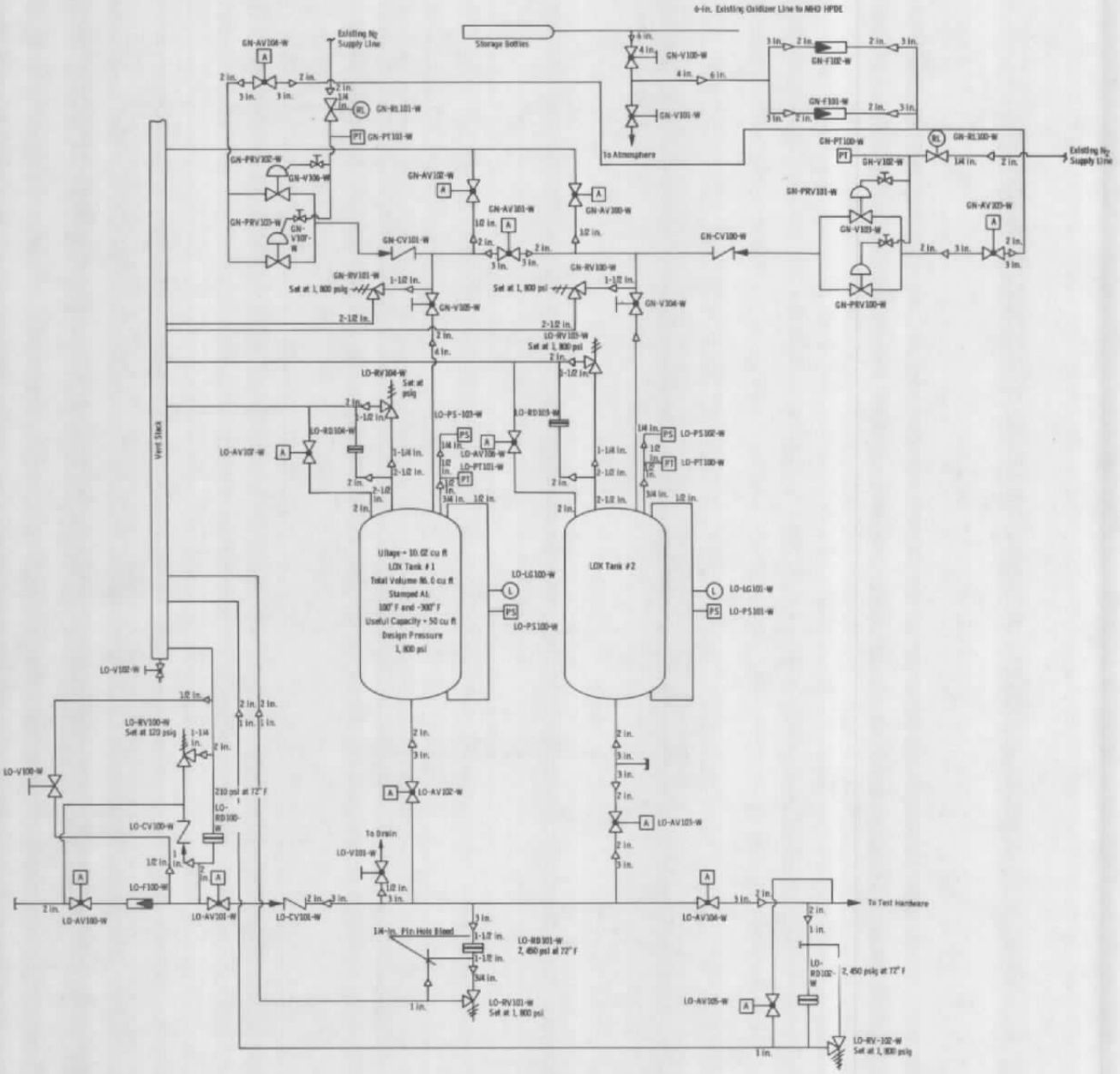

a. Schematic layout

Figure 10. Liquid oxygen system.

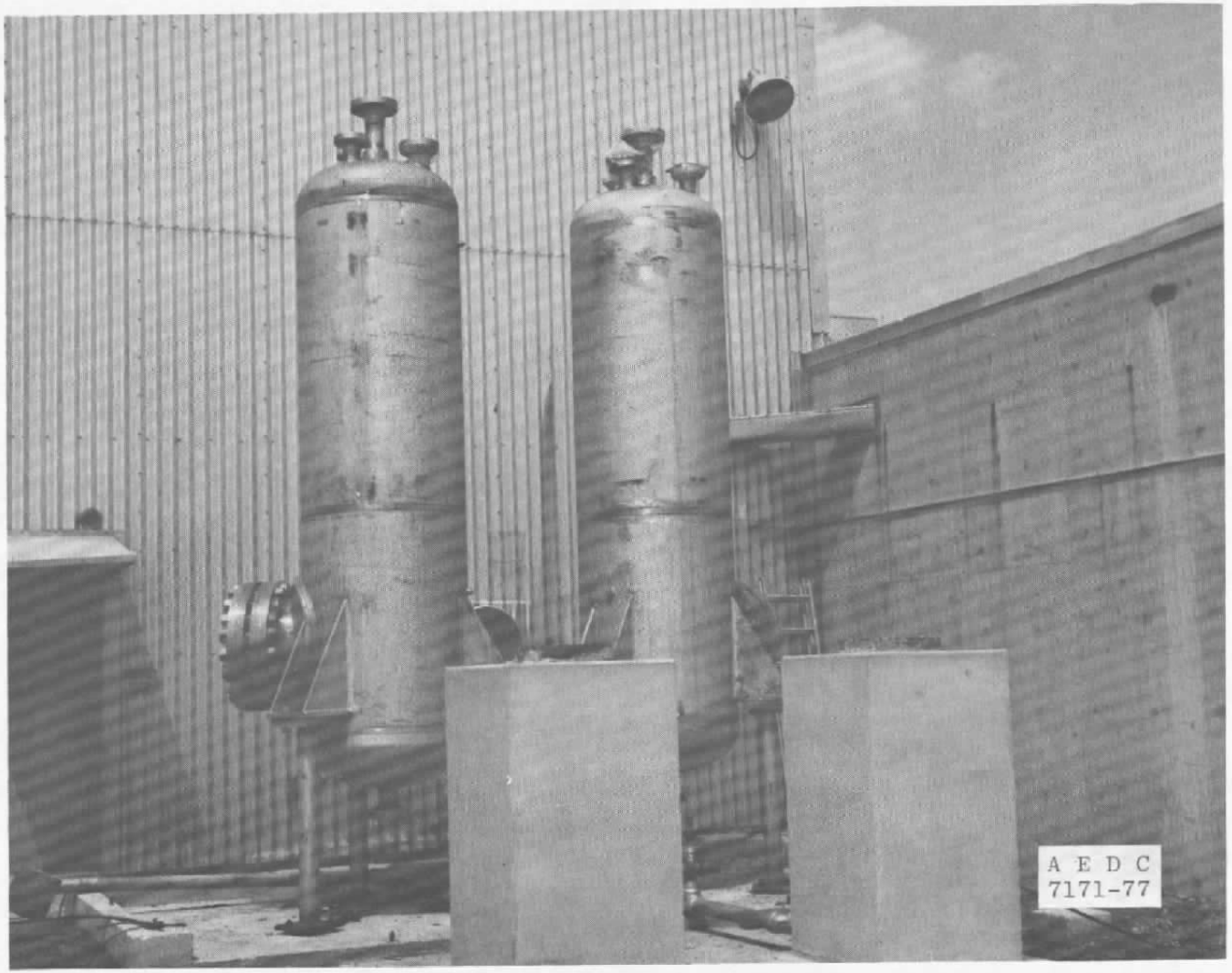

b. LOX tanks at high temperature laboratory
Figure 10. Concluded.

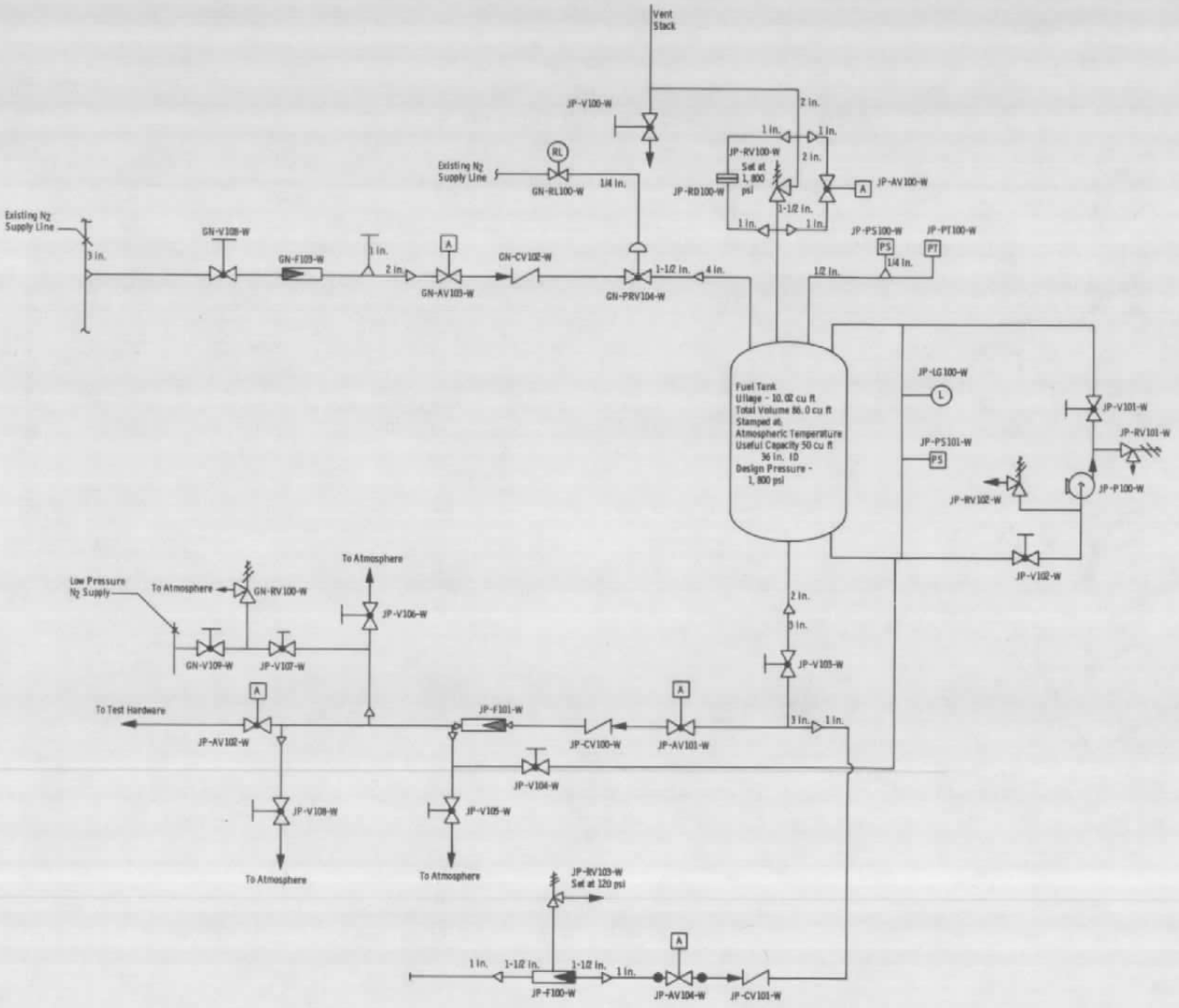

a. Schematic layout

Figure 11. HPMS fuel system.

b. Fuel tank at high temperature laboratory
Figure 11. Concluded.

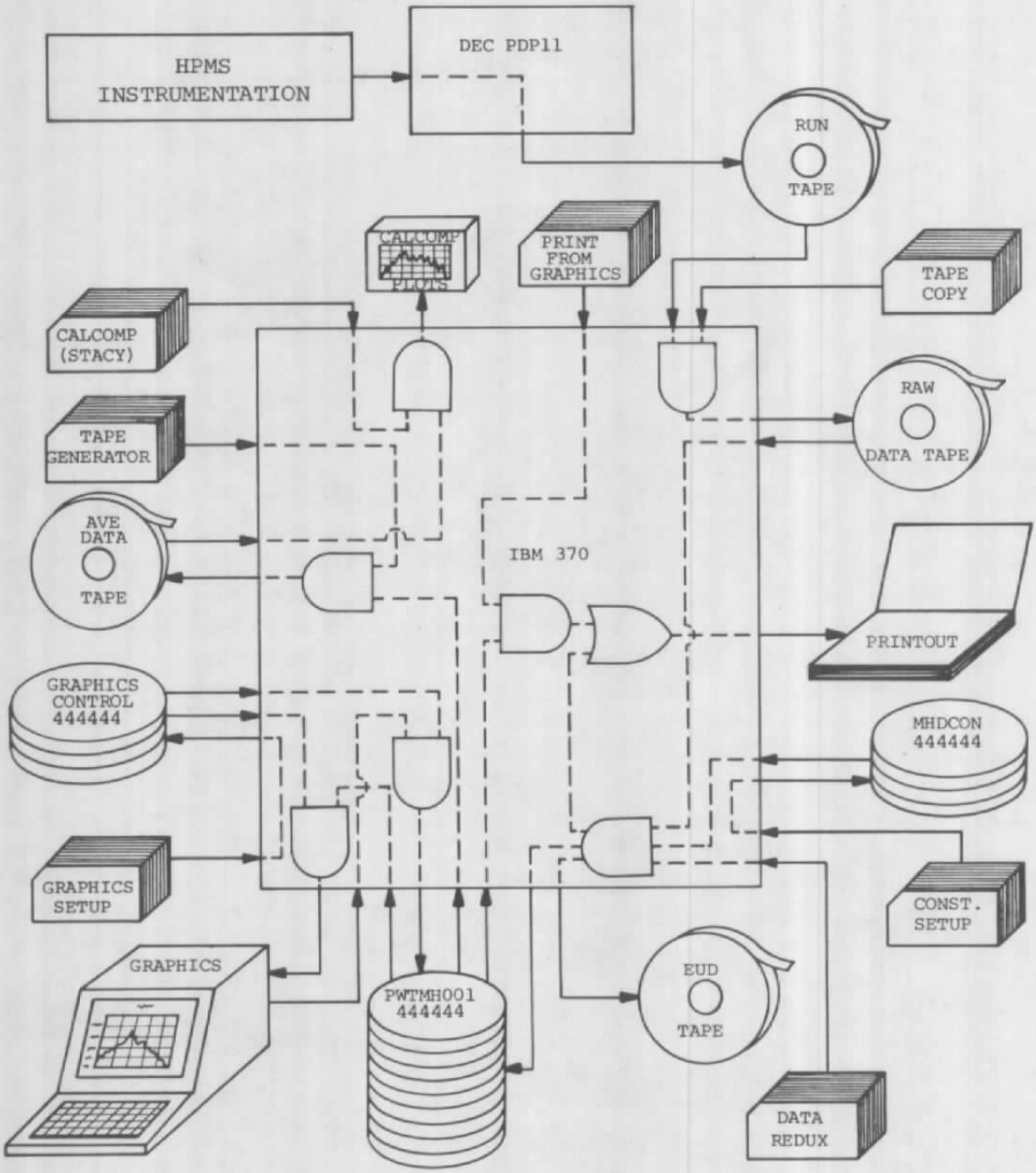

Figure 12. HPMS data acquisition and data reduction system.

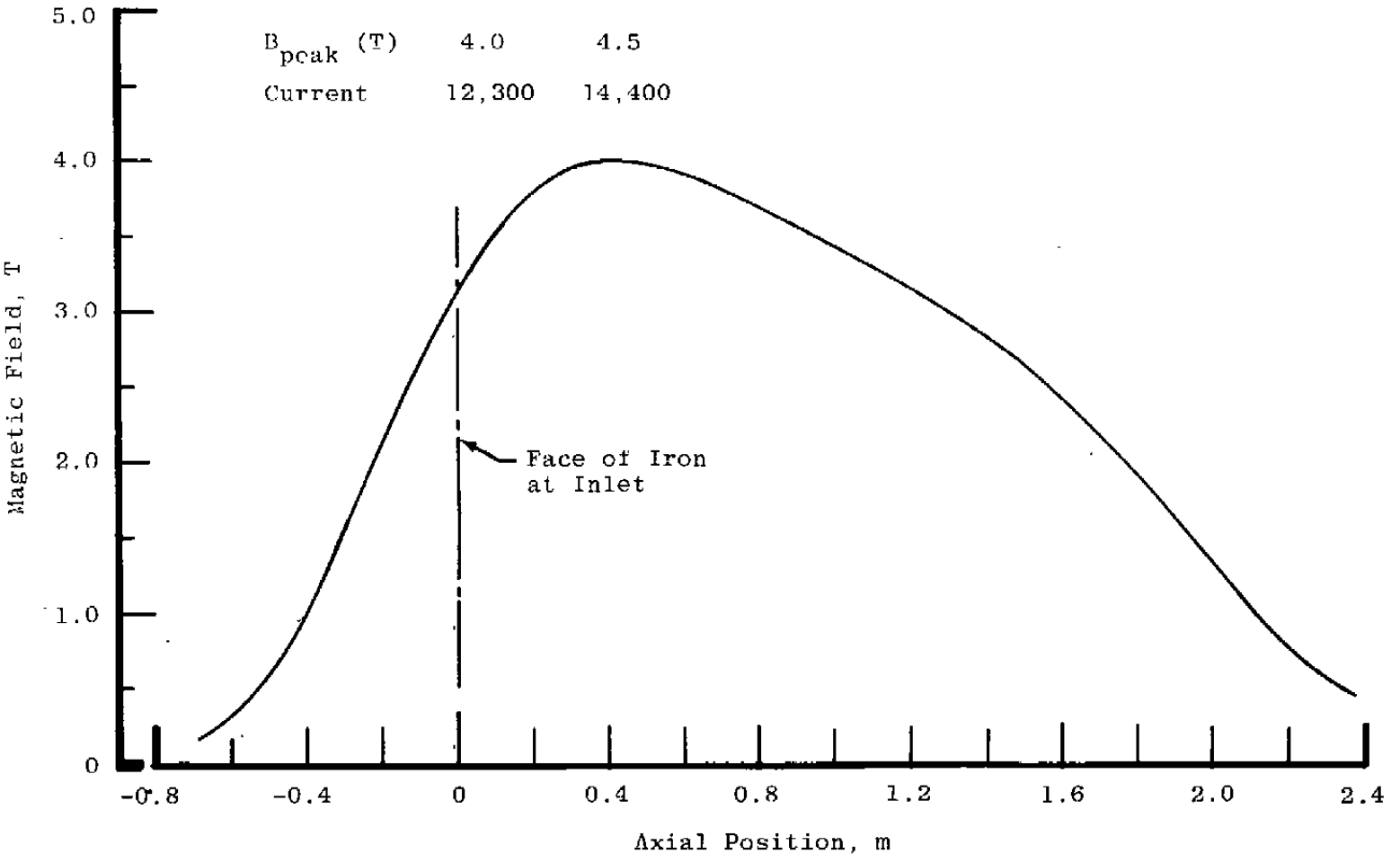

Figure 13. Magnetic field distribution on magnet centerline.

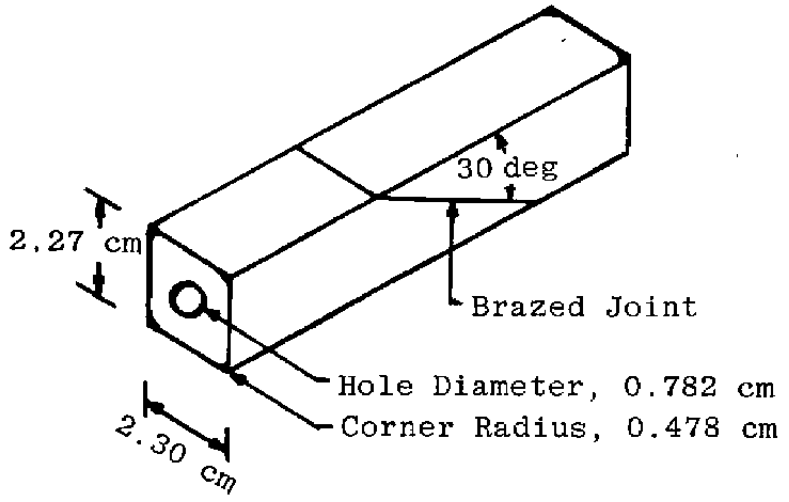

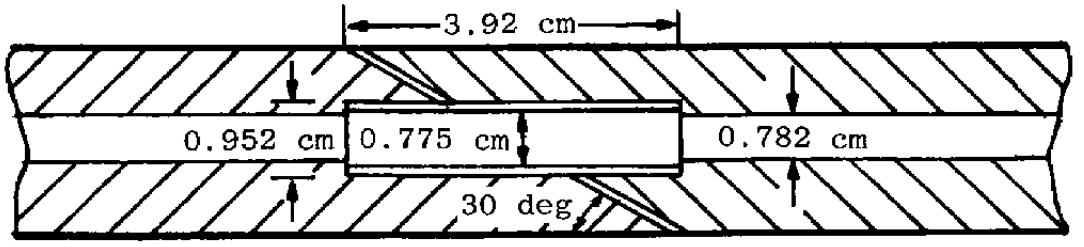

Figure 14. Typical conductor scarf joint.

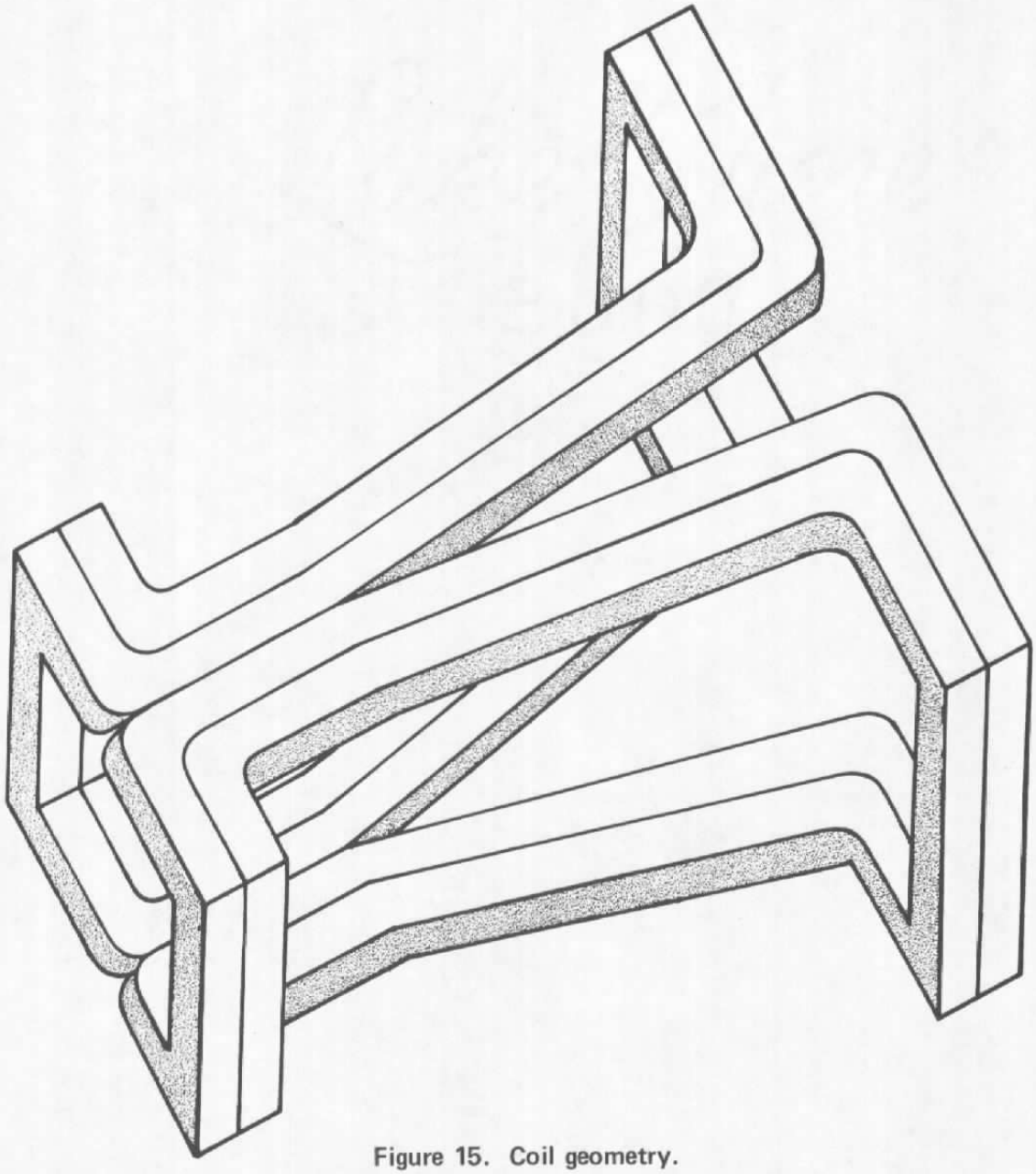

Figure 15. Coil geometry.

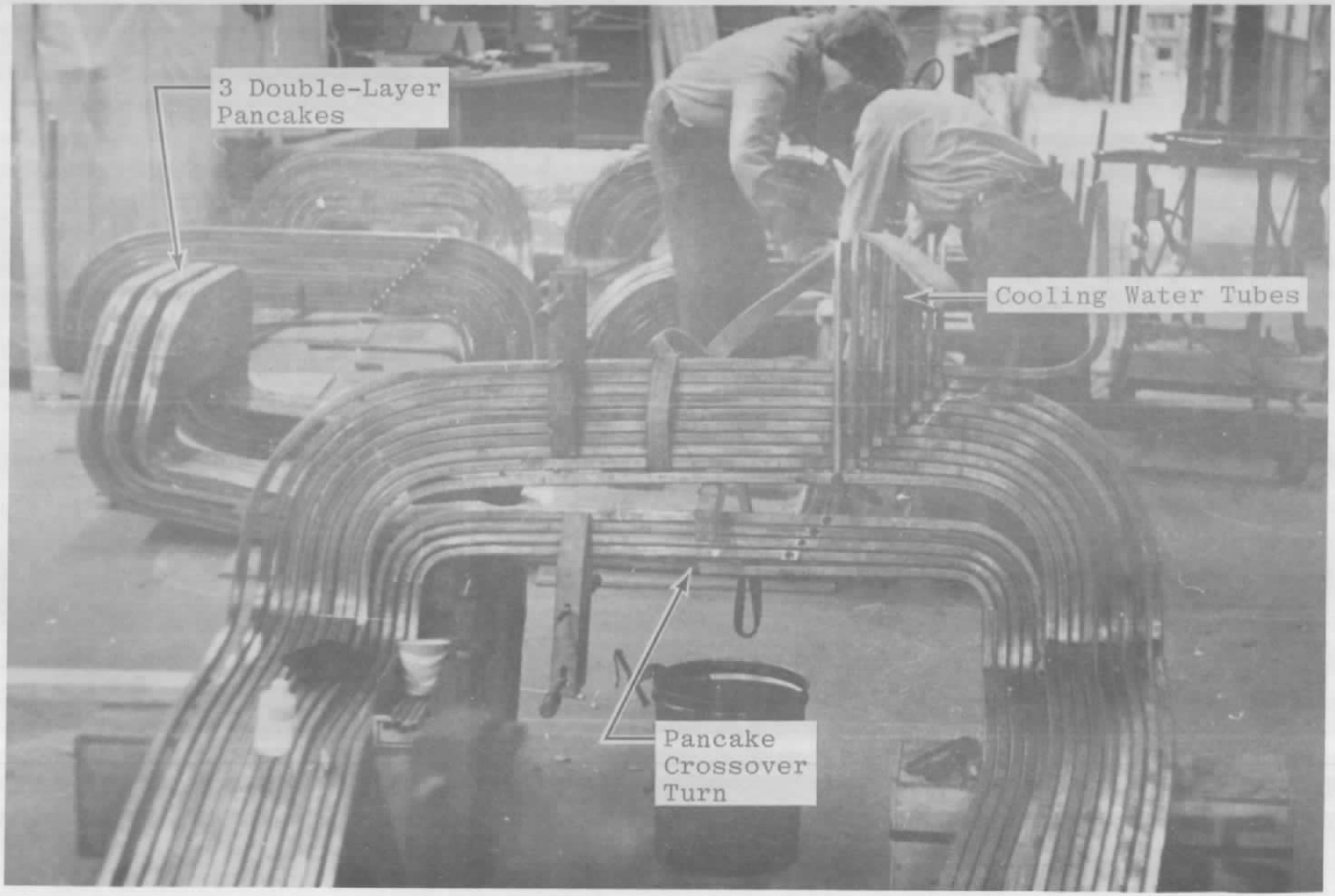

Figure 16. Coils after removal from winding fixture.

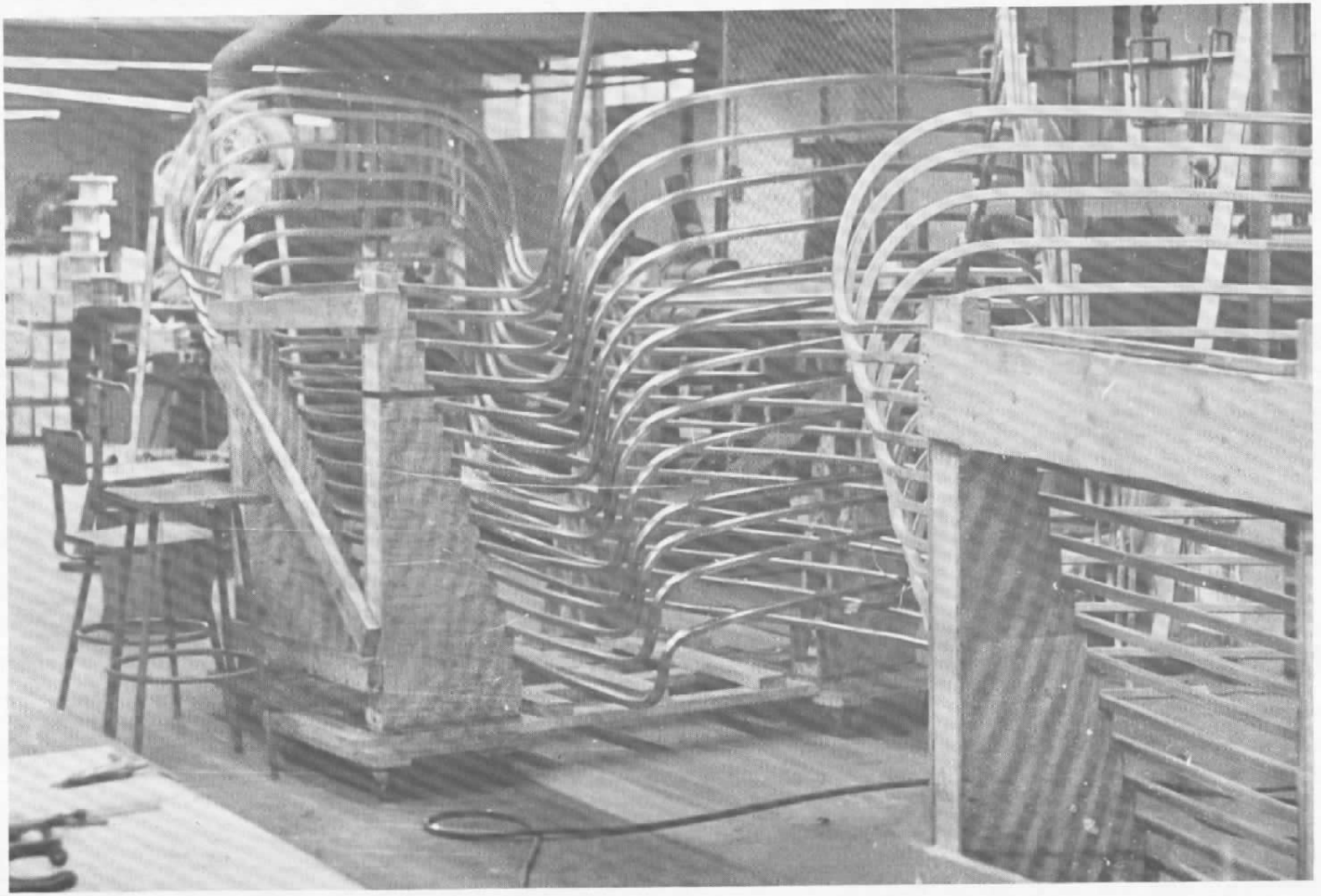

Figure 17. Coil separated for installation of turn-to-turn insulation.

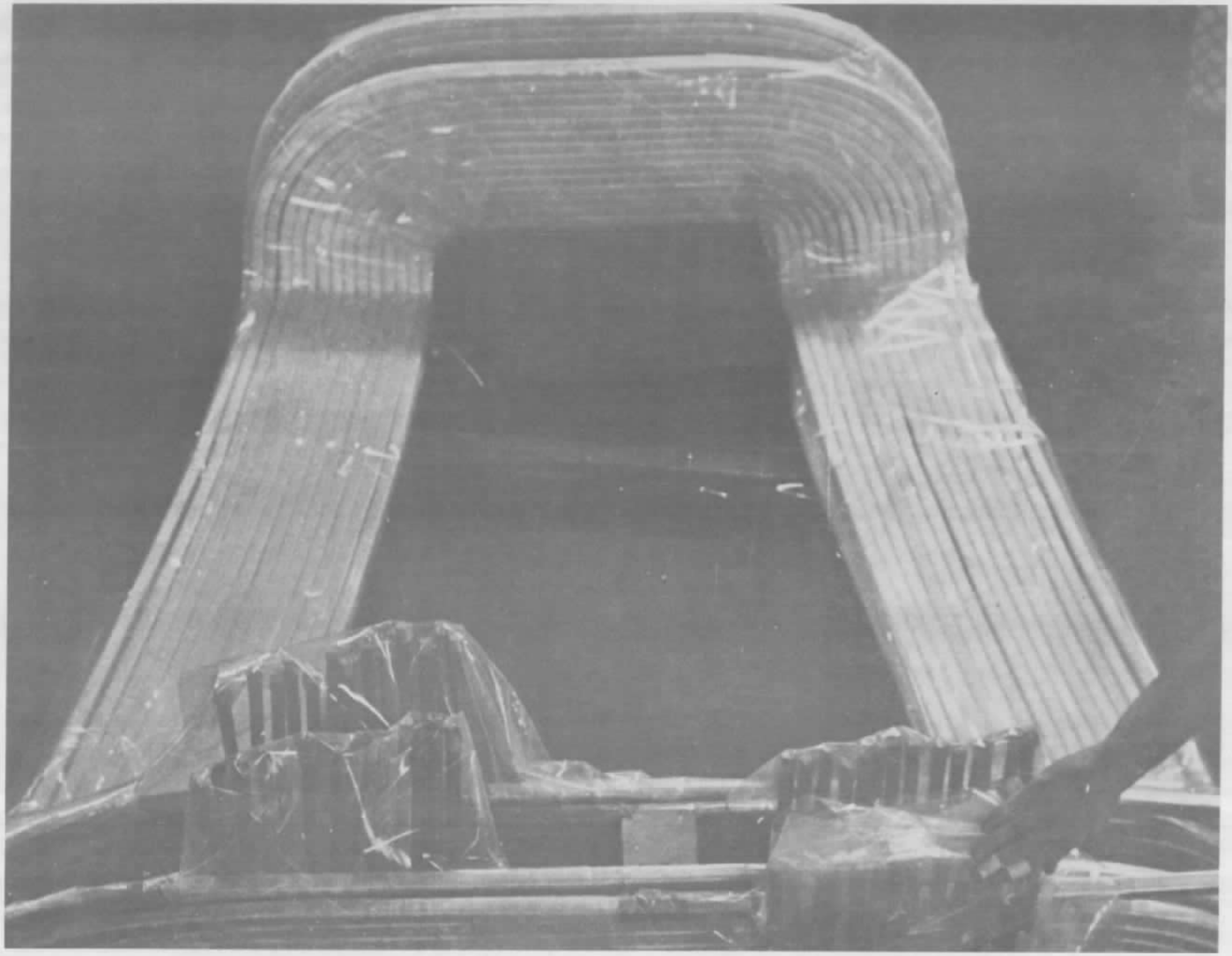

Figure 18. Coil complete with turn-to-turn insulation.

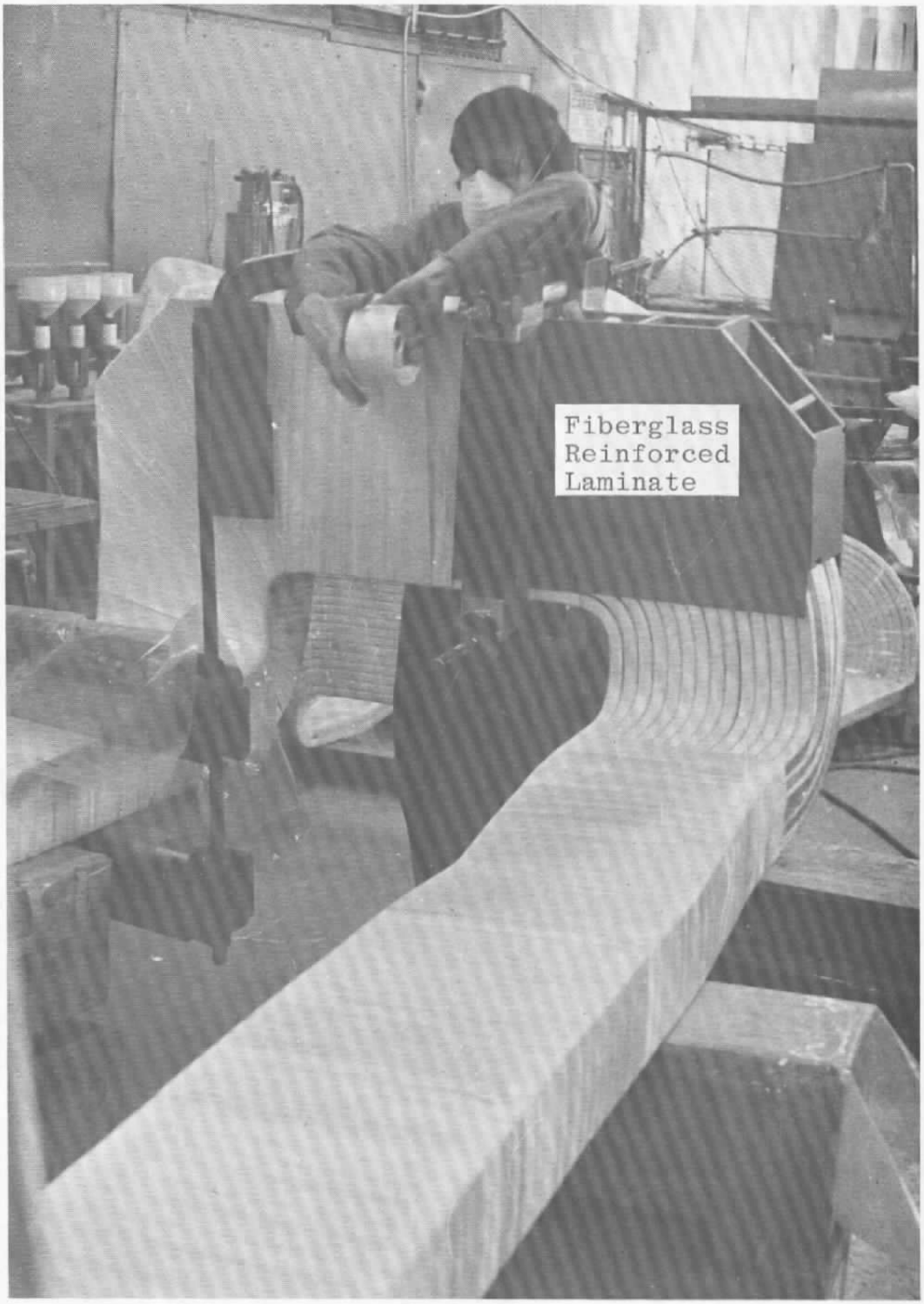

Figure 19. Coils as the final ground wrap is being applied.

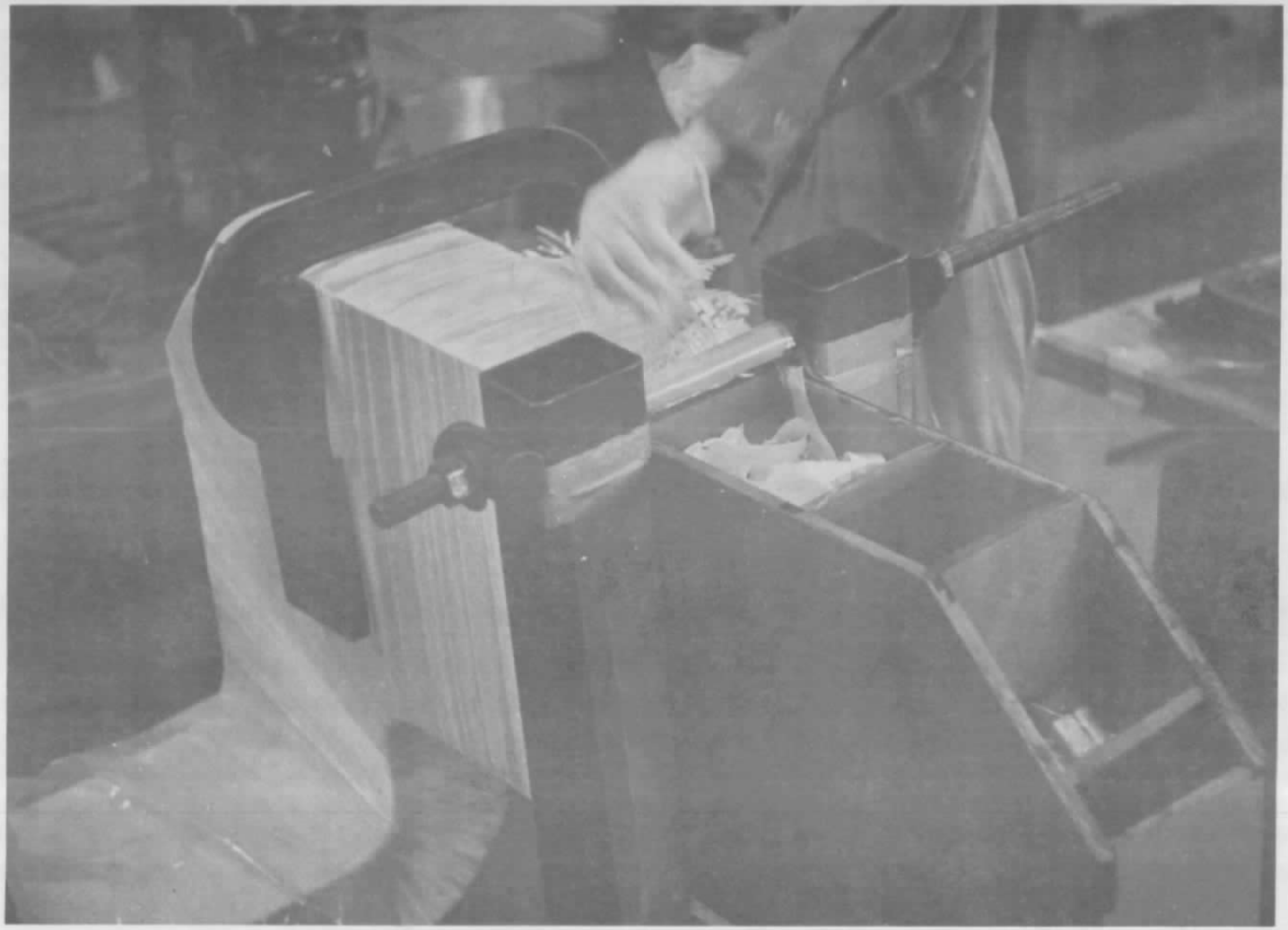

Figure 20. Blocks being filled with shredded fiberglass.

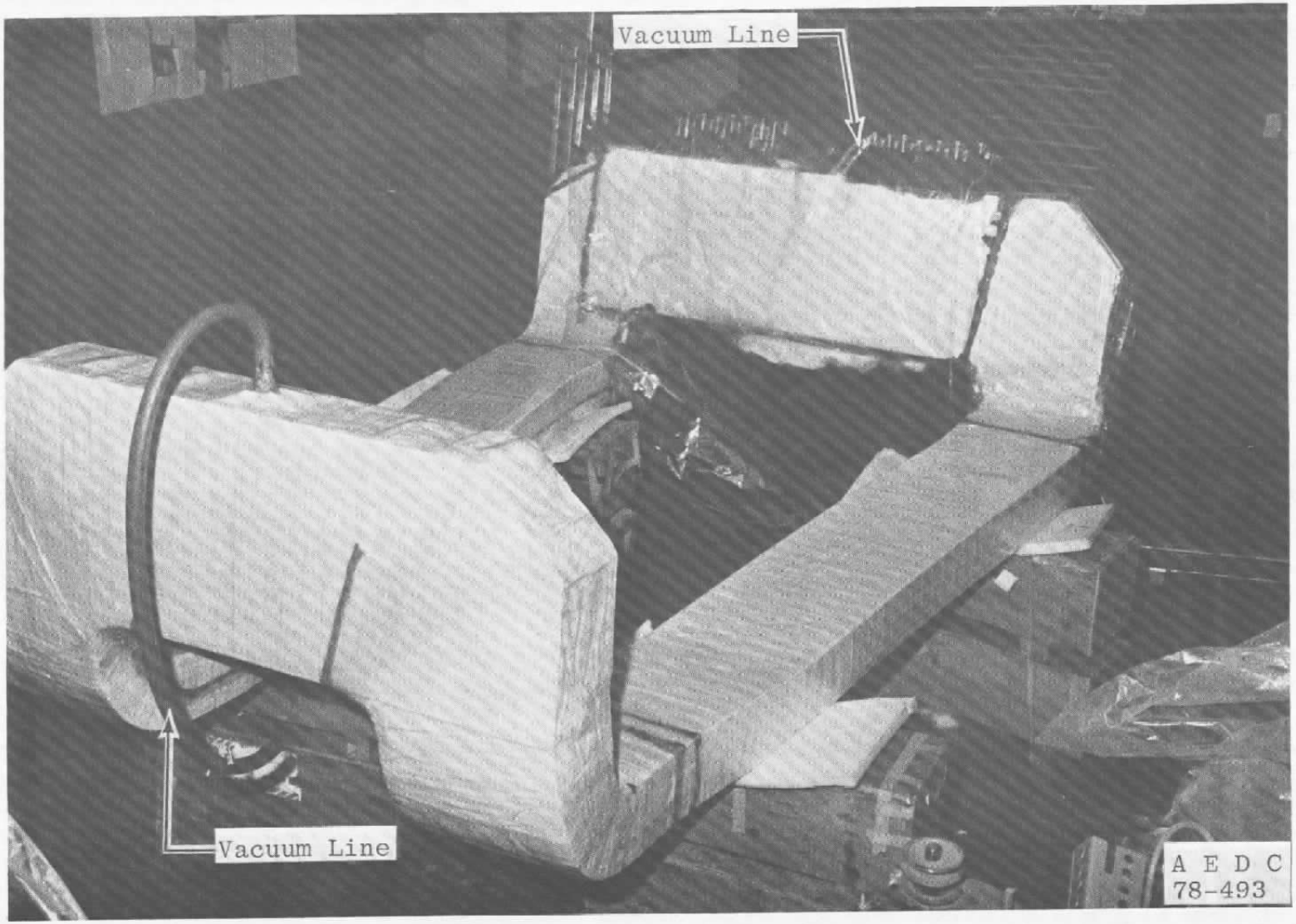

Figure 21. Coil after the final ground wrap in preparation for impregnation.

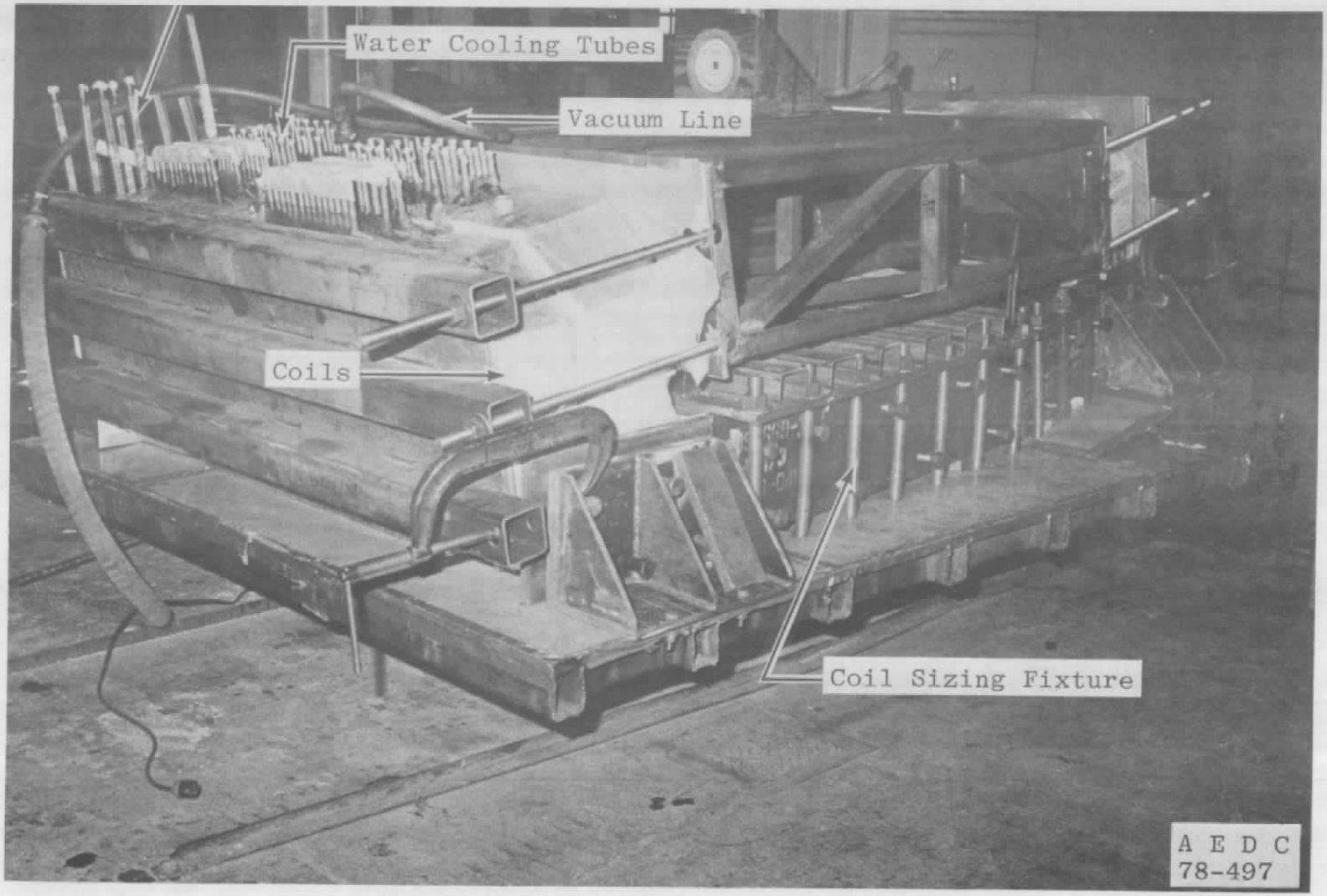

Figure 22. HPMS coils placed in sizing fixture.

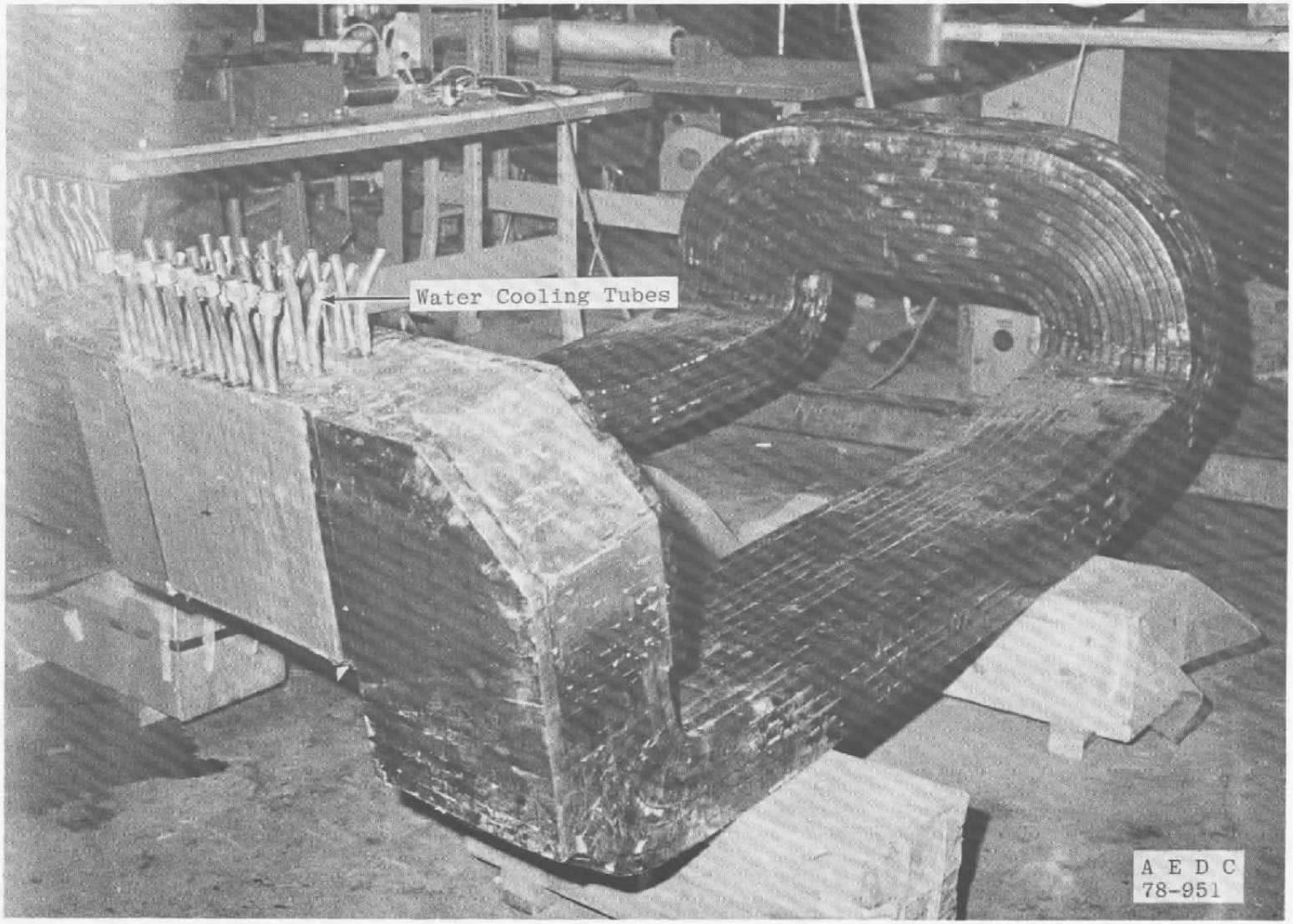

Figure 23. HPMS impregnated coil partially cleaned.

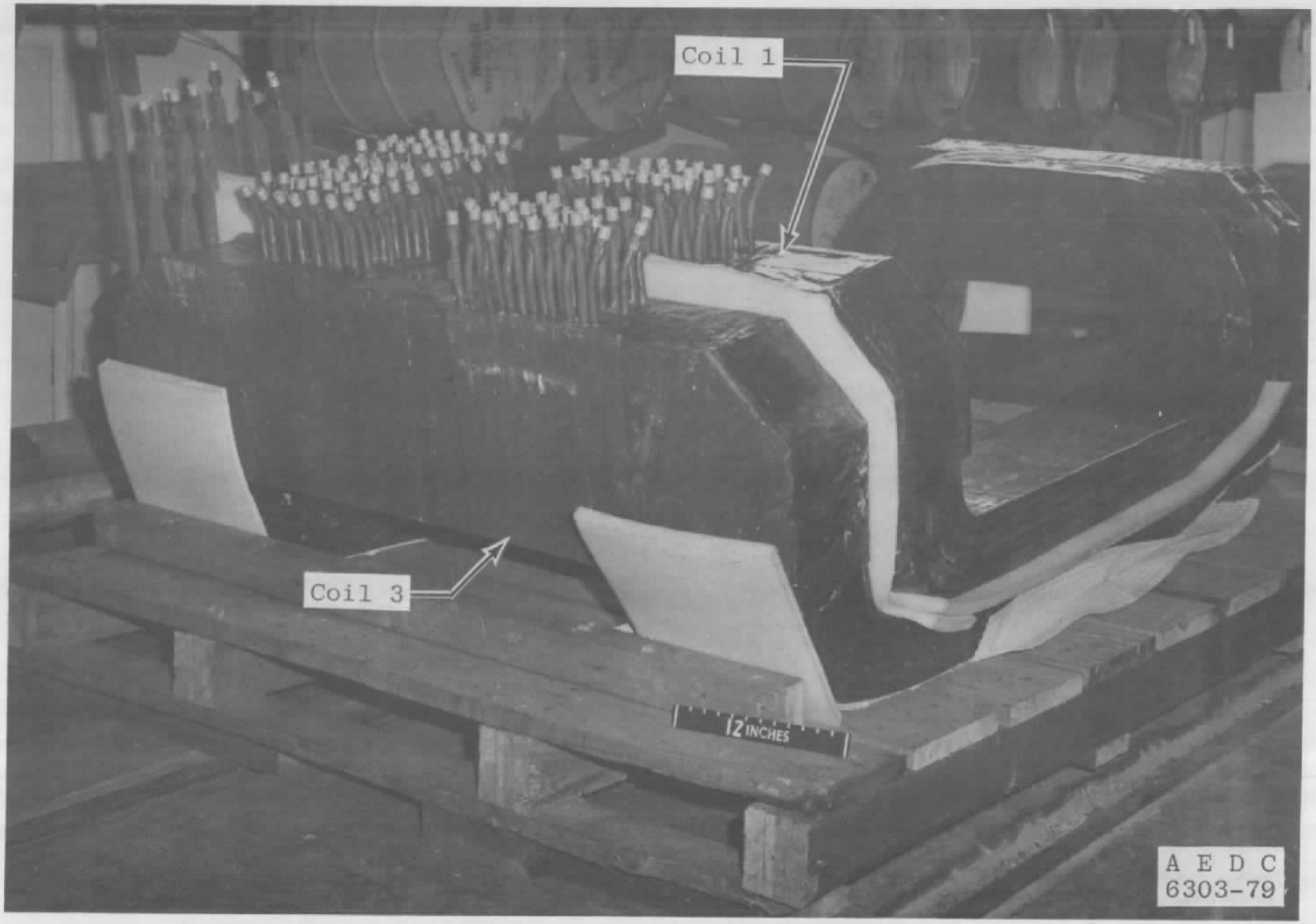

Figure 24. Completed coils as received.

Figure 25. HPMS magnet coils - as received.

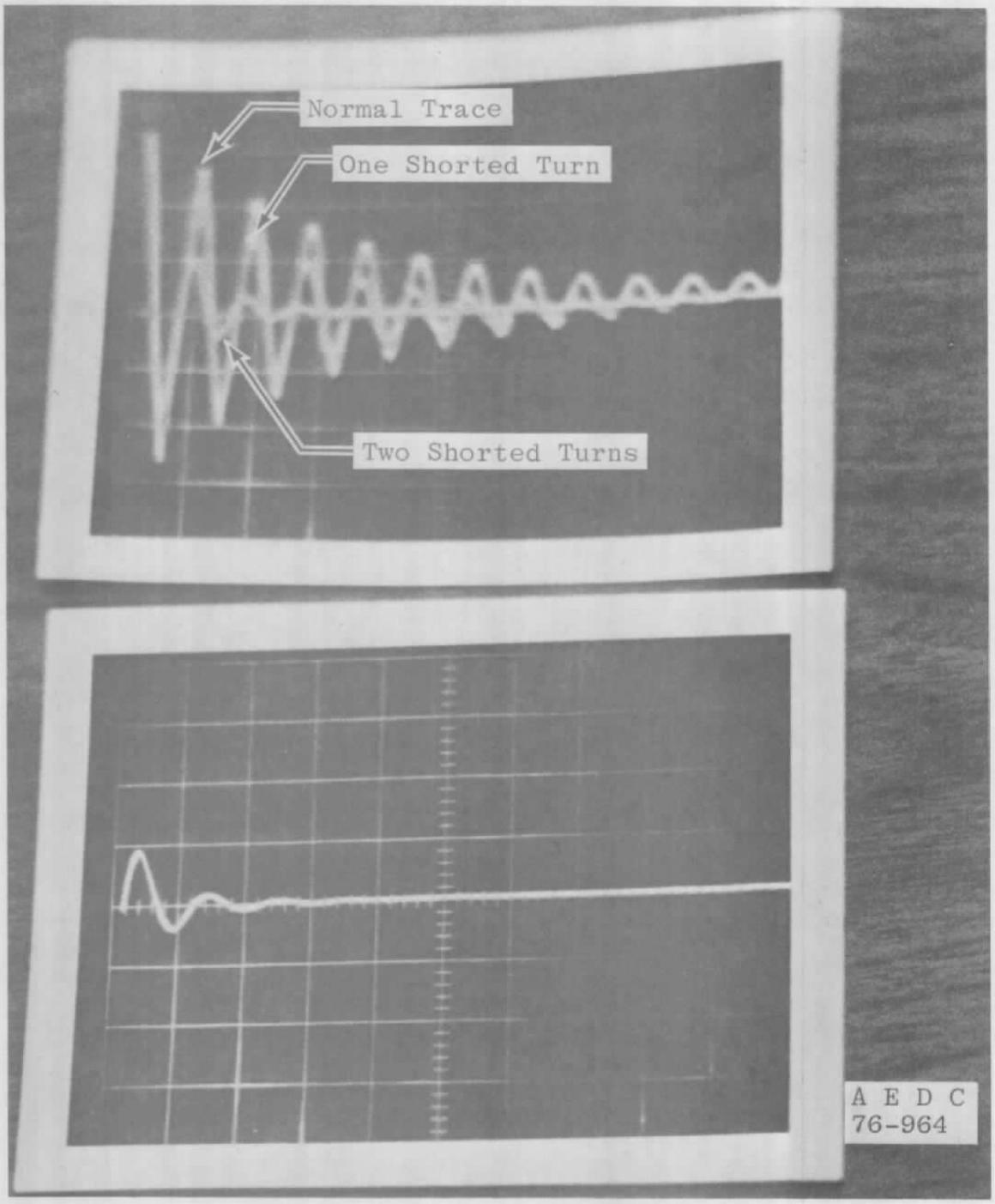

Figure 26. Capacitive discharge test results.

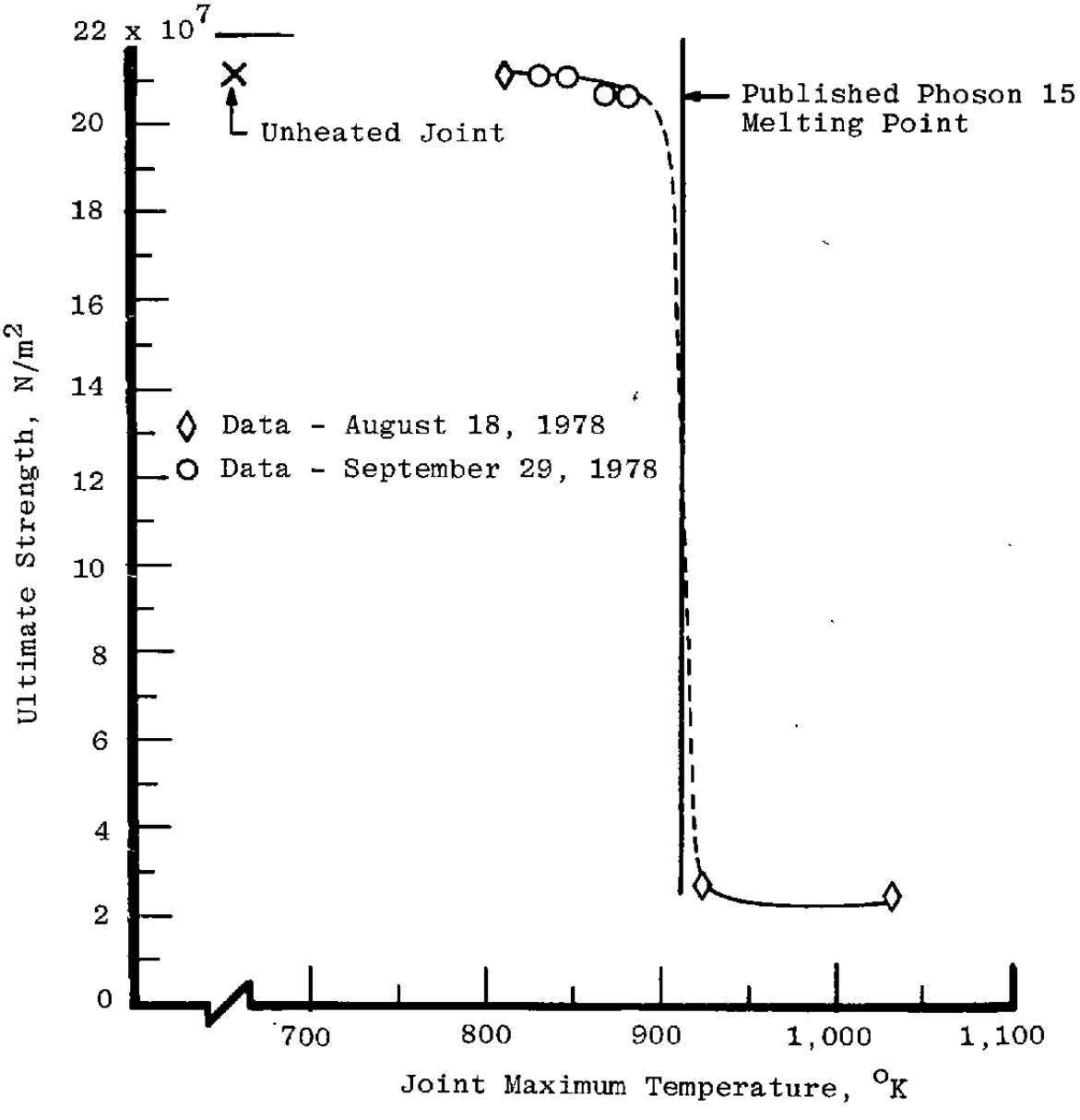

Figure 27. Tensile tests on heated joint specimens.

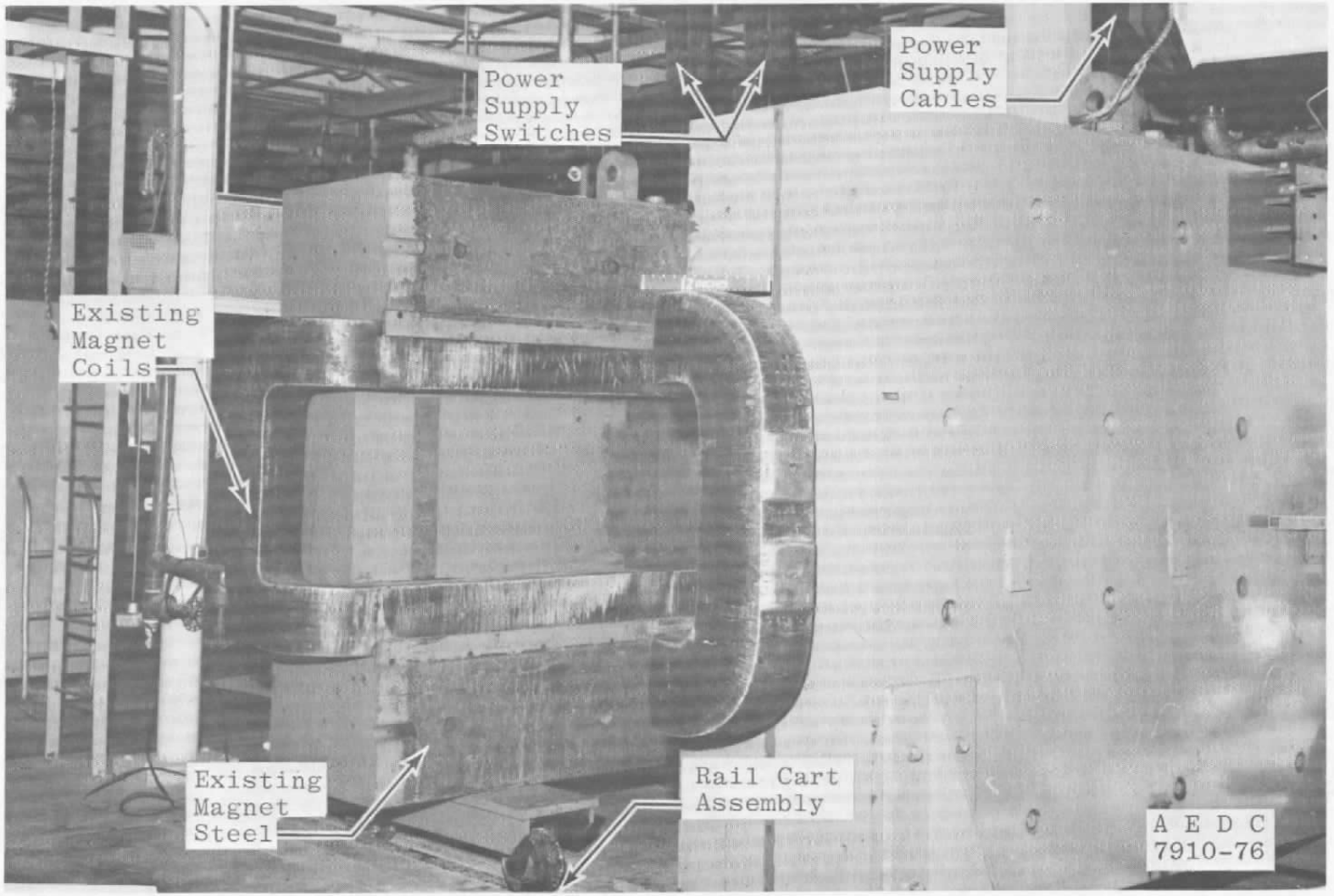

Figure 28. Original magnet assembly.

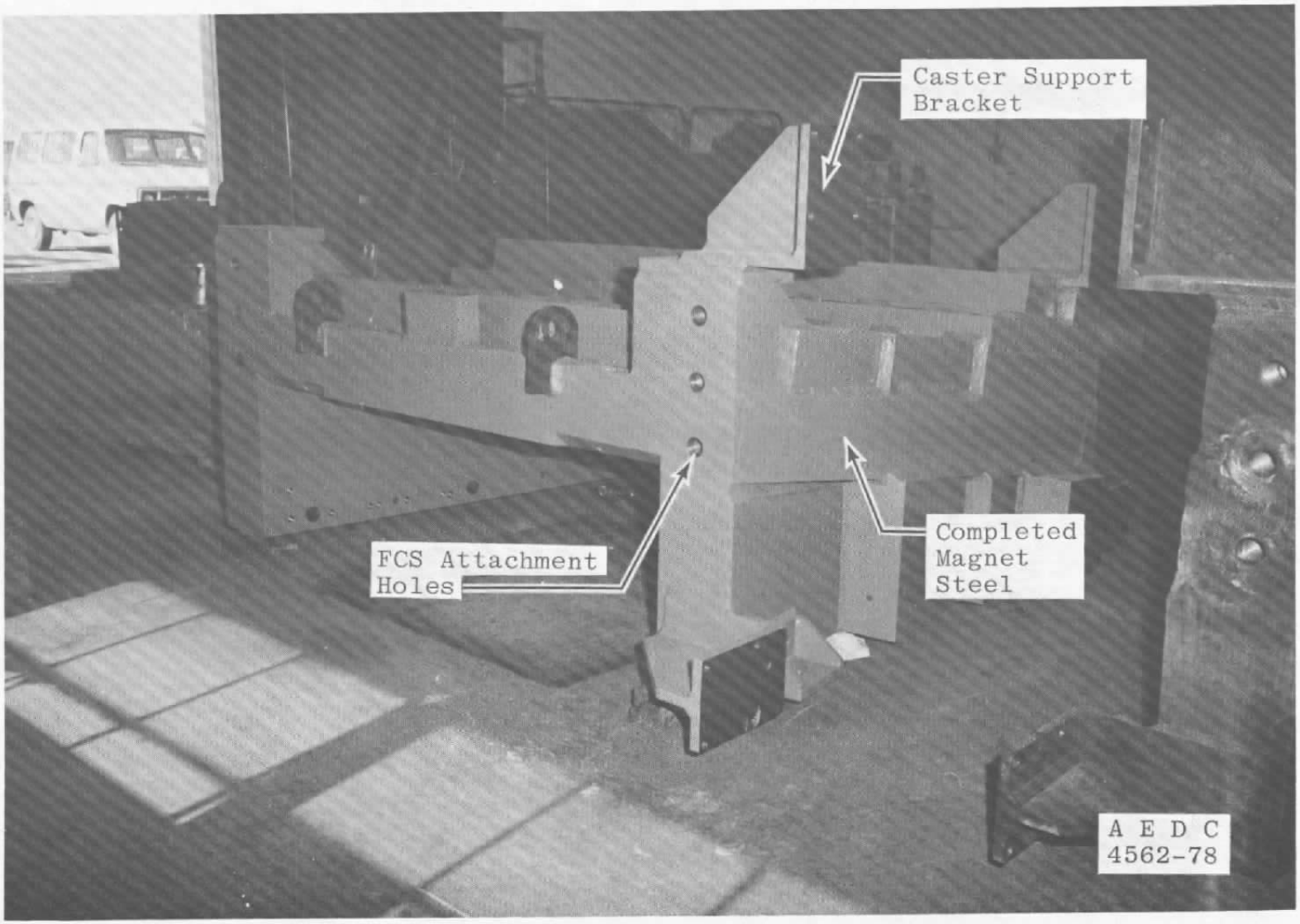

Figure 29. Modified HPMS magnet steel.

Figure 30. Axial force containment structures - before final cleaning and painting.

Figure 31. End turn force containment structure and attractive load spacers.

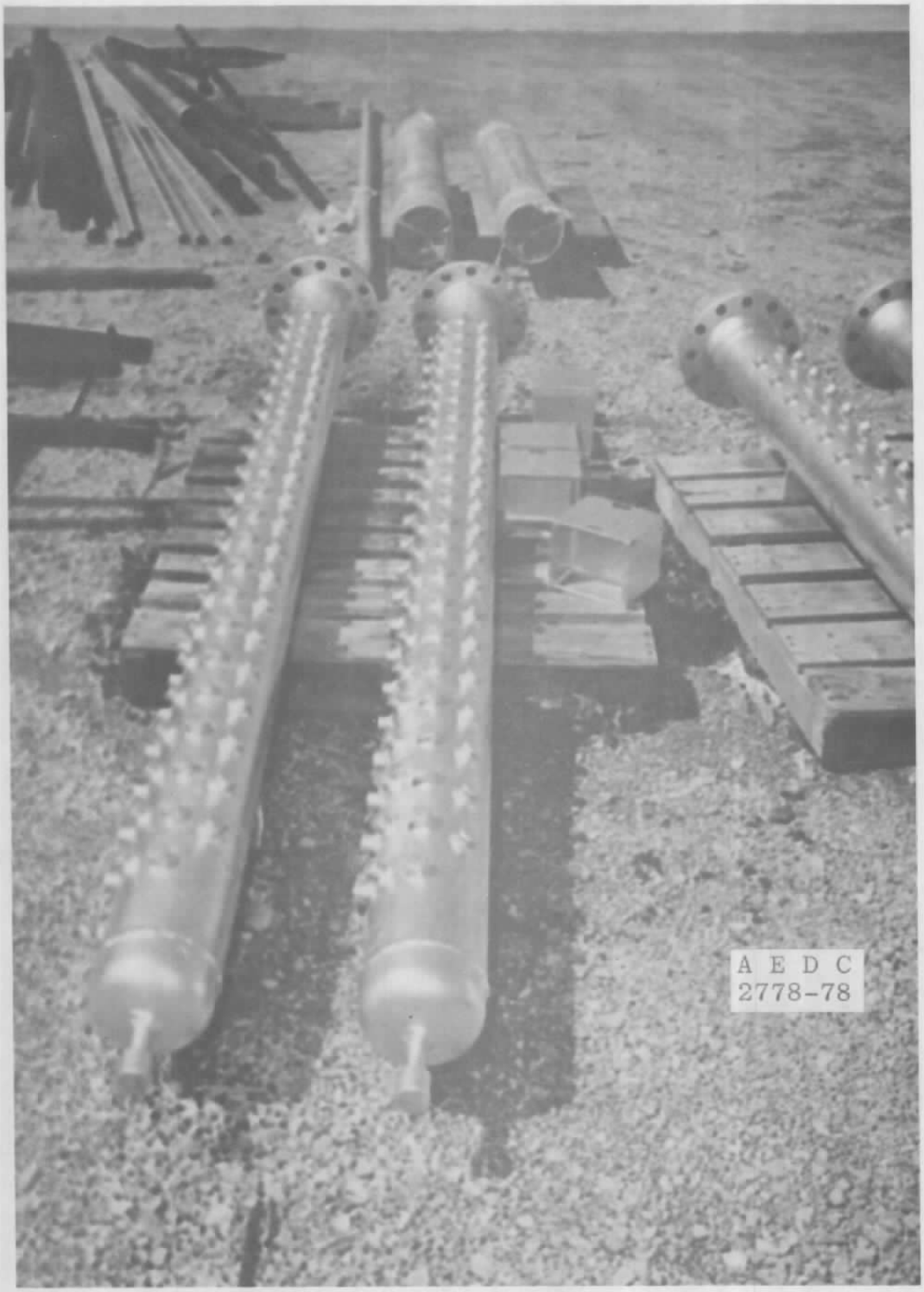

Figure 32. Water cooling manifolds.

Figure 33. Nonuniform spacing on coils no. 2 and no. 4.

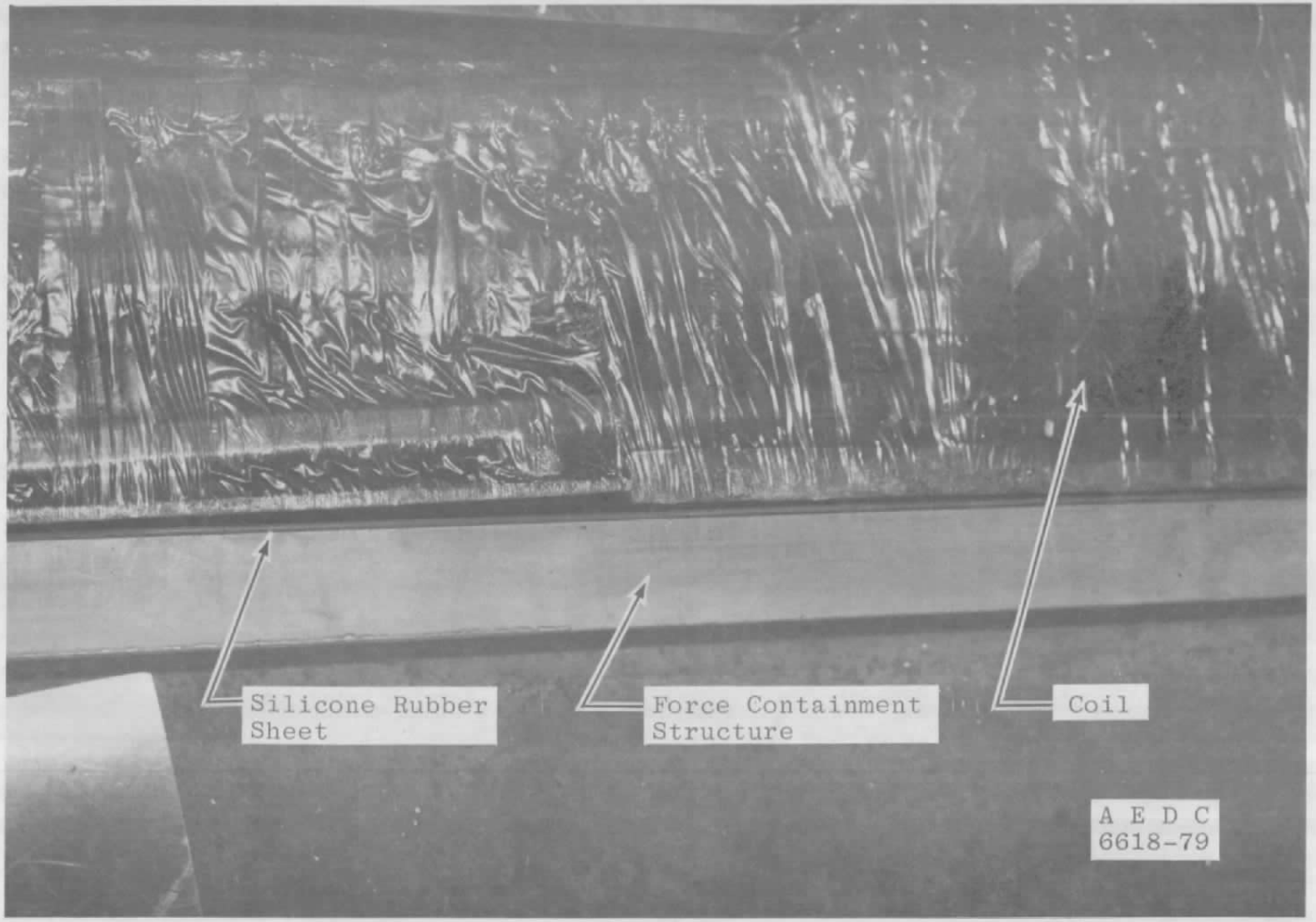

Figure 34. Nonuniform spacing between coil and FCS.

Figure 35. Nonuniform spacing between coils no. 2 and no. 4.

Figure 36. Nonuniform spacing between coils no. 2 and no. 4.

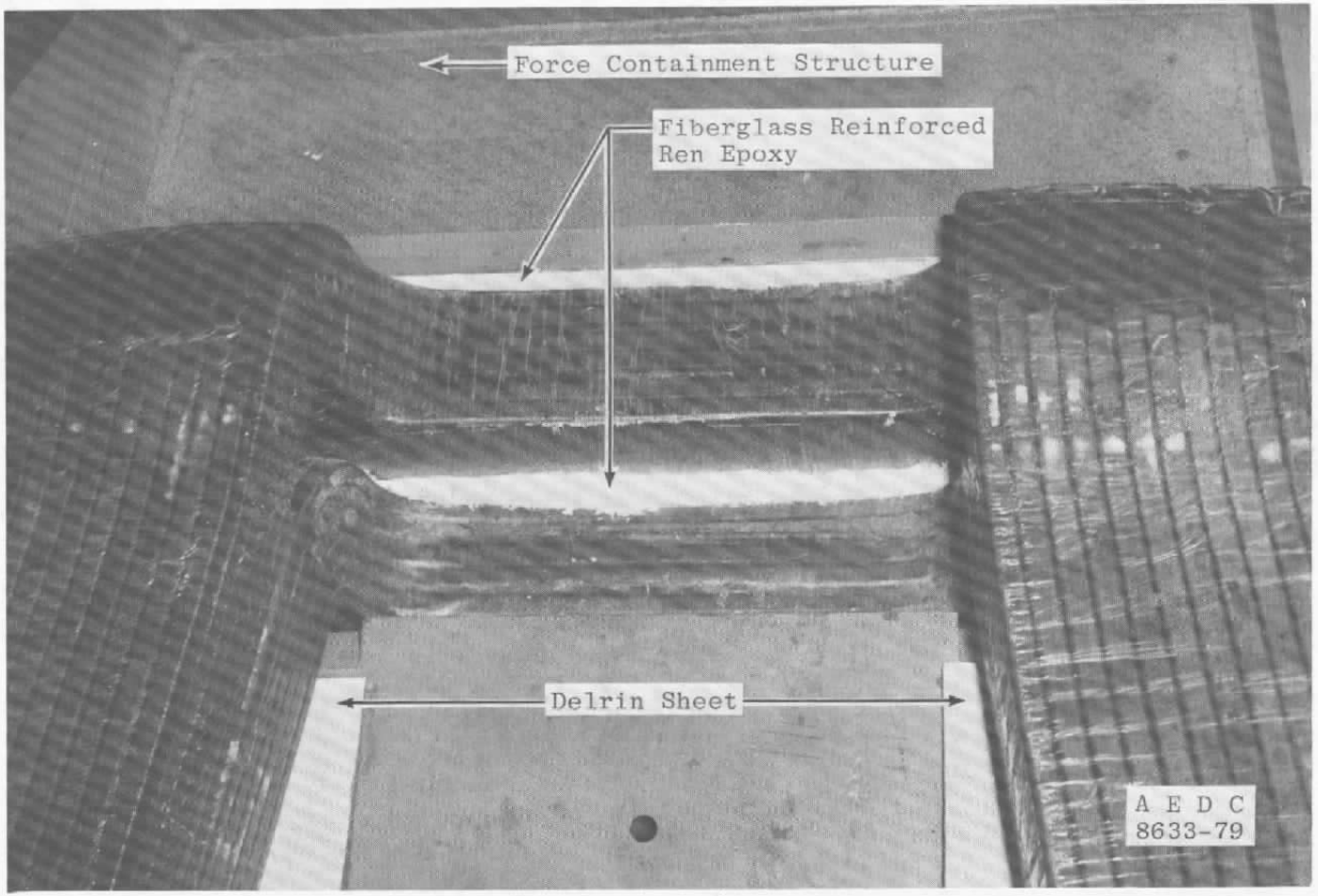

Figure 37. Saddle region after pouring of the epoxy.

Figure 38. Force containment structure beams installed.

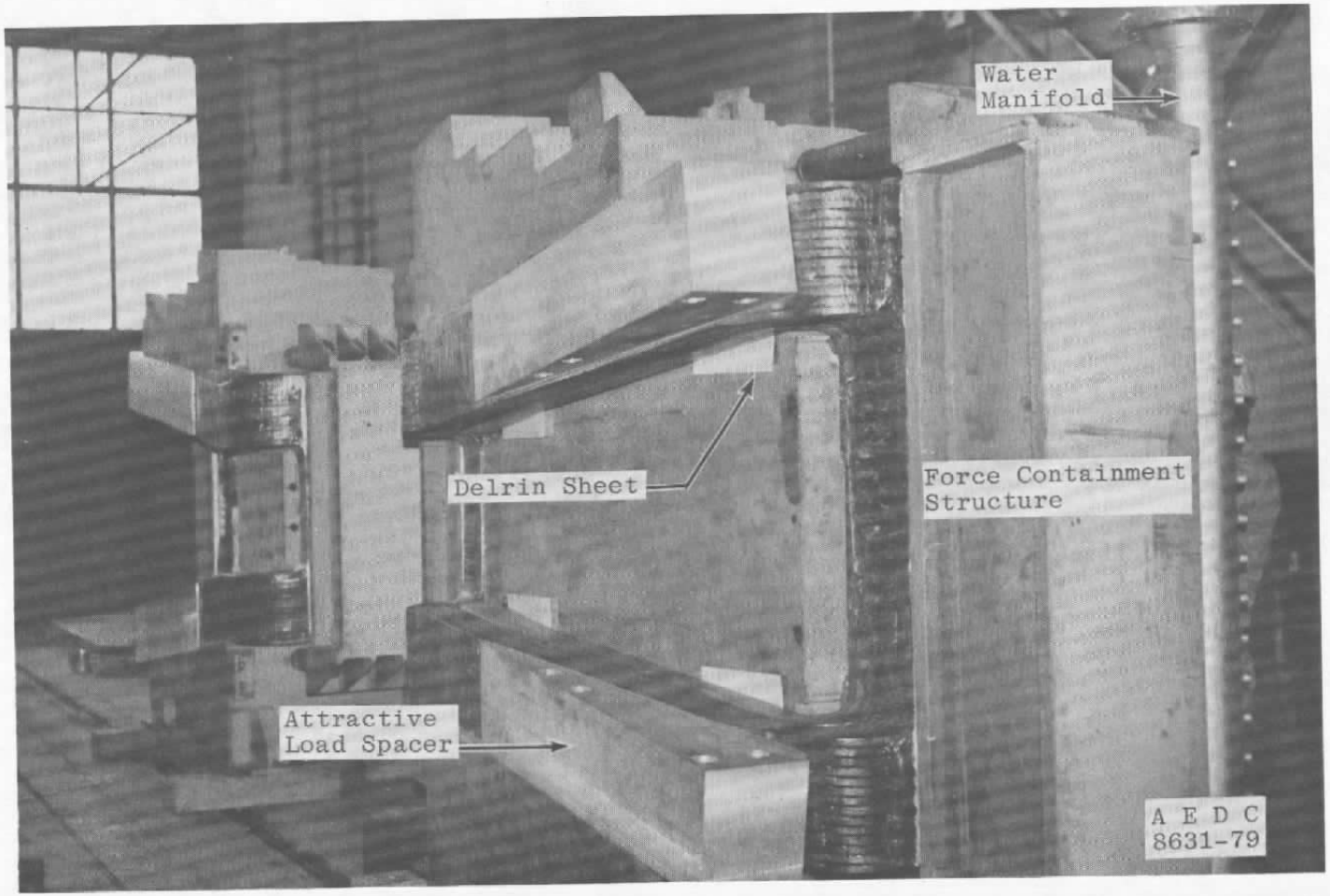

Figure 39. Assembled magnet halves.

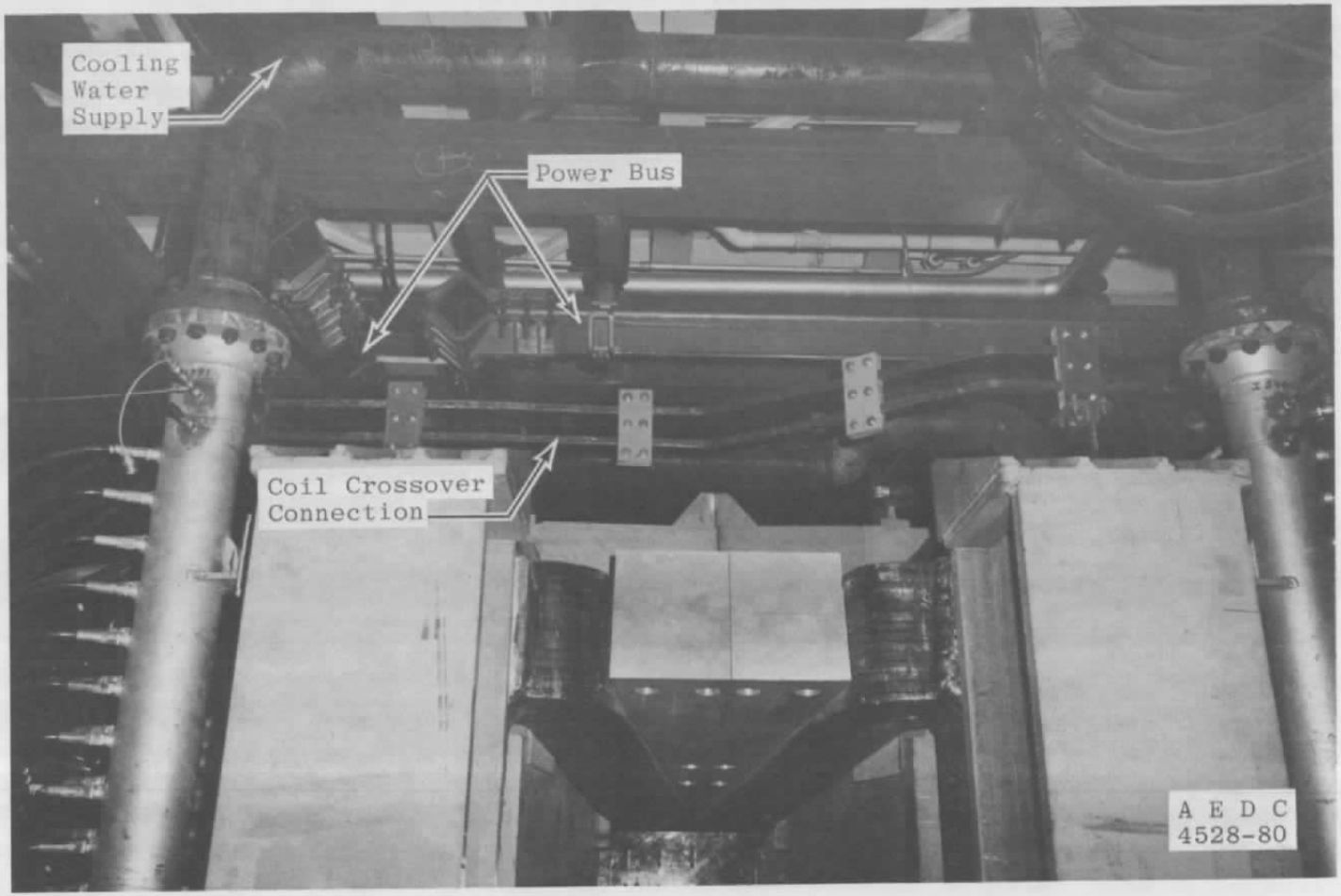

Figure 40. HPMS magnet.

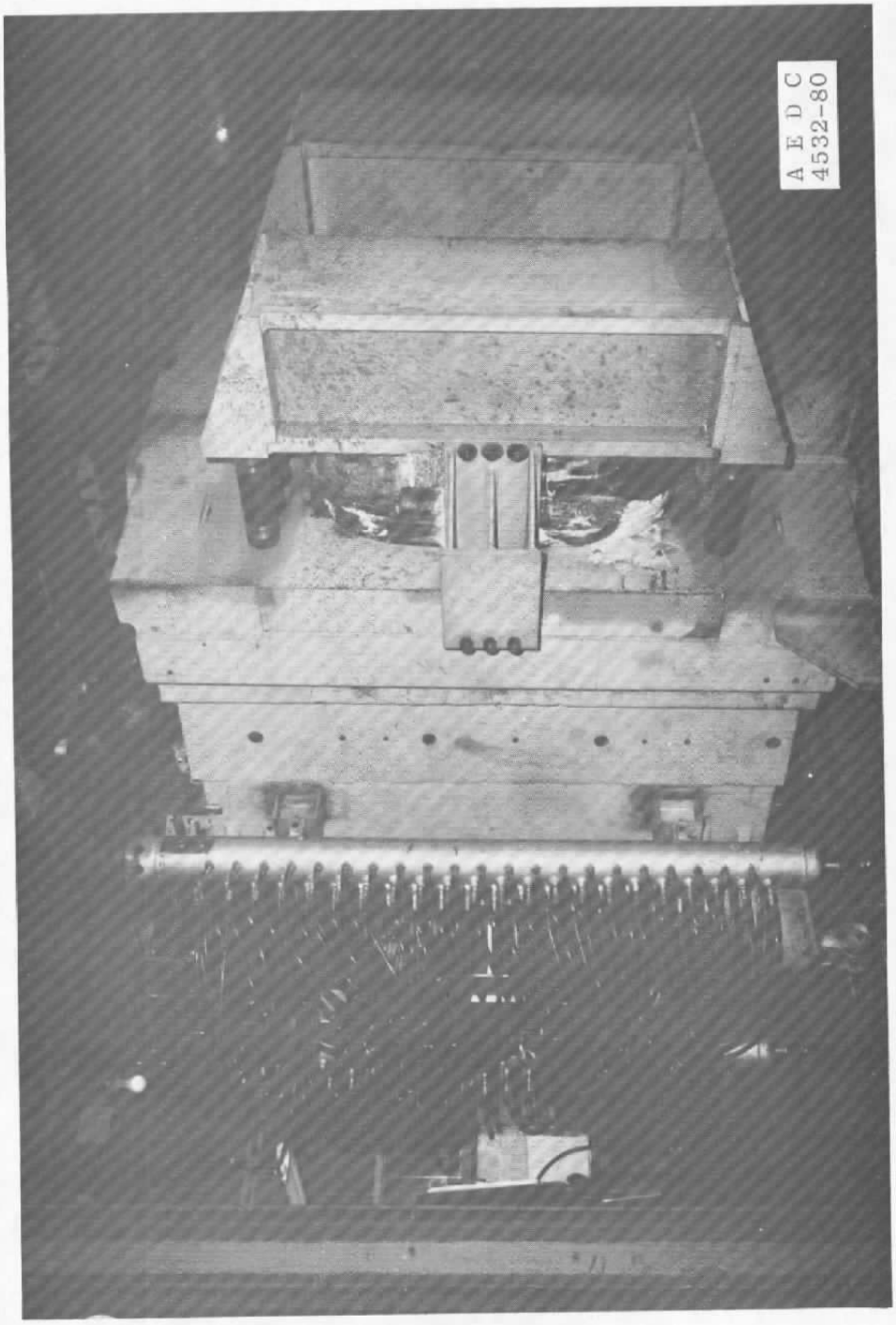

Figure 41. HPMS magnet as installed.

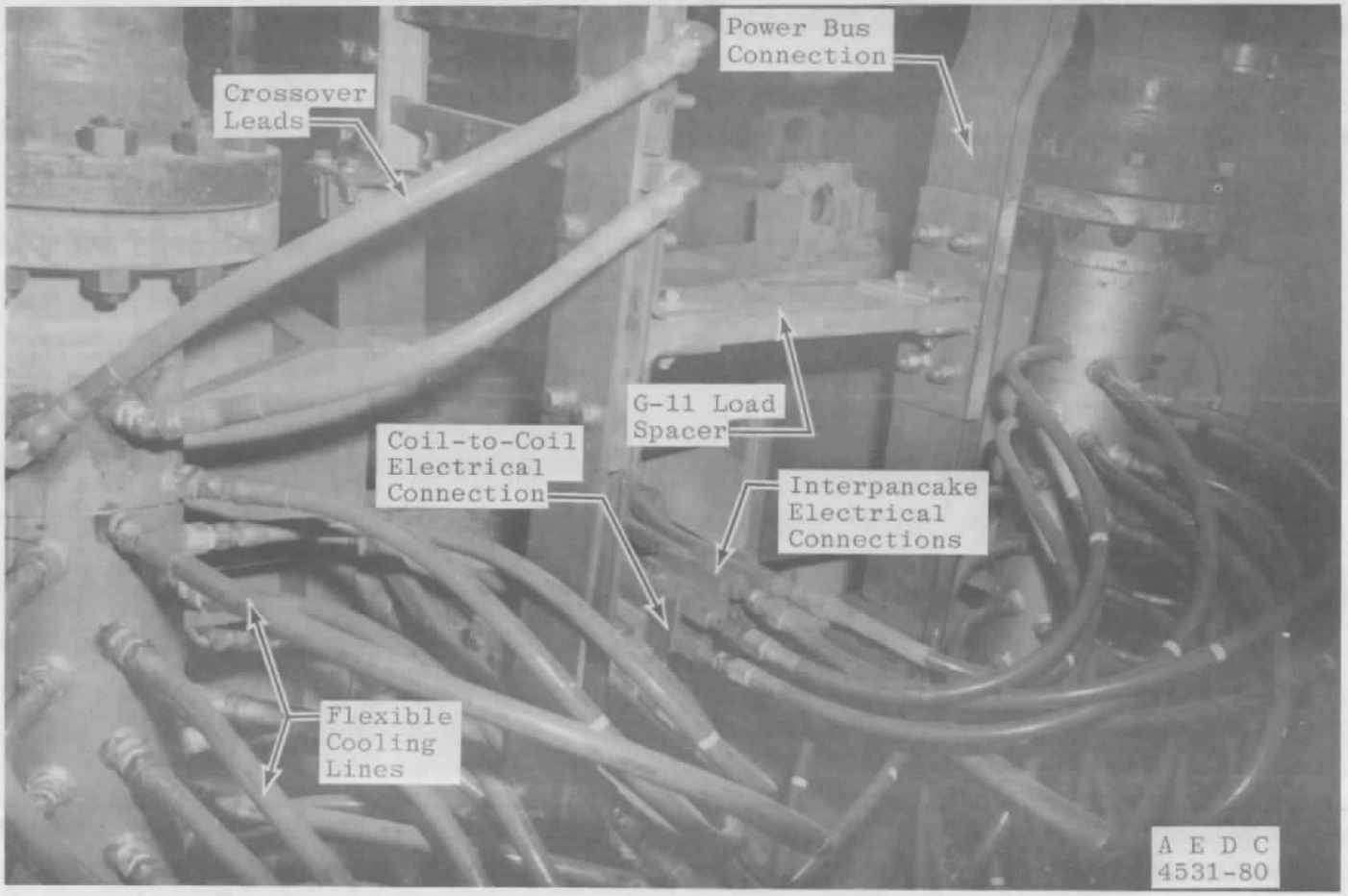

Figure 42. Closeup photograph of the cooling, power, and electrical connections.

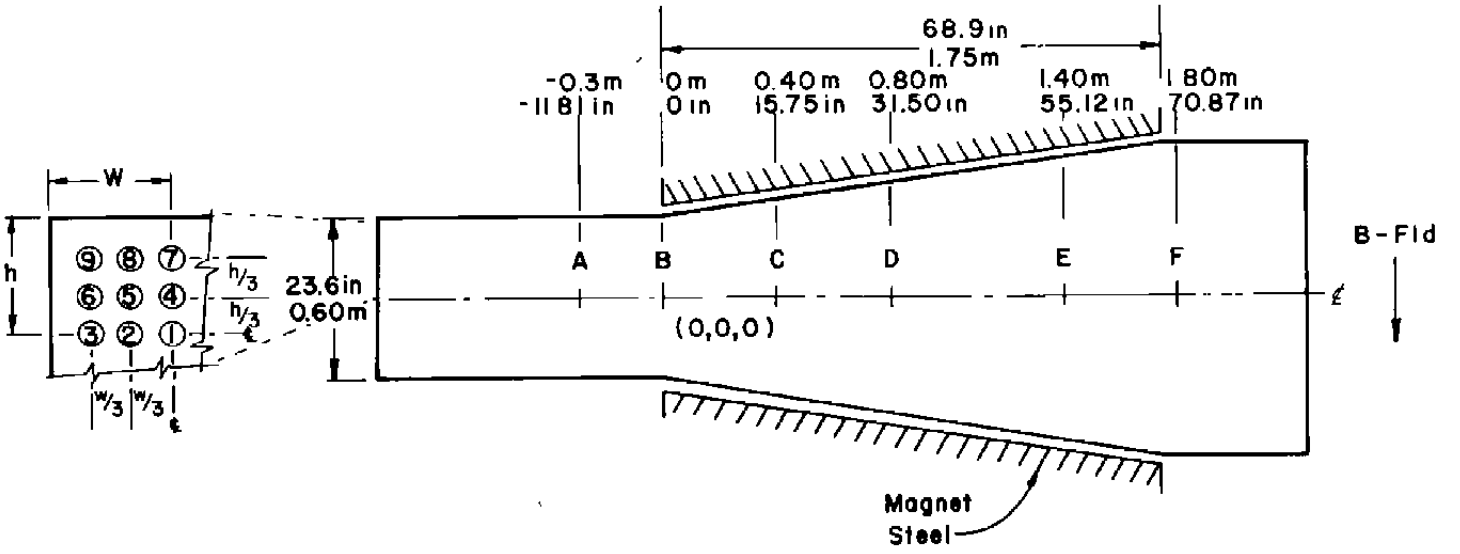

Figure 43. Location of HPMS Hall probes.

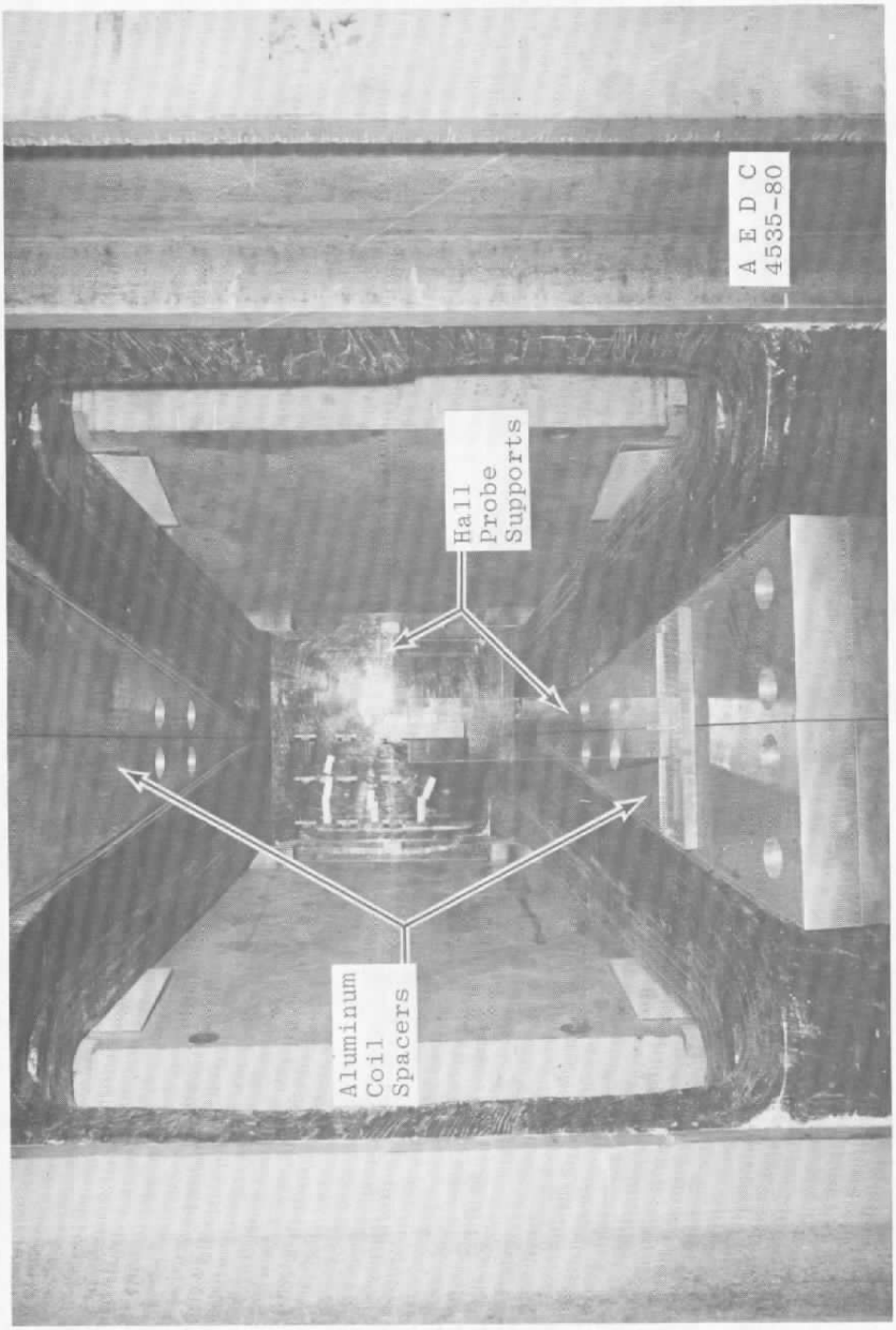

Figure 44. HPMS magnet.

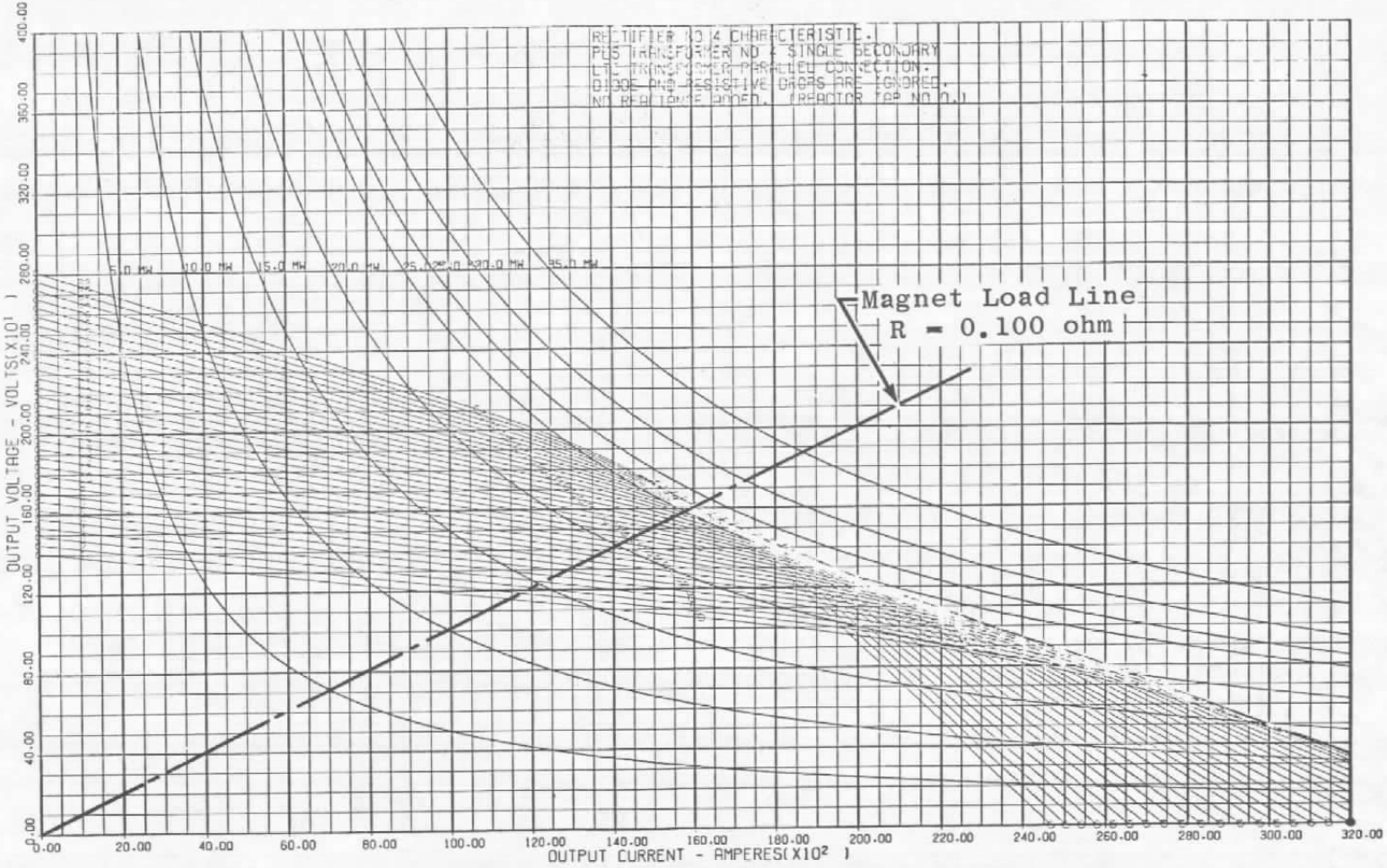

Figure 45. Power supply performance curves with no external reactance, reactor tap 0.

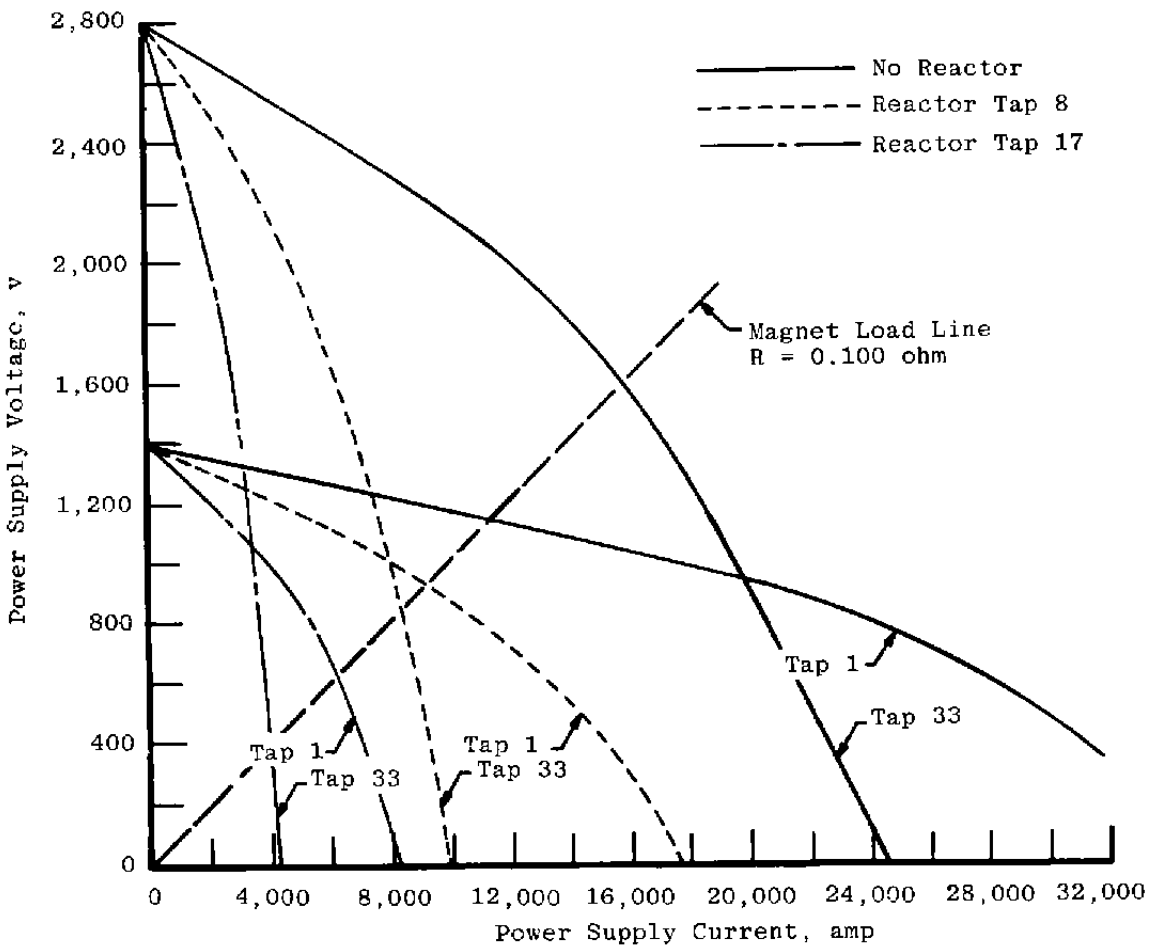

Figure 46. Power supply performance curves for several transformer and reactor tap settings.

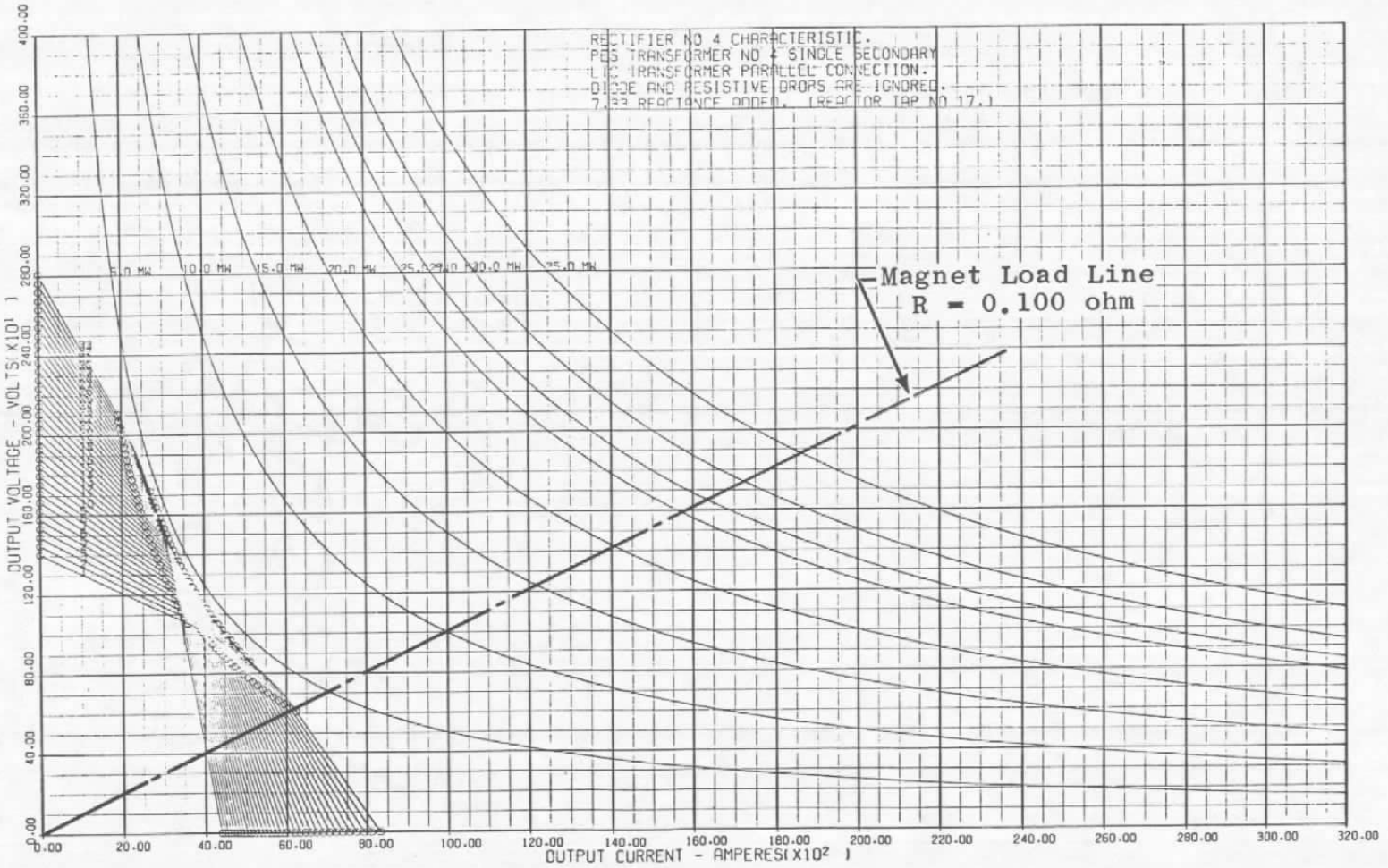

Figure 47. Power supply performance curves with maximum external reactance, reactor tap 17.

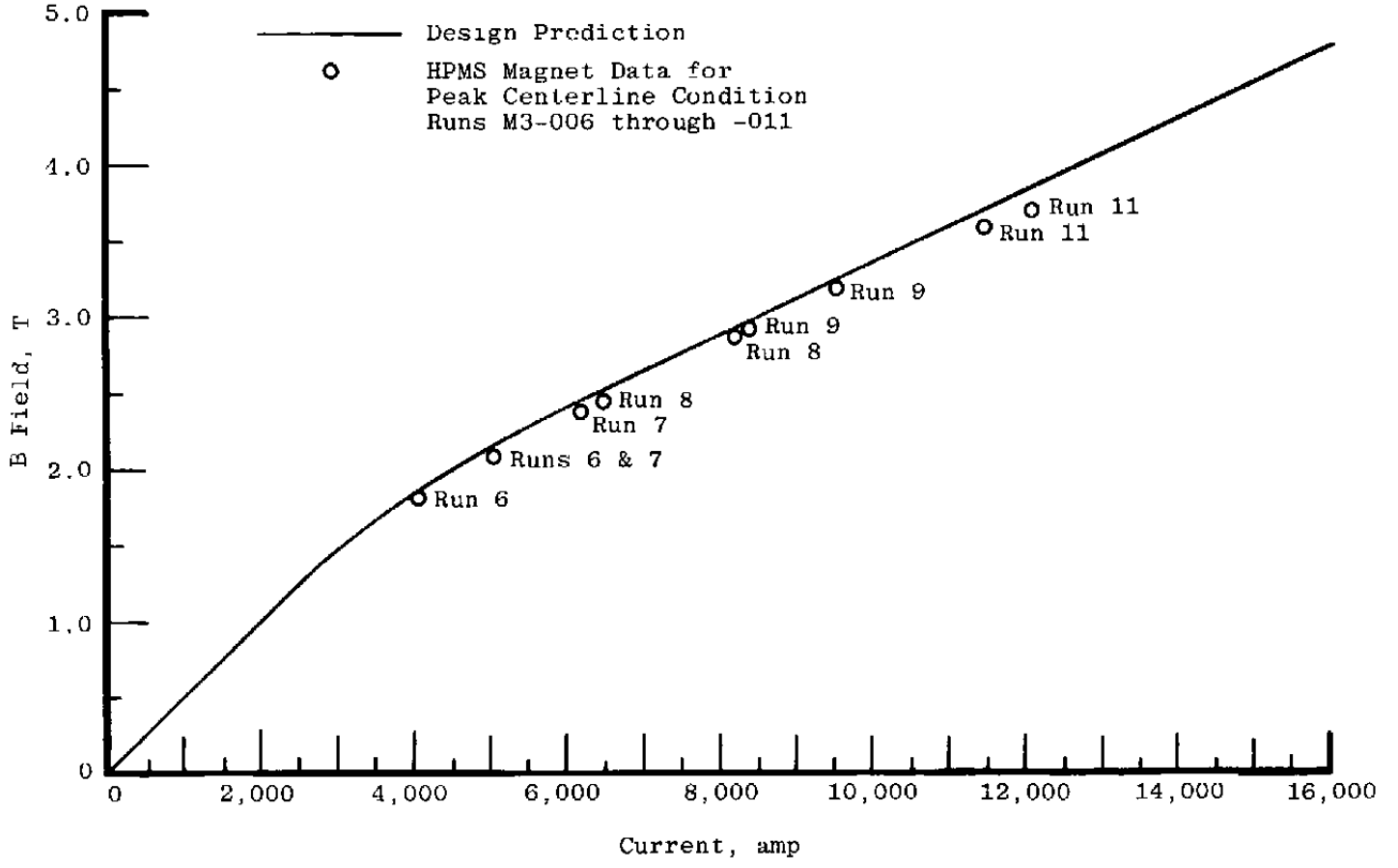

Figure 48. HPMS magnet steady-state characteristics.

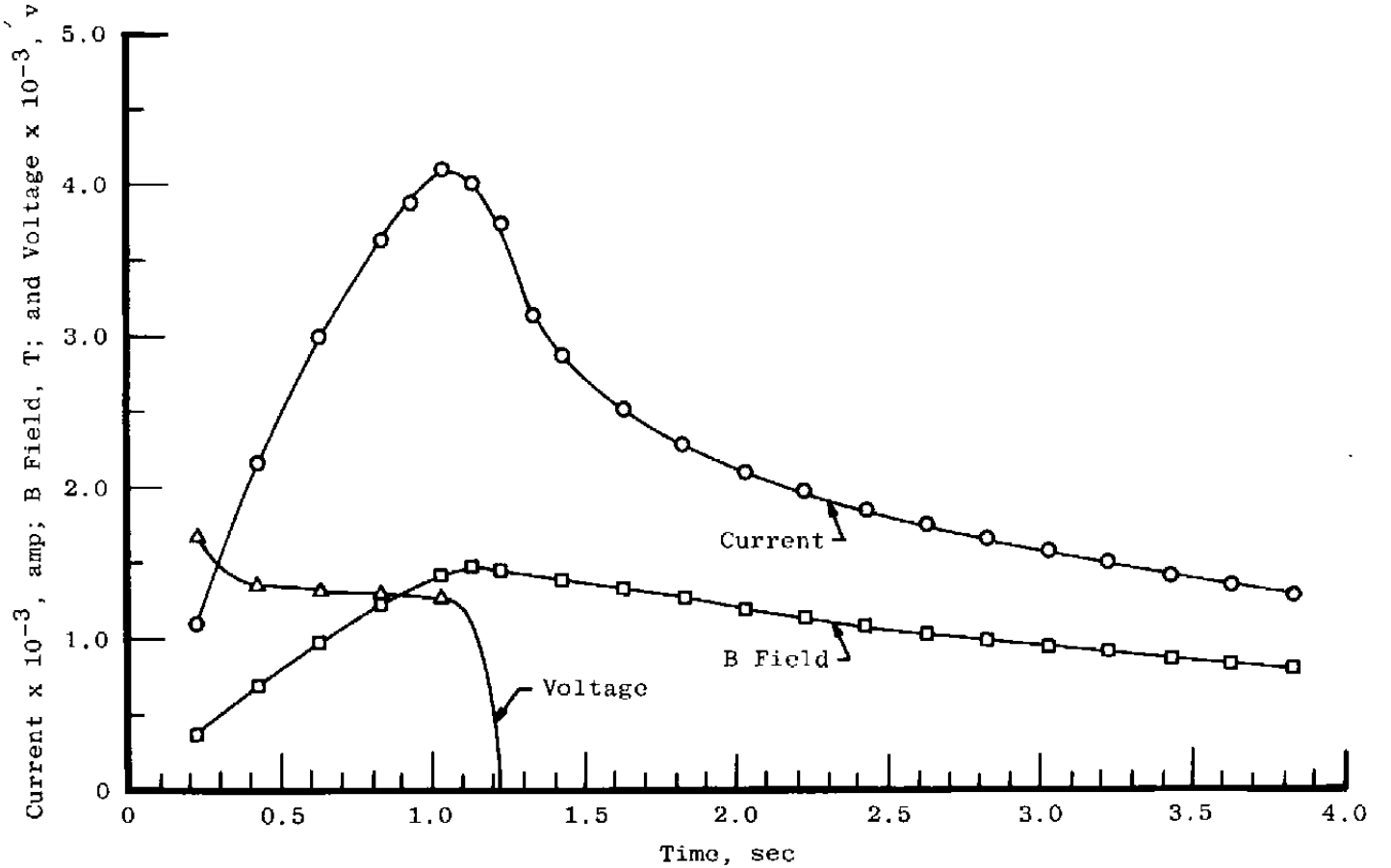

Figure 49. Performance variation with time on run M3-003, reactor tap 17, transformer tap 17.

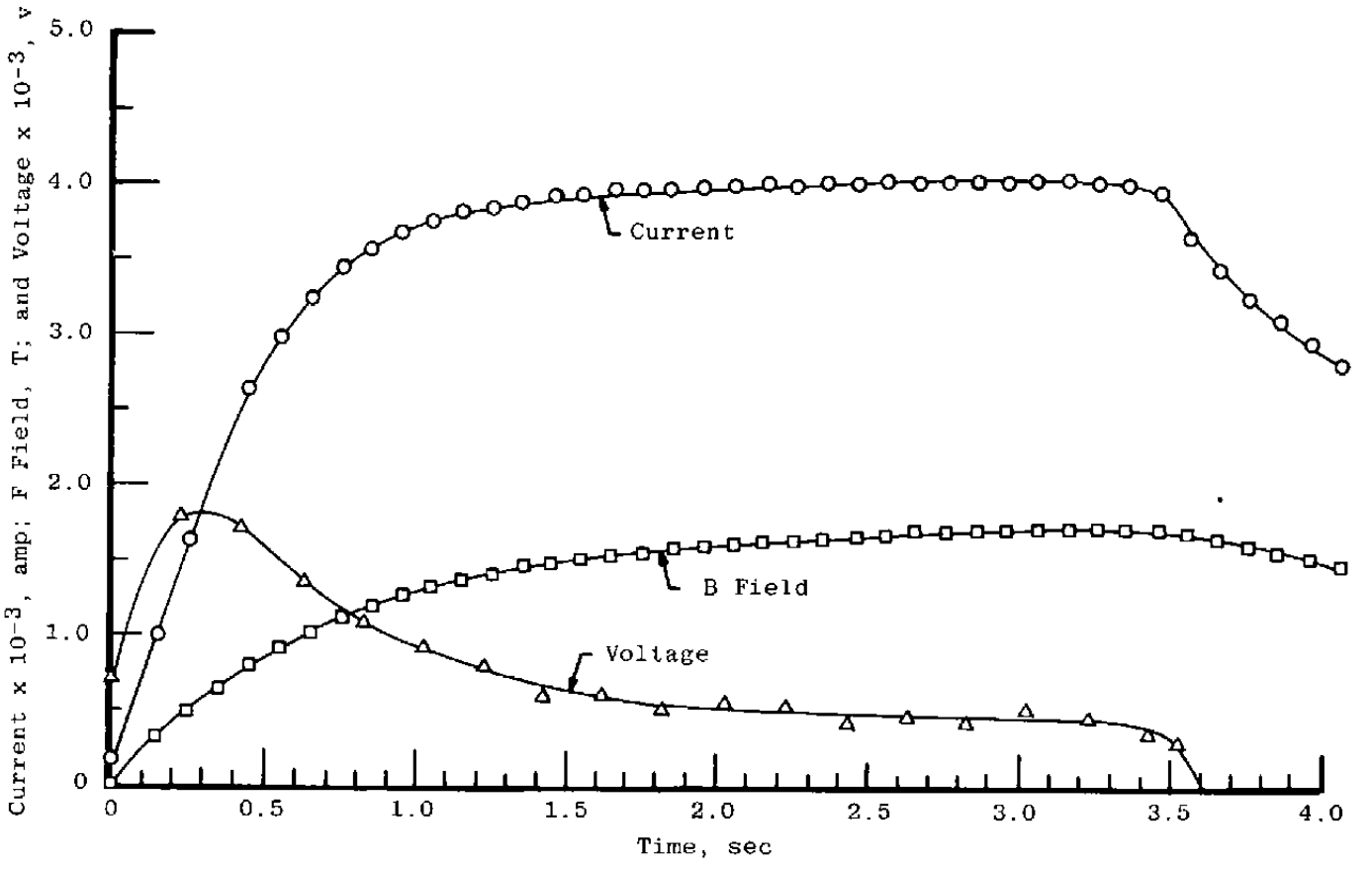

Figure 50. Performance variation with time on run M3-004, reactor tap 17, transformer tap 33.

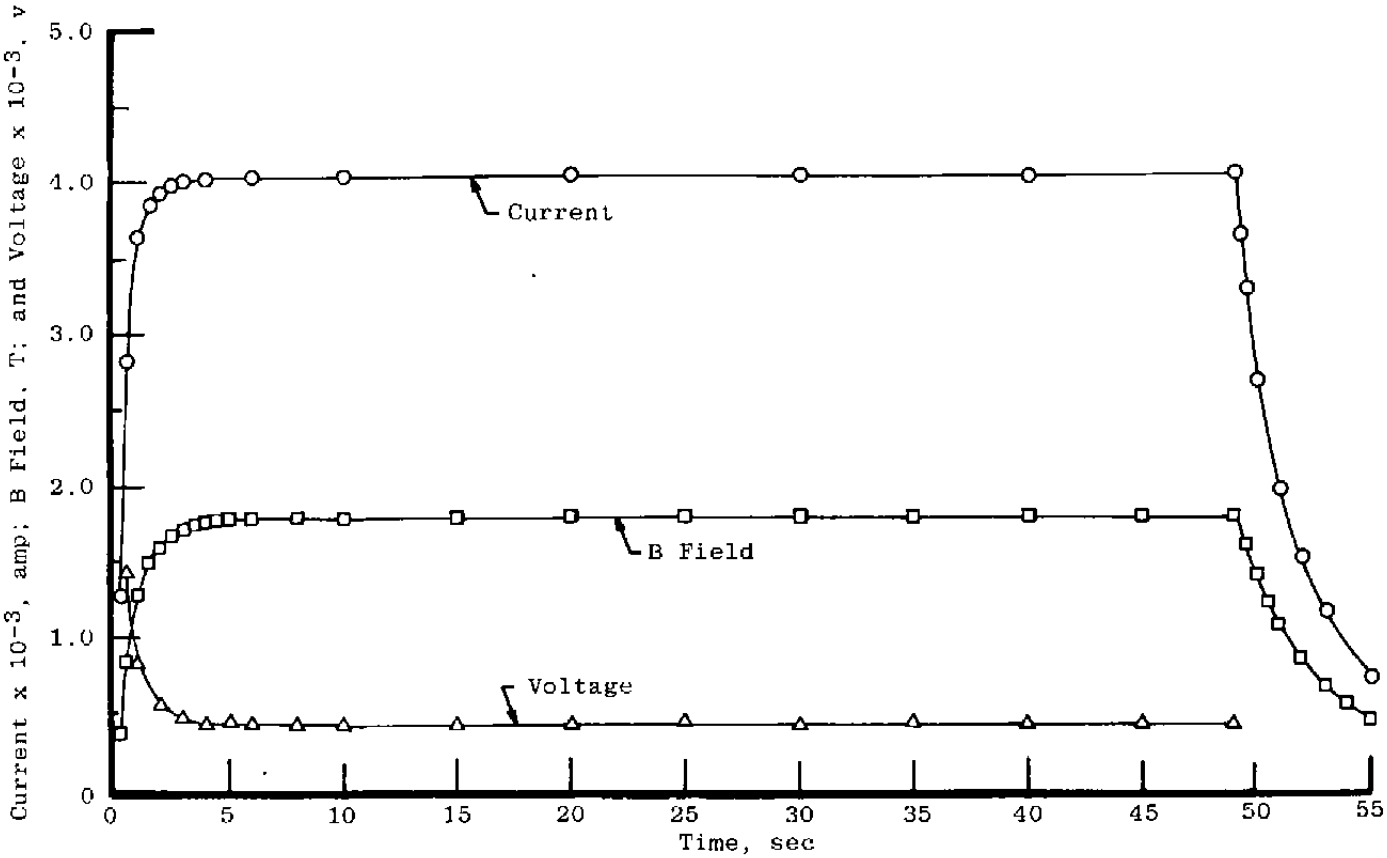

Figure 51. Performance variation with time on run M3-005, reactor tap 17, transformer tap 33.

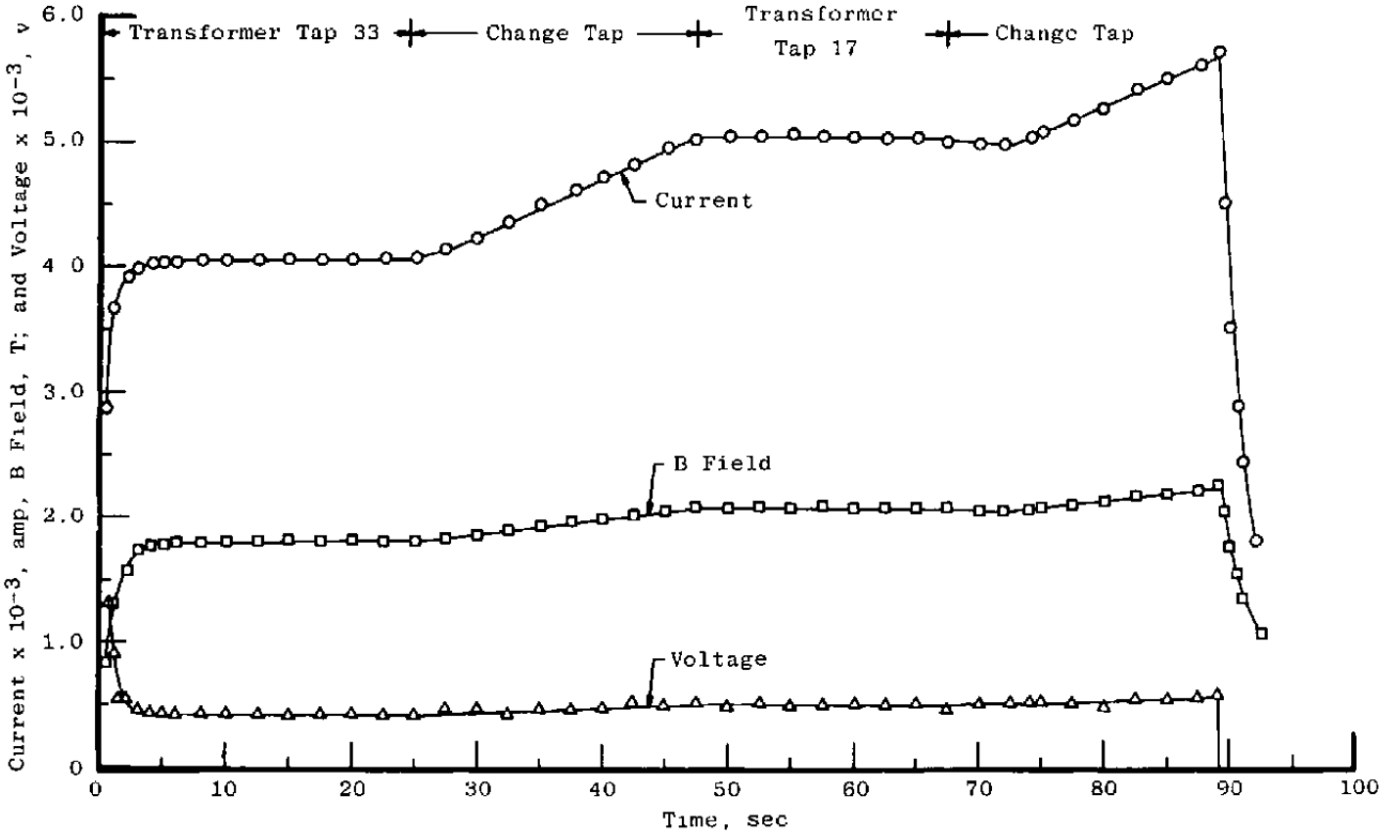

Figure 52. Performance variation with time on run M3-006, reactor tap 17.

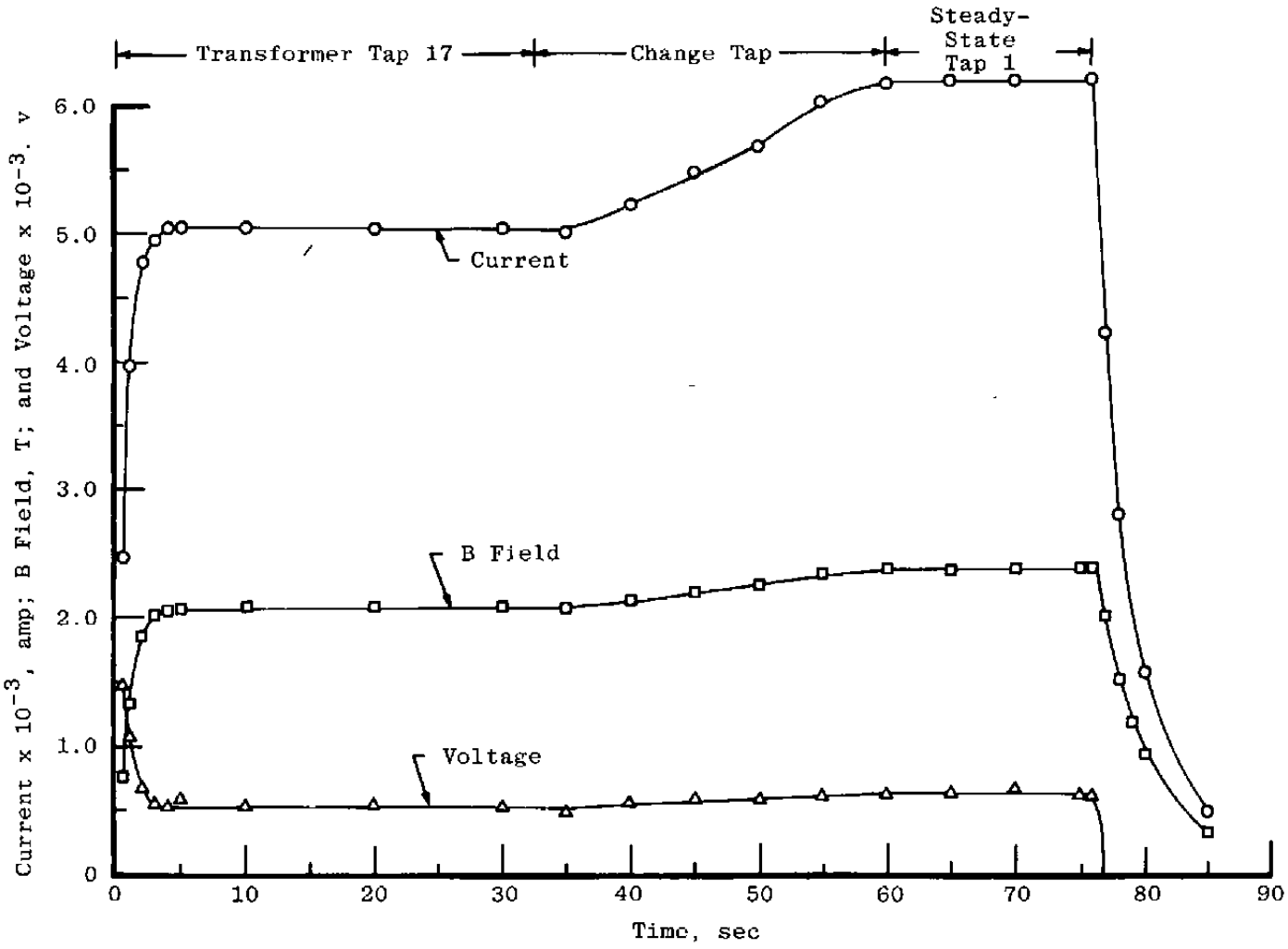

Figure 53. Performance variation with time on run M3-007, reactor tap 17.

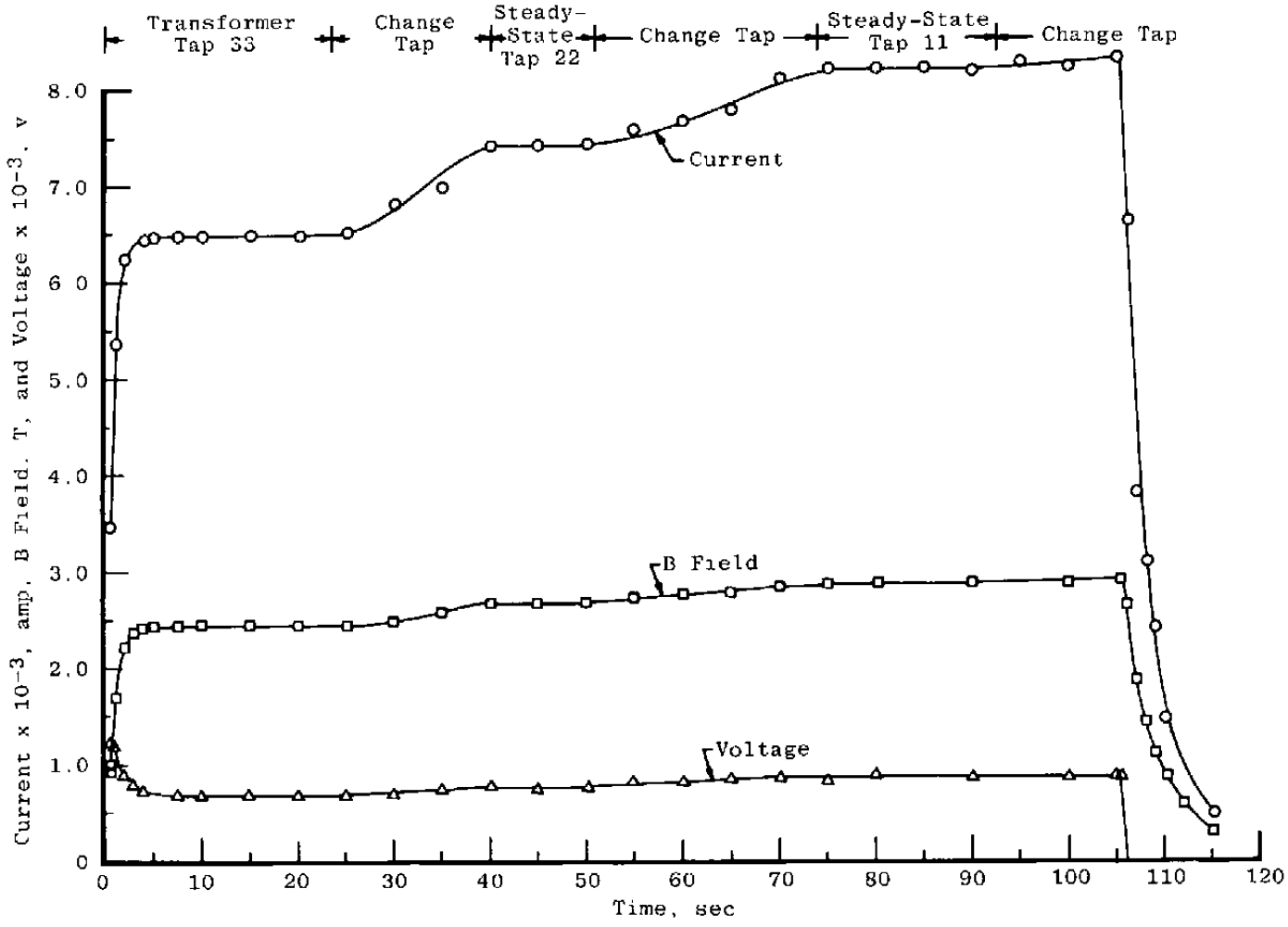

Figure 54. Performance variation with time on run M3-008, reactor tap 10.

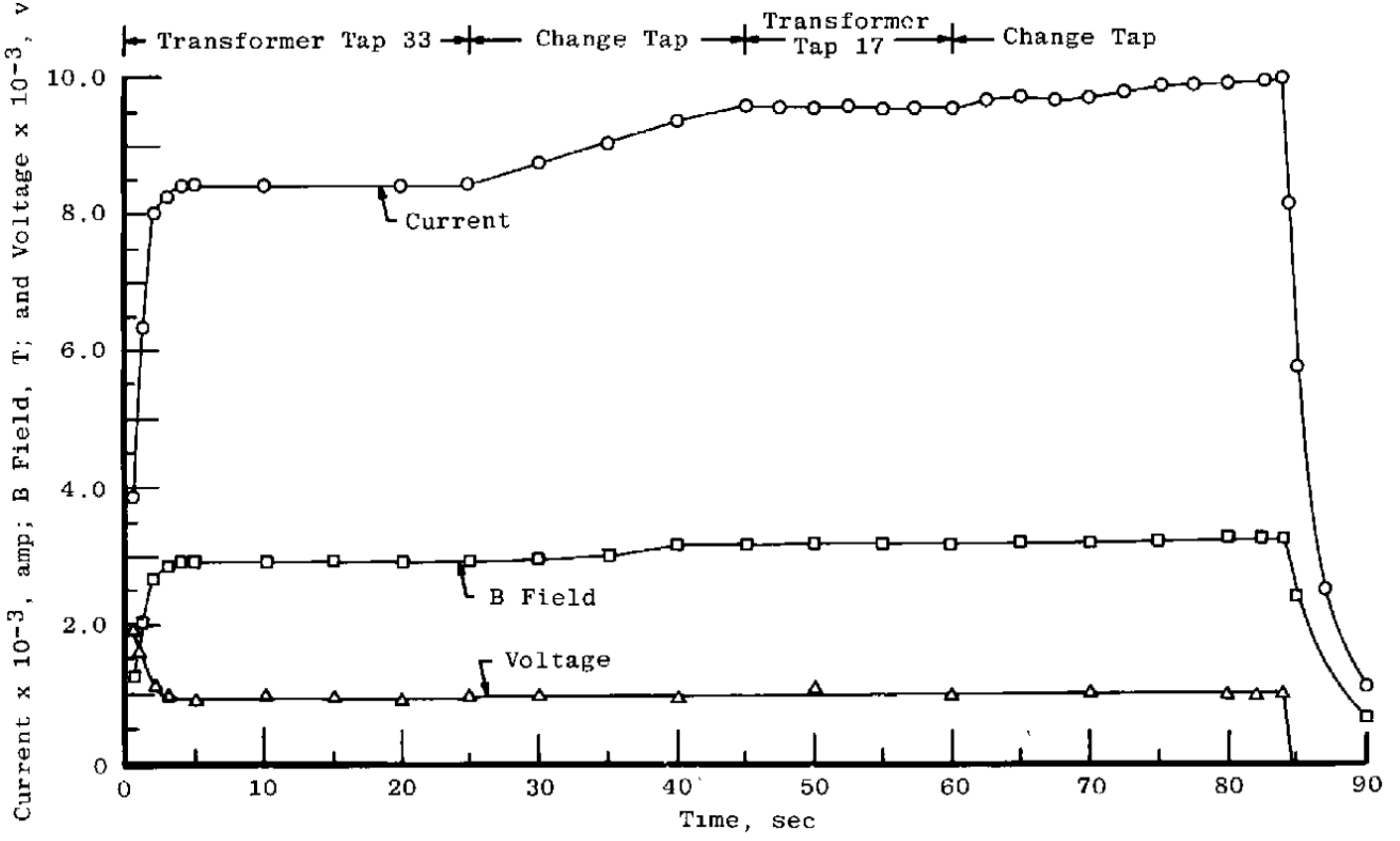

Figure 55. Performance variation with time on run M3-009, reactor tap 8.

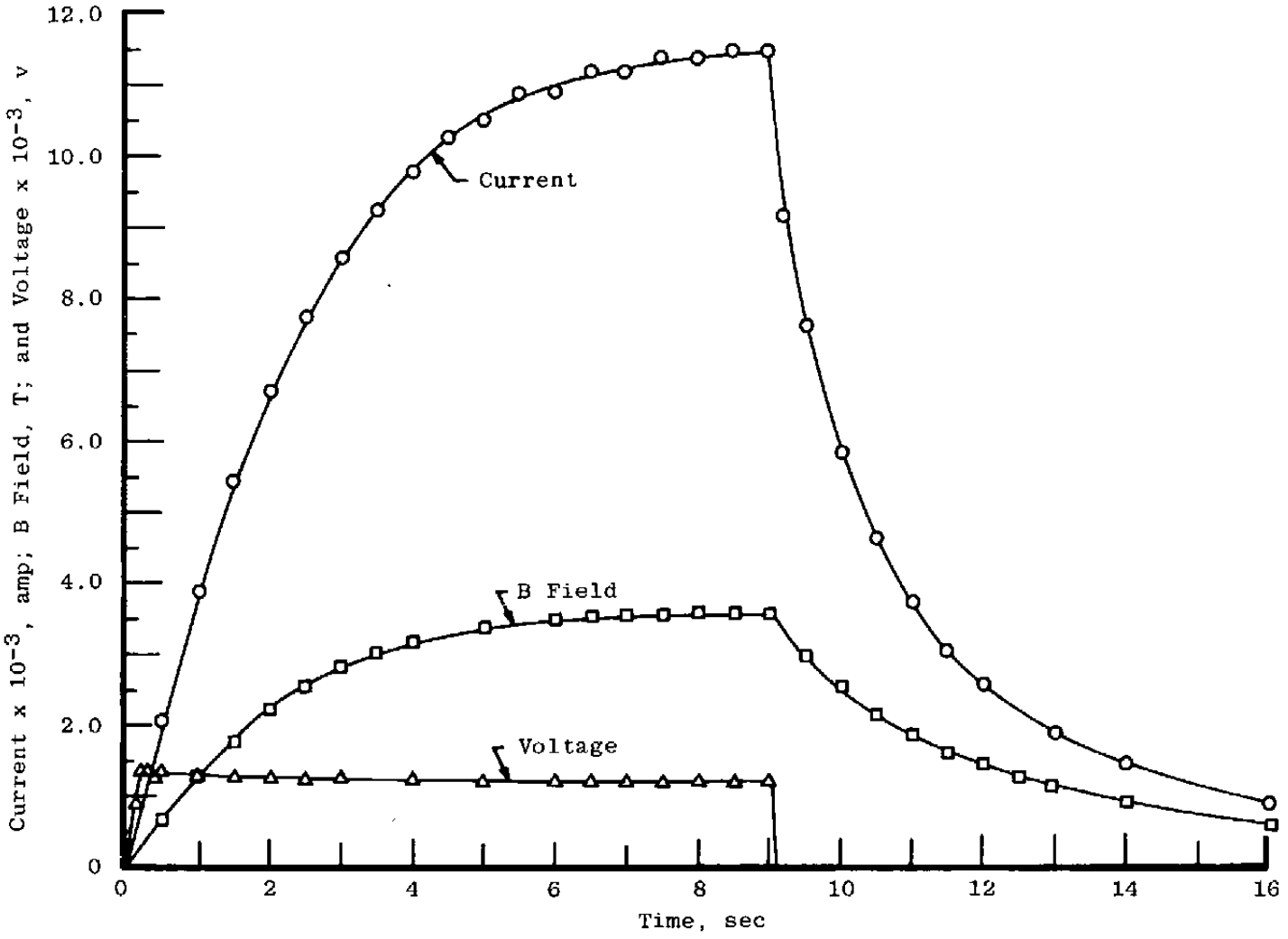

Figure 56. Performance variation with time on run M3-010, reactor tap 0, transformer tap 1.

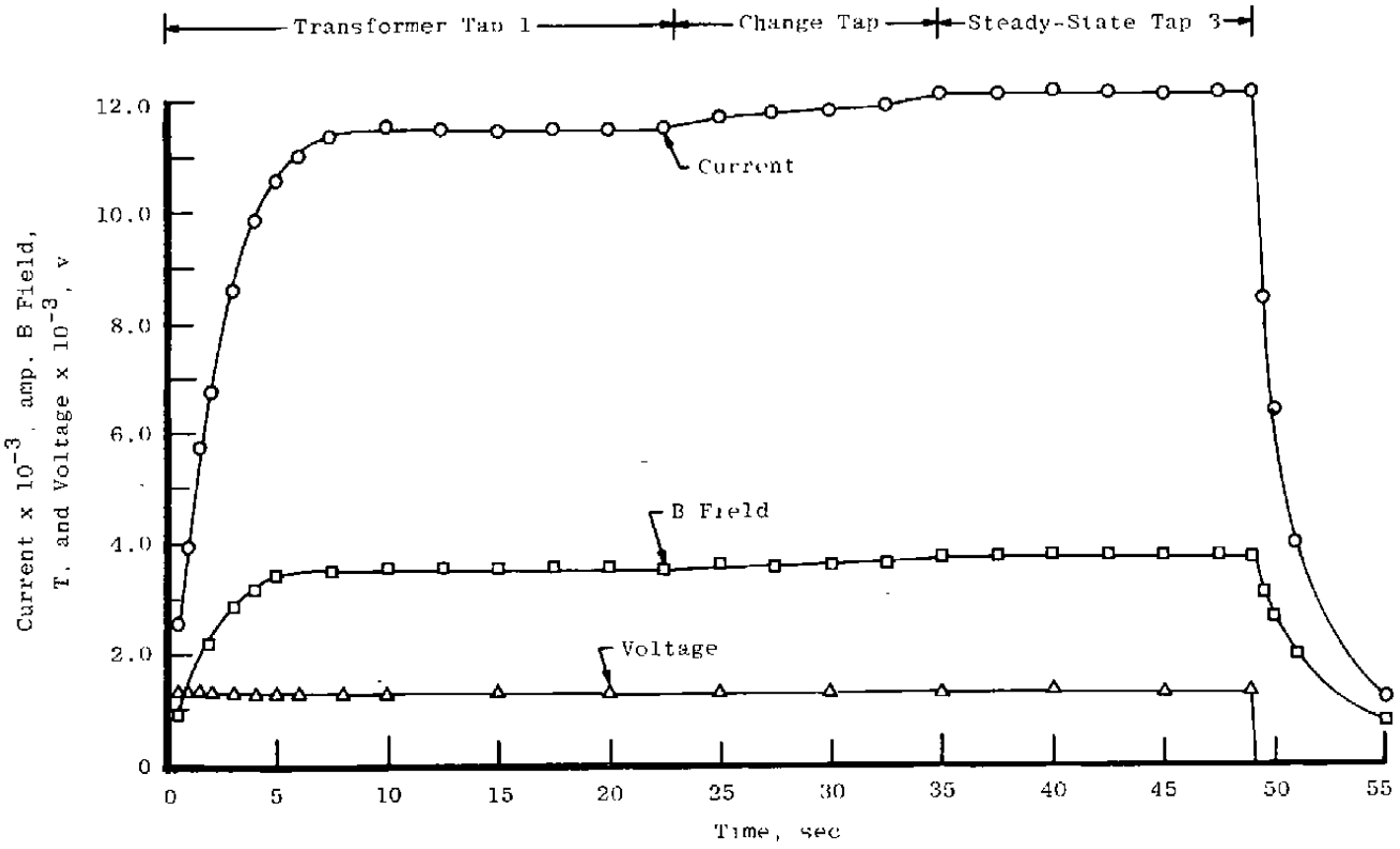

Figure 57. Performance variation with time on run M3-011, reactor tap 0.

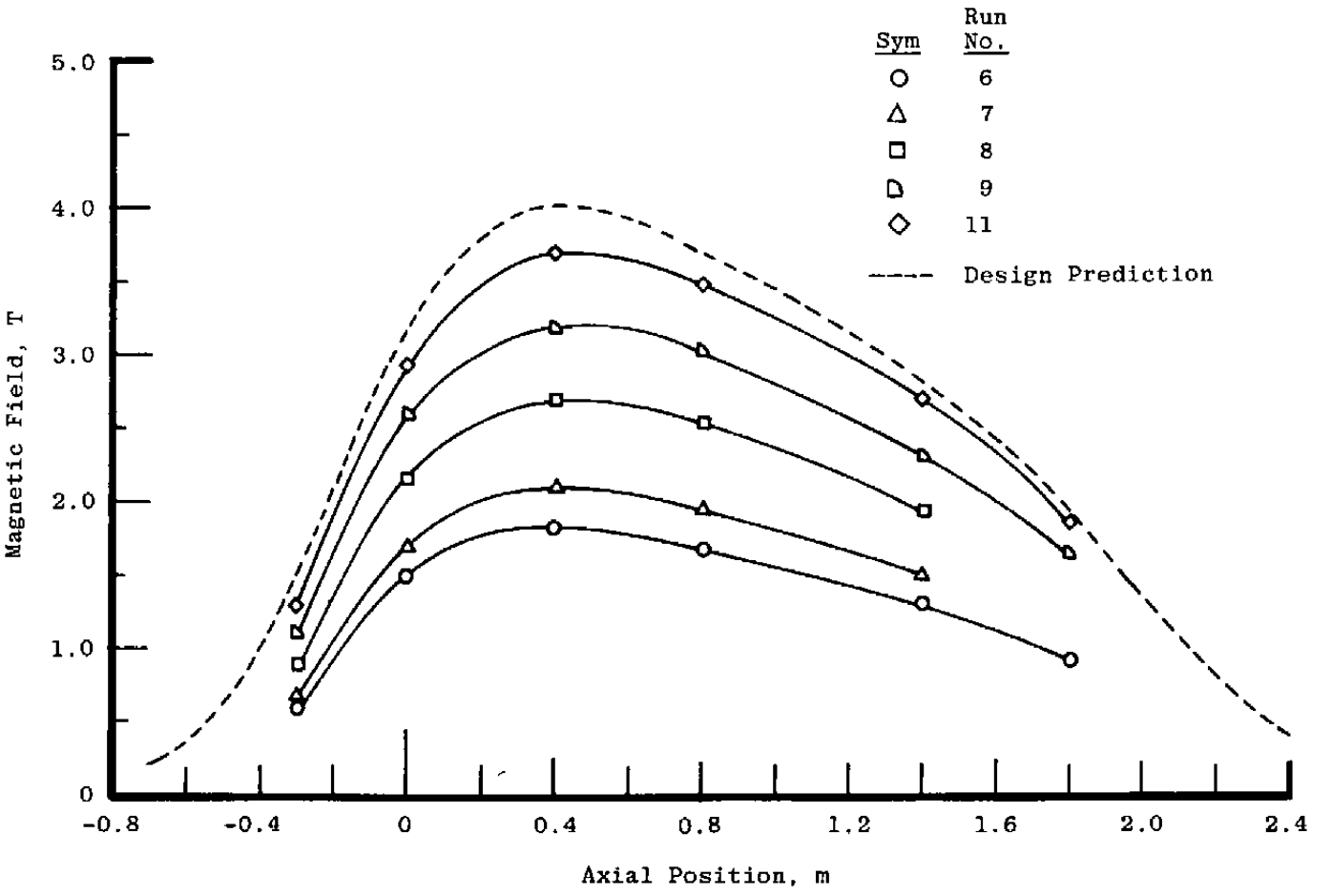

Figure 58. Axial magnetic field strength profile on magnet centerline.

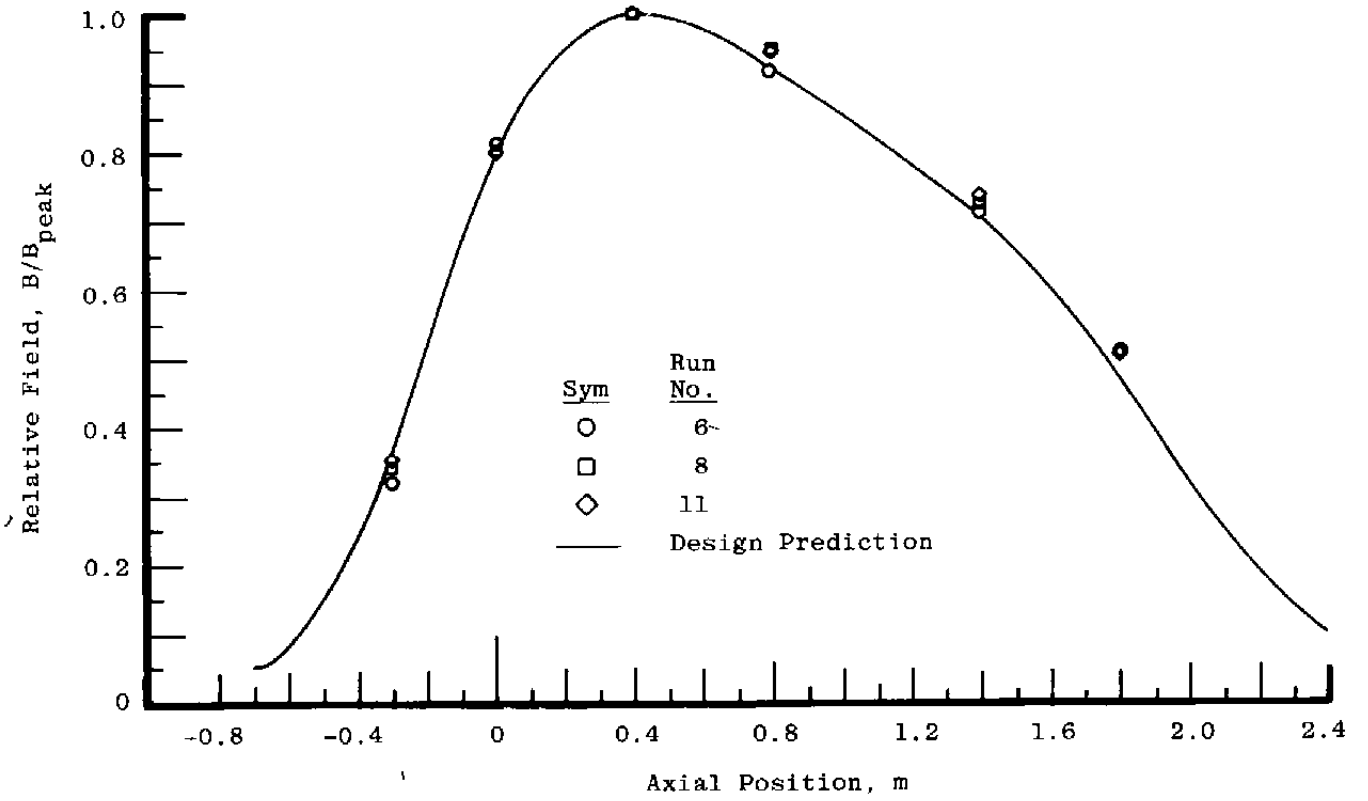

Figure 59. Normalized axial magnet field strength profile on magnet centerline.

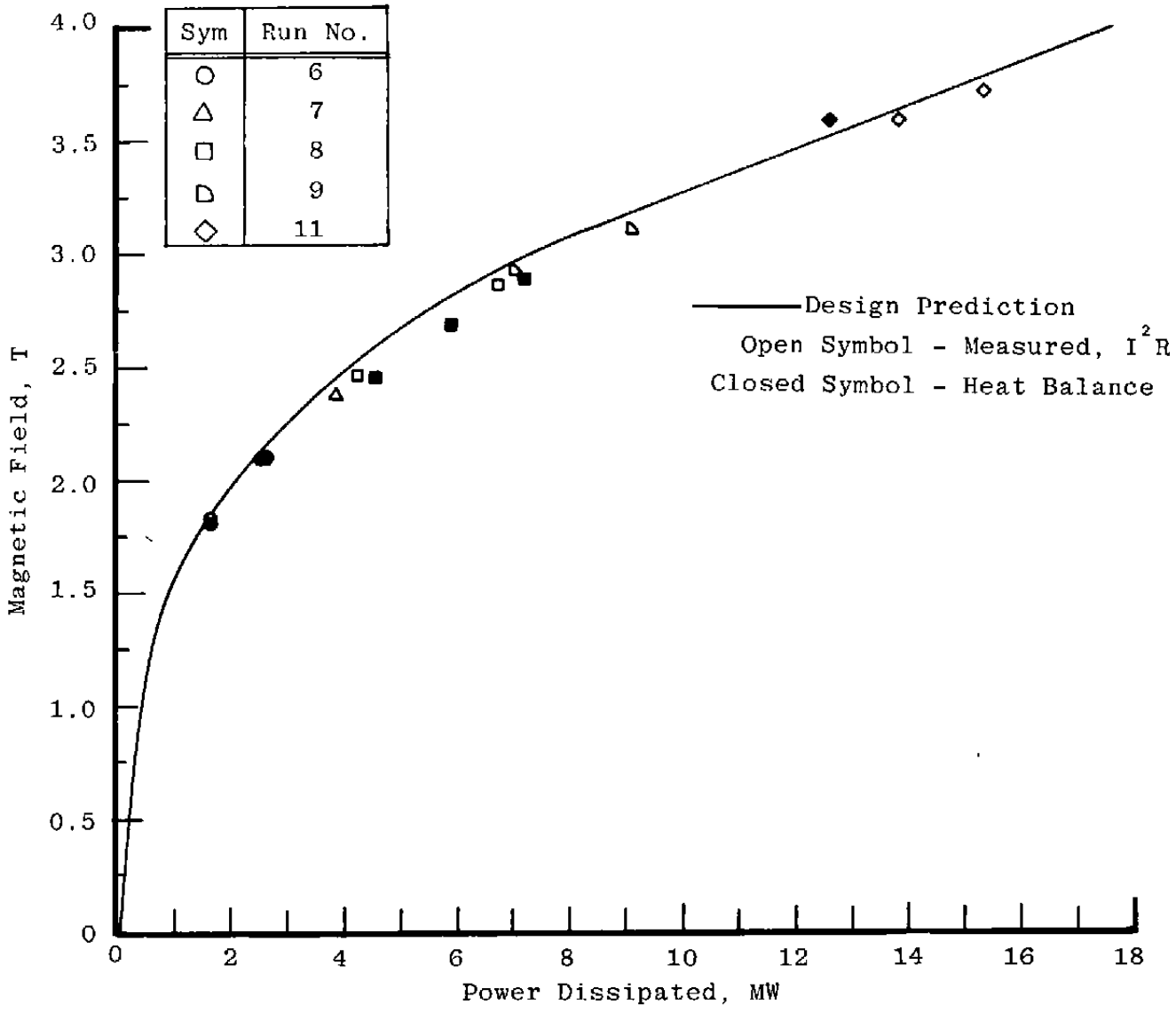

Figure 60. Power requirement versus peak magnetic field strength.

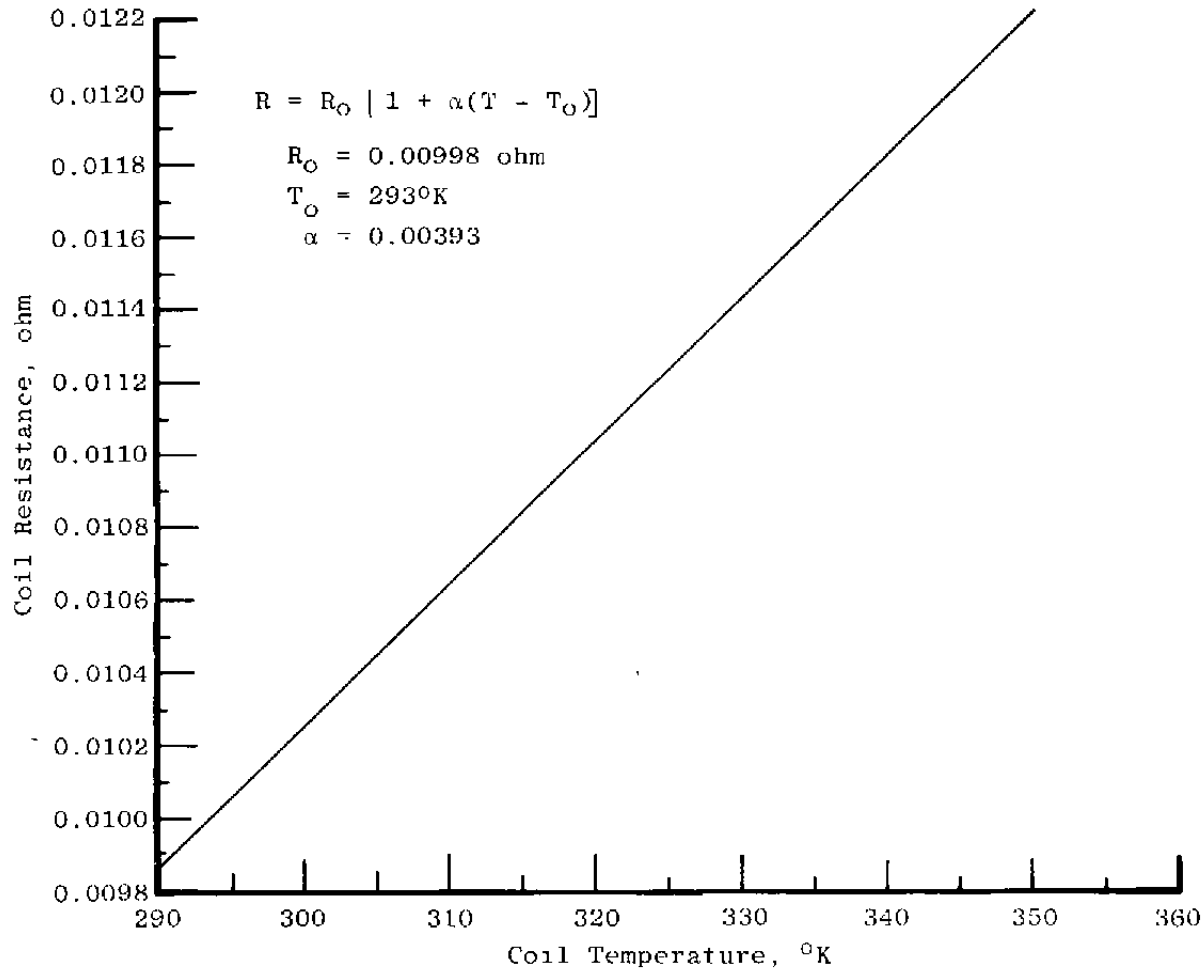

Figure 61. Coil resistance versus coil temperature.

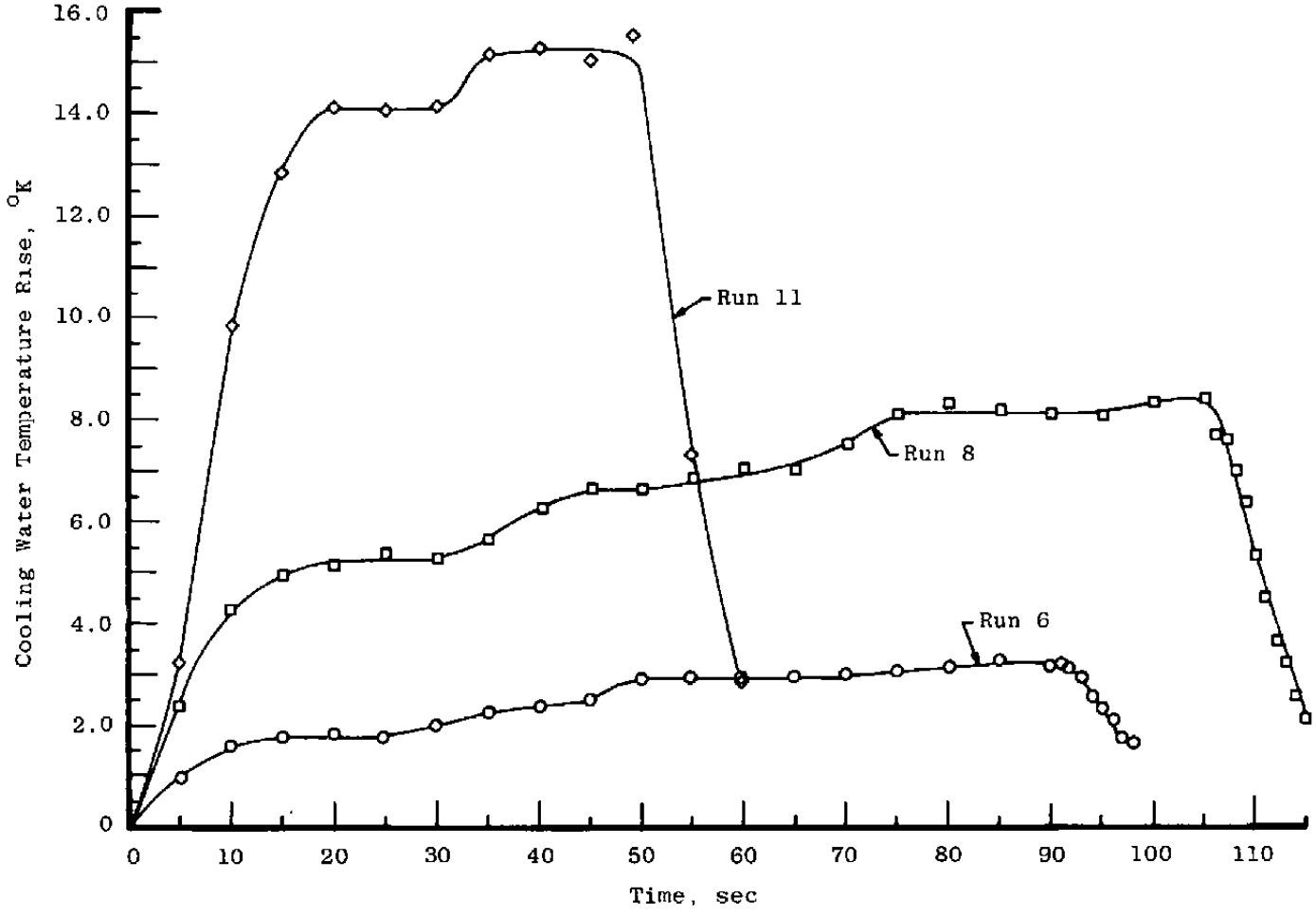

Figure 62. Cooling water temperature rise during runs M3-006, -008, and -011.

Table 1. HPMS Performance Objectives

Power Output	30 MW
Energy Extraction	1 MJ/kg
Power Desity	200 MW/m^3
Run Time	Up to 150 sec
Operation	Steady-state and multipulse
Startup	Full power within 1 sec (Excluding magnet startup)

Table 2. HPMS Channel Design Parameters

Diagonal Wall Angle	40 deg (ϕ = 1.2)
Electrodes	OFHC copper with Inconel and castable ceramic inset
Outer Structure	Filament wound, glass epoxy composite
Cooling Water	Water
Mass Flow	30 kg/sec
Inlet Pressure	3.5 atm
Inlet Temperature	2,800°K
Inlet Mach Number	2.0
Seed Rate	2 to 10 percent (5 percent nominal)
Magnetic Field Strength	4 T (Maximum)
Power Output	30 MW
Output Current	6,800 amp
Output Voltage	4,400 v

Table 3. Combustor Characteristics

Chamber Pressure	30 atm
Chamber Temperature	3,450°K
Total Flow Rate	30.4 kg/sec
O/F Ratio (LOX/JP-4)	3.41
Oxidizer	Liquid Oxygen
Fuel	JP-4 and Span-80 (7 percent Span-80 by weight)
Seed	Cs_2CO_3 in H_2O (72 percent Cs_2CO_3)
Ignition System	Dual, Augmented Spark Ignition
Ignition Reactants	Methane and Gaseous Oxygen

Table 4. Ballast Resistance Load Bank

OD, in.	Thickness, in.	No. Tubes	R, ohms	Bulk ΔT, °F	Water Flow, gpm	Max Amps/Tube	kw/Tube	Total Mw
0.250	0.010	147	0.90	100	5.8	330	93	14
0.375	0.010	36	0.54	100	16.7	640	220	8
0.625	0.010	93	0.35	100	63.5	1,600	900	84

Table 5. Summary of Electrical Characteristics

	4 T Performance	Projected 4.5 T Performance
B_{peak} on Axis (T)	4.0	4.5
Power Level (MW)	17.5	24.7
Operating Current (A)	12,300	14,400
Number of Turns	336	336
Ampere Turns	4.13×10^6	4.84×10^6
Nominal Resistance (Ω)	0.116	0.119
Terminal Voltage (V)	1,430	1,720
Copper Current Density (A/m^2)	2.71×10^7	3.17×10^7
Overall Current Density (A/m^2)	2.09×10^7	2.45×10^7

Table 6. Summary of Mechanical Characteristics

Conductor: OFHC Hollow Copper (based on average of actual dimensions)		
Conductor Dimension (cm)	2.30 by 2.27	
Hole Diameter (cm)	0.782 cm	
Corner Radius (cm)	0.478	
Cross Section Area (cm^2)	4.54	
Insulation		
Turn	0.018-cm thick fiberglass tape, half-lap wrap per turn	
Interlayer Spacer	0.076-cm thick G-10 strips	
Ground Wrap	0.030-cm thick fiberglass tape, half-lap wrap (two layers)	
Coils		
	Inner	Outer
Length Between End Turns (cm)	182.48	223.52
Length, Overall (cm)	219.71	260.76
Number of Layers	6	6
Number of Turns/Layer	14	14
Conductor Bundle Height (cm)	33.32	33.32
Conductor Bundle Width (cm)	14.81	14.81
Minimum Bend Radius (cm)	5.08	5.08
Average Conductor Length (m)	7.74	8.66
Total Conductor Length (m)	655.32	731.52
Conductor Weight (kg)	2,635	2,939
Total Conductor Weight, 4 Coils (kg)	11,149	---

Table 6. Concluded.

Magnet Dimensions (Nominal)	
Length, Overall (cm)	363.22
Width, Overall (cm)	196.09
Height, Overall (cm)	289.56
Centerline Height from Floor (cm)	152.40
Assembled Iron: Low Carbon Steel (Nominal)	
Length, Overall (cm)	175.01
Width, Overall (cm)	196.09
Height, Overall (cm)	274.07
Horizontal Gap at Inlet (cm)	61.21
Horizontal Gap at Outlet (cm)	107.44
Weight (kg)	41,278
Weight Summary	
Total Coil Weight - Conductor and Epoxy (kg)	12,066
Assembled Iron (kg)	41,278
Axial Force Containment Structure (kg)	3,130
Miscellaneous (Casters, Brackets, etc.) (kg)	726
Total Magnet Weight (kg)	57,200

Table 7. Summary of Hydraulic Characteristics.

	4 T Performance	Projected 4.5 T Performance
Pressure Drop in Long Turn (psi)	324	324
Cooling Water Flow Rate (lpm)	12,850	12,850
Inlet Water Temperature (°K)	300	300
Water Temperature Rise (°K)	25	35
Average Cu/Water Temperature Rise (°K)		
Outer Coil	6	7
Inner Coil	7	8

Turn Lengths (m)

	Outer Coil	Inner Coil
Longest Coil	11.22	10.15
Shortest Coil	8.26	7.35

Table 8. ARN-02 Coil Material List

Item	Type	Origin	Notes
Conductor	2.29-cm square w/0.478-cm corner radius and 0.782-cm diam center hole	Phelps Dodge	OFHC
Epoxy*	Resin Hardner Accelerator Wax	Ciba Geigy Ciba Geigy Ciba Geigy Union Carbide	Araldite 6005 Araldite 906 Araldite 064 CarboWax 600
Turn Insulation	Straight sections of coil 0.018 cm by 3.81 cm by 32.92 m. Corner sections of coil 0.018 cm by 1.90 cm by 32.92 m.	J. P. Stevens	"E" glass fiber Volan finish
Ground Wrap	Straight section of coil 0.030 cm by 5.08 cm by 45.72 m. Corner section of coil 0.030 cm by 2.54 cm by 45.72 m.	J. P. Stevens	"E" glass fiber Volan finish
Sleeving	0.051 by 1.59-cm diam by 38.1 m	Nat Var Corp.	Fiberglass Volan finish
Interlayer Insulation	0.076 by 1.905-cm sanded two sides	Synthane Taylor	Nema G-10 Glass cloth/epoxy
Preformed Ring	0.079 wire	Handy & Harmon	Sil Fos 15% Ag
Copper Bar (Bus)	7.62 by 12.7 by 1.905 cm	Local Supplier	ETP copper
Copper Bar (Thermostat mount)	3.175 by 1.59 by 0.95 cm	Local Supplier	ETP copper
Water Fitting	Machined from 1.90-cm square stock	Local Supplier	ETP copper
Tube Cooling	B10-1MC-8	Tylok Int.	Copperplated brass
Tubing	1.27-cm nom Type K	Local Supplier	Copper
Thermostat	#4344-176 w/30.48-cm lead	Texas Instrum.	MIL Std 202
Thermal Joint Compound	Type 120	Local Supplier	----
Filler Blocks	Phenolic	Synthane Taylor	Nema C Phenolic/Canvas
Ferrule	0.9525-cm diam by 0.081 cm by 3.81 cm	Local Supplier	OFHC copper

*Note: Cure Cycle - 4 hrs @ 352.59°K, 10 hrs @ 394.26°K

Table 9. HPMS Test Sequence

Run No.	Duration, sec	Maximum Current	Initial Tap Setting	Final Tap Setting	Reactor Tap No.	Hall Probe Uniformity Grid
M3-001	1	2,000	1	1	17	Location C
M3-002	1	4,000	1	1	17	Location C
M3-003	2	4,000	17	17	17	Location C
M3-004	4	4,000	33	33	17	Location C
M3-005	50	4,200	33	33	17	Location C
M3-006	88	6,400	33	1	17	Location C
M3-007	76	6,400	17	1	17	Location C
M3-008	105	8,400	33	6	10	Location C
M3-009	84	10,000	33	8	8	Location C
M3-010	9	11,500	1	1	0	Location C
M3-011	49	11,500	1	3	0	Location B